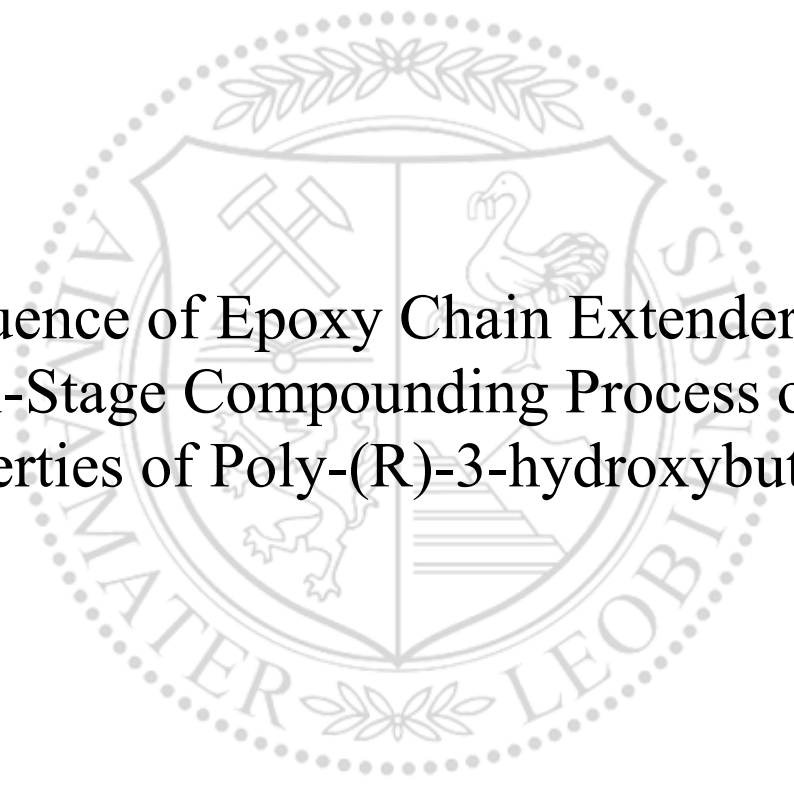Chair of Polymer Processing

Master's Thesis

Influence of Epoxy Chain Extender and Multi-Stage Compounding Process on the Properties of Poly-(R)-3-hydroxybutyrate

Klaus Hinterberger, BSc

September 2023

EIDESSTATTLICHE ERKLÄRUNG

Ich erkläre an Eides statt, dass ich diese Arbeit selbständig verfasst, andere als die angegebenen Quellen und Hilfsmittel nicht benutzt, und mich auch sonst keiner unerlaubten Hilfsmittel bedient habe.

Ich erkläre, dass ich die Richtlinien des Senats der Montanuniversität Leoben zu "Gute wissenschaftliche Praxis" gelesen, verstanden und befolgt habe.

Weiters erkläre ich, dass die elektronische und gedruckte Version der eingereichten wissenschaftlichen Abschlussarbeit formal und inhaltlich identisch sind.

Datum 05.09.2023

Unterschrift Verfasser/in
Klaus Hinterberger

I

Acknowledgments

Foremost, I want to express my gratitude to the European Union funded C–PlaNeT project for initiating, financing, and organizing this project. Without this project, this thesis would not have been possible.

I would like to express special thanks to MTech Priyanka Main, assoz.Prof. Dipl-Ing. Dr.mont. Thomas Lucyshyn, Martin Glehr, and all the employees from the Chair of Polymer Processing, who supported me through this work and helped me with questions and difficulties, which arose during this thesis.

I also want to thank the Chair of Materials Science and Testing of Polymers and the Chair of Chemistry of Polymeric Materials for using their instruments and for their support in proceeding the measurements.

Further thanks to my friends and fellow students for their support, motivation in difficult times, and especially for the enjoyable times we shared during my study.

Especially I would like to thank my family for their support in every possible way. Without you, achieving the goal of completing this study would not have been possible.

Great thanks to all the developers and contributors of Python and all the Python libraries used in this work for the tremendous work in these open-source projects.

Thank you to all the people I have not mentioned who have supported me over the years.

Abstract

Poly-(R)-3-hydroxybutyrate (PHB) is a semi-crystalline biobased biodegradable polymer, which has the potential of being a future replacement for the fossil-based non-degradable polypropylene (PP), especially as a packaging material. PHB meets high barrier properties to O_2, CO_2, and H_2O, but it is very sensitive to thermo-mechanical and hydrolytic degradation. To improve the ductility of the material and reverse a significant amount of the degradation during processing and recycling, a Joncryl® chain extender was added in a simulated recycling process on a twin-screw extruder. To evaluate the effects of processing and the addition of the chain extender on the properties, thermal gravimetric analysis (TGA), differential scanning calorimetry (DSC), small strain oscillatory plate-plate rheometry, tensile tests, and notched impact Charpy tests were carried out. With the addition of Joncryl® a decline in crystallinity and peak crystallization temperature in the DSC measurements was found; for the rheological measurements, an increase in zero shear viscosity was detected; and for the mechanical properties, an increase in elongation at break and a decline in the tangent modulus was observed. Each additional processing step had a vast negative effect on the zero shear viscosity, elongation at break, the notched impact strength, and a positive effect on the tangent modulus. The impact of the processing is more dominant compared to the addition of Joncryl®, and therefore, the usage of Joncryl® is limited in the recycling process of PHB to reverse the thermo-mechanical degradation due to processing. While Joncryl® is a proven chain extender for polyethyleneterephthalate (PET) and polylactic acid (PLA), the significantly lower processing temperature of PHB seemed to limit the full potential of Joncryl® due to the slow reaction speed at this temperature.

Kurzfassung

Poly-(R)-3-hydroxybutyrat (PHB) ist ein teilkristallines biobasiertes, biologisch abbaubares Polymer, das das Potenzial hat, das fossil basierte, nicht abbaubare Polypropylen (PP) zu ersetzen, insbesondere als Verpackungsmaterial. PHB weist hohe Barriereeigenschaften gegenüber O_2, CO_2 und H_2O auf, ist aber sehr empfindlich gegenüber thermomechanischem und hydrolytischem Abbau. Um die Duktilität des Materials zu verbessern und einen Großteil des Abbaus während der Verarbeitung und des Recyclings rückgängig zu machen, wurde in einem simulierten Recyclingprozess in einem Doppelschneckenextruder ein Joncryl®-Kettenverlängerer hinzugefügt. Um die Auswirkungen der Verarbeitung und des Zusatzes des Kettenverlängerers auf die Eigenschaften zu bewerten, wurden eine thermogravimetrische Analyse (TGA), eine Differential-Scanning-Kalorimetrie (DSC), eine oszillatorische Plattenrheometrie mit kleinen Deformationen, Zugversuche und Kerbschlagversuche nach Charpy durchgeführt. Mit der Zugabe von Joncryl® wurde bei den DSC-Messungen ein Rückgang der Kristallinität und der Peakkristallisationstemperatur festgestellt, bei den rheologischen Messungen wurde ein Anstieg der Nullviskosität festgestellt, und bei den mechanischen Eigenschaften wurde ein Anstieg der Bruchdehnung und ein Rückgang des Tangentenmoduls beobachtet. Jeder zusätzliche Verarbeitungsschritt hatte einen erheblichen negativen Effekt auf die Nullviskosität, die Bruchdehnung und die Kerbschlagzähigkeit und einen positiven Effekt auf den Tangentenmodul. Die Auswirkung der Verarbeitung ist im Vergleich zur Zugabe von Joncryl® dominanter und daher ist die Verwendung von Joncryl® im Recyclingprozess von PHB begrenzt, um die thermomechanische Degradation aufgrund der Verarbeitung umzukehren. Joncryl® ist zwar ein bewährter Kettenverlängerer für Polyethylenterephthalat (PET) und Polylactide (PLA), aber die deutlich niedrigere Verarbeitungstemperatur von PHB scheint das volle Potenzial von Joncryl® aufgrund der langsamen Reaktionsgeschwindigkeit bei dieser Temperatur zu begrenzen.

Contents

List of Symbols and Abbreviations

Abbreviations

CI   Confidence interval

DSC   Differential scanning calorimetry

e.g.   exempli gratia

et al. et alia

EU27+3 EU Member States, Norway, Switzerland, and the United Kingdom

MFR Melt flow rate

PHB   Poly-(R)-3-hydroxybutyrate

SEC   Size exclusion chromatography

TGA   Thermal gravimetric analysis

Mechanical Symbols

ϵ_b Elongation at break

σ_m Ultimate tensile strength (UTS)

a_{cN} Charpy notched impact strength

E_t Tangent modulus according to DIN EN ISO 527-1

Rheological Symbols

η^* Complex viscosity

η_0 Zero shear viscosity (analog to A in *Bird-Carreau-Yasuda* model)

λ_L Shear at limit of the linear visco-elastic range

ω Angular frequency

A, B, a, n *Bird-Carreau-Yasuda* parameters

Thermal Symbols

ΔH_m^0 Heat fusion of 100 % crystalline sample

ΔH_m Specific melting enthalpy

T_{pc} Peak crystallization temperature

T_{pm} Peak melting temperature

w_c Crystallinity

1 Introduction

According to Hundertmark et al. (2018), by 2030, a third of the demand for polymers might be met by polymers that had already been used for at least one application. For 2050, they predict that the supply of recycled polymers could rise to nearly 60 % of the total manufactured polymer products. The recovered polymers from recycling are in competition with their virgin counterparts; the production costs of the virgin materials depend mainly on the oil price (Hundertmark et al., 2018). Therefore, for recycled polymers to have a competitive advantage, either the oil price has to rise, government regulations or subsidies have to provide a competitive advantage, or a reduction in production costs of recycled polymers due to innovation creates this advantage. Another driving factor for the recycling of polymers is the increasing problem of polymer waste in the whole world (Rosenboom et al., 2022). A possible solution to this problem is recycling as part of the circular economy model. The landfill of polymer waste results only in the Asia-Pacific region in damages of estimated US$1.3 billion per year for tourism, fishing, and shipping, and a worldwide total damage of estimated US$13 billion per year (Messerli et al., 2019). Till now there are two established ways to recycle polymers (recycling definition according to ISO 15270 Hopewell et al., 2009): mechanical recycling, and chemical recycling. In 2020, in the EU27+3, which includes the EU Member States, Norway, Switzerland, and the United Kingdom, 35 % of the polymer waste was recycled, 42 % was used for energy recovery and 23 % was landfilled (PlasticsEurope, 2022).

To become more independent of non-renewable resources and reduce greenhouse-gas emissions, biobased polymers can be part of the solution. The polymer production in 2019 demanded approximately 5 % to 7 % of the total oil supply and caused 2 % of the total CO_2 emissions; 61 % of the emissions are caused by the material extraction, 30 % by the polymer production, and 9 % are produced in the end-of-life stage (Hamilton & Feit, 2019; Rosenboom et al., 2022; Zheng & Suh, 2019). The complete substitution of fossil feedstock for polymer production with sugarcane would reduce the greenhouse-gas emission by approximately 25 %, as the simulation of Zheng and Suh (2019) predicts. Polyhydroxybutyrate (PHB) is a polymer that belongs to the group of polyesters, it is biodegradable and biobased (Turco et al., 2021). PHB also belongs to the polyhydroxyalkanoates (PHAs), a subgroup of the polyesters, which are produced by a variety of microorganisms as a carbon and energy storage (McAdam et al., 2020). Generally, PHB melts between 170 °C to 180 °C and the processing window is around 180 °C to 190 °C; the degradation process at the temperature range of the processing windows is fast and makes the processing of PHB challenging (Janigová et al., 2002; Turco et al., 2021). PHB shows high crystallinity of 50 % to 90 %, is brittle with an elongation at break of 1 % to 15 % (Bugnicourt et al., 2014; Keskin et al., 2017; Rajan et al., 2019).

The overall properties of PHB change dramatically with each additional processing step (Pachekoski et al., 2013; Plavec et al., 2022), which is due to the thermo-mechanical degradation initiated by the processing. To enhance the mechanical properties of PHB, especially for recycled PHB, which is even more brittle than the virgin material, different additives and blends were investigated by multiple authors (Bousfield, 2014; Choi et al., 2003; Duangphet et al., 2014; Kolahchi & Kontopoulou, 2015; Przybysz et al., 2018; L. Wang et al., 2008; Weinmann & Bonten, 2019). Duangphet et al. (2014) showed that the addition of Joncryl® to PHB increases the activation energy for the thermal degra-

dation and enhances the complex viscosity. The effect of the Joncryl® chain extender on the mechanical properties was not investigated till now and these are the most important properties for future application and the recycling of PHB, especially the change in brittleness is necessary to investigate. The effect of multiple addition of Joncryl® in a simulated multistage recycling process on the mechanical properties is also important for the application of PHB and the consideration of a recycling process after the end-of-life.

The assumption at the core of this investigation is, that the addition and reaction of Joncryl® results in the formation of side-chains and cross-linking, which decreases the crystallinity of PHB and enhances the fracture toughness. The addition of Joncryl® in a simulated multi-stage recycling process should therefore, result in an increase in thermal stability and ductility of the material. This is backed up due to the thermal, rheological, and mechanical tests performed during this thesis.

2   State of the Art

In the state of the art section, the topics of mechanical recycling, properties and degradation of PHB, effects of additives on the properties of PHB, and the use of chain extenders with polyesters and the effect on the properties are discussed.

2.1   Mechanical Recycling

With the steady increase of worldwide polymer production of 365.5 Mt in 2018 to 390.7 Mt in 2021 the end-of-life management becomes more challenging every year (PlasticsEurope, 2022). Of the 390.7 Mt in 2021, 90.2 % were fossil-based, 8.3 % post-consumer recycled, and 1.5 % bio-based/bio-attributed plastics (PlasticsEurope, 2022). The main options for waste treatment are recycling, landfill, and energy recovery. The exact numbers for the evolution of waste treatment from 2006 to 2020 for the EU27+3 can be seen in figure 1.
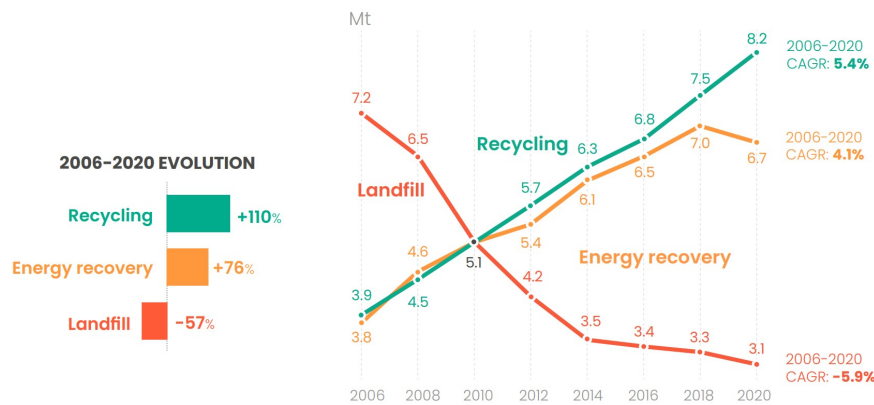

Figure 1: Waste management of the EU27+3 (PlasticsEurope, 2022). With CAGR as the compound annual growth rate.

The waste management hierarchy is as follows: most preferred is the prevention of waste, second most is the re-use of products, third most is the recycling of waste, fourth is the energy recovery of waste, and the least preferred is disposal or landfill of the waste (Delva et al., 2019). The recycling step of the waste management hierarchy can be further distinguished into closed-loop, open-loop, and chemical recycling with a decreasing preference in the order as mentioned (World Economic Forum et al., 2016). Closed-loop mechanical recycling processes use the waste to create products with the same quality as the previous application, in open-loop mechanical recycling the waste is used to produce products with fewer requirements on quality and/or material properties of the recycling material (World Economic Forum et al., 2016).

Most of the recycling nowadays is of a mechanical nature in open-loop form, e.g. 80 % of polyethylene terephthalate bottles are turned into polyester fibers (World Economic Forum et al., 2016). The open-loop mechanical recycling process is more common today, due to the degradation of the properties with each recycling process and economic challenges. The degradation of the waste during the recycling process limits the application area of the recycling material, and therefore, results in an open-loop recycling process. In figure 2 a mechanical recycling process for an open or closed-loop cycle is shown.

Figure 2: Mechanical recycling process (Nizamuddin et al., 2021).

Hamad et al. (2013) provide an overview of the degradation of a wide range of properties for the polymers polyethylene, polypropylene, and polystyrene. A review of the main methods, challenges, degradation mechanisms, decline of properties, and used additives for the mechanical recycling of the five main packaging polymers: polyethylene terephthalate, polyethylene, polypropylene, polystyrene, and poly(vinyl chloride) is provided by Schyns and Shaver (2021).

In figure 3, the ambition of World Economic Forum et al. (2016) is shown. This represents a circular economy to reduce plastic waste and decouple the polymer production from fossil-based feedstocks, which also includes the production of virgin material from renewable feedstocks and the reuse of products. To achieve these problems, also the design and production phase has to be considered, to design and manufacture products for reuse and recycling.
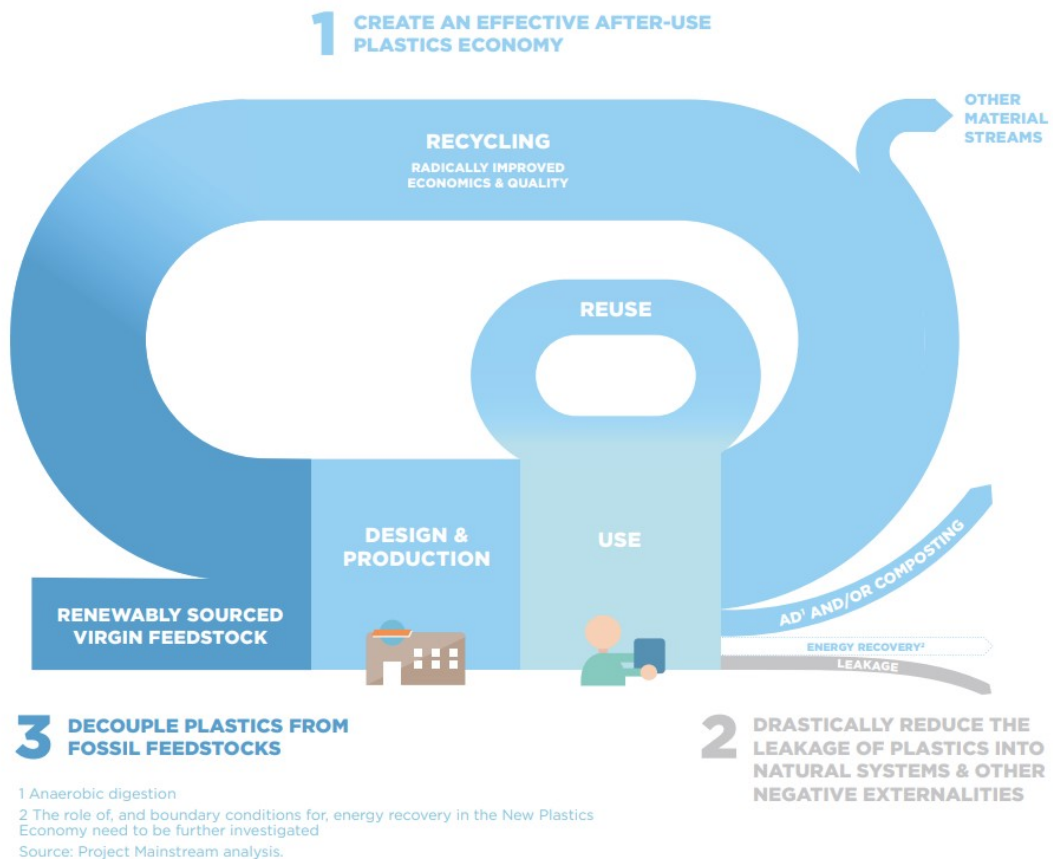
Figure 3: Ambition of the new plastic economy (World Economic Forum et al., 2016).

2.2 PHB

PHB is a biobased and biodegradable polymer, which belongs to the group of polyesters. Polyesters are generally synthesized with a polycondensation reaction. This is typically achieved by an equilibrium reaction of alcohol and acids. To shift the equilibrium towards the products, water is deducted during the synthesis (Endres & Siebert-Raths, 2011). In figure 4 the general structure of a polyester is shown. The organic group R represents the different polyesters. PHB is presented in figure 5.

Figure 4: General structure of a polyester.

Figure 5: Structure of PHB.

2.2.1   Properties

In table 1, the main thermal and mechanical properties of PHB published by two research groups are shown. Most of the properties from both rese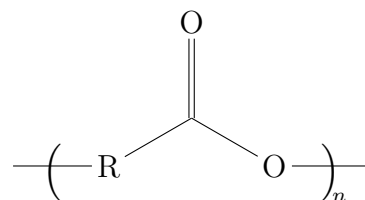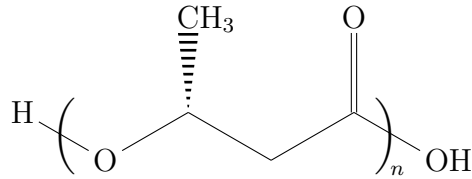arch groups show at least a large overlap, except for the tensile modulus and the glass transition temperature. Polypropylene has a tensile modulus of $1.95\,\text{GPa}$, an elongation at break of $50\,\%$ to $145\,\%$, and a glass transition temperature of $-20\,°\text{C}$ to $-5\,°\text{C}$; therefore PHB is stiffer but more brittle compared to polypropylene, the other properties are similar (McAdam et al., 2020). The heat of fusion for a $100\,\%$ crystalline PHB sample is $146.6\,\text{J/g}$ according to Barham et al. (1984).

Table 1: The main properties of PHB.

Properties	McAdam et al. (2020)	Bugnicourt et al. (2014)
Tensile modulus in GPa	3-3.5	1-2
Tensile strength in MPa	20-40	15-40
Elongation at break in %	5-10	1-15
Degree of cystallinity in %	50-60	40-60
Melting temperature in °C	165-175	160-175
Glass transition temperature in °C	5-9	2

2.2.2   Degradation due to Processing and Influence on Properties

In the following section, the main degradation effects during processing are shown and the effect of the degradation process on the properties of PHB.

The thermal degradation reaction is shown in figure 6. PHB is prone to random chain scission when it is subjected to heat. During processing, the main degradation mechanism is of thermo-mechanical nature and cannot be explained purely by thermal degradation (Dos Santos et al., 2018). The thermo-mechanical degradation is significant compared to a pure thermal degradation model during processing, as shown by Pachekoski et al. (2013); they did measurements in which PHB got processed and the molar mass distribution was measured with size exclusion chromatography (SEC) and compared with the theoretical decrease in molar mass due to thermal degradation (theoretical decrease of $0.3\,\%$ and measured decrease of $29\,\%$ of initial average molecular mass). Rivas et al. (2017) have found a decline in tensile stress at break of $32.1\,\text{MPa}$ to $13.4\,\text{MPa}$ after three extrusion cycles. The significant decline of the complex viscosity in the time sweep is also a well-researched phenomenon (Lajewski et al., 2021; Melik & Schechtman, 1995; Park et al., 2001; Plavec et al., 2022). Pachekoski et al. (2013) reported an increase in melt flow rate

(MFR) from $19\,g/10min$ to $26\,g/10min$ (at $190\,°C$ and with $2.16\,kg$) and in crystallinity from $56.6\,\%$ to $61\,\%$ after two processing cycles of extrusion and injection molding.
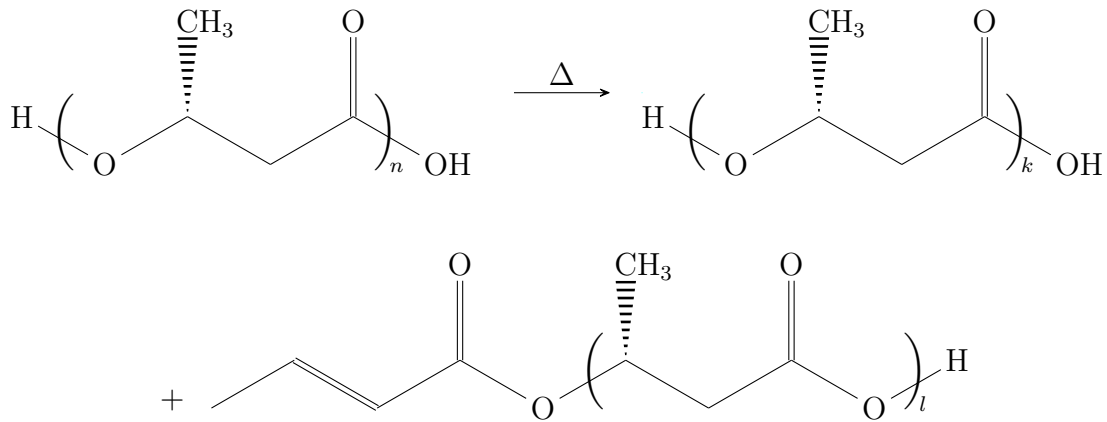

Figure 6: Random chain scission reaction of PHB (Bordes et al., 2009; Turco et al., 2021).

2.3 Effects of Additives on the Properties of PHB

Commonly used additives for polyesters or PHB in specific are stabilizers, chain extenders, plasticizers, and antioxidants (Schyns & Shaver, 2021). For stabilizers and antioxidants, no or negative effects on the thermal melt stability were found by Arza et al. (2015) (Rheometry and SEC) and Tocháček et al. (2021) (MFR), and a positive effect by L. Wang et al. (2008) in an MFR measurement. Longé et al. (2022) reported a tremendous increase for the elongation at break from $11\,\%$ for the pure PHB to $260\,\%$ for a blend with $30\,wt\%$ butanediol diferulate. This result for the elongation at break was measured five minutes after the extrusion process and then rapidly declined to $27\,\%$ one hour after the extrusion process and continued declining. L. Wang et al. (2008) reported a decline of the glass transition temperature from $6.1\,°C$ to $-30.7\,°C$, melting enthalpy from $82.1\,J/g$ to $60.6\,J/g$, and peak melting temperature from $169\,°C$ to $156.8\,°C$ with an increase from $0\,\%$ to $30\,\%$ in acetyl tributyl citrate concentration for the second heating scan of a DSC measurement. They also found a decline from $14\,MPa$ to $6.1\,MPa$ in tensile strength, $1510.4\,MPa$ to $192.7\,MPa$ in Young's modulus, and an increase in elongation at break from $2.5\,\%$ to $9.7\,\%$ for the same change in concentration. Chain extenders and specifically the Joncryl® chain extender will be discussed in the next section.

2.4   Chain Extenders and Polyesters

Chain extenders react with functional groups of polymers and can lead to side-branching and/or cross-linking in the polymer. This is often used when the polymer is prone to degradation to reverse or even enhance the degraded properties compared to the initial state of the properties. A schematic example can be seen in figure 7 of an epoxy chain extender, which reacts with a carboxyl and a hydroxy group. Two commonly used multi-functional epoxy chain extenders are Joncryl® 4400 and 4468 (both produced by BASF, Germany), which were used in this thesis. The general structure of a multi-functional epoxy chain extender is illustrated in figure 8. The reaction mechanism of Joncryl® with polyesters is visible in figure 9 for an undegraded and a degraded polymer chain. In the case of the undegraded polymer chain the Joncryl® reacts with the carboxyl end-group and in the case of the degraded polymer chain the Joncryl® reacts with the vinylic ester or acid end groups (compare with figure 6).
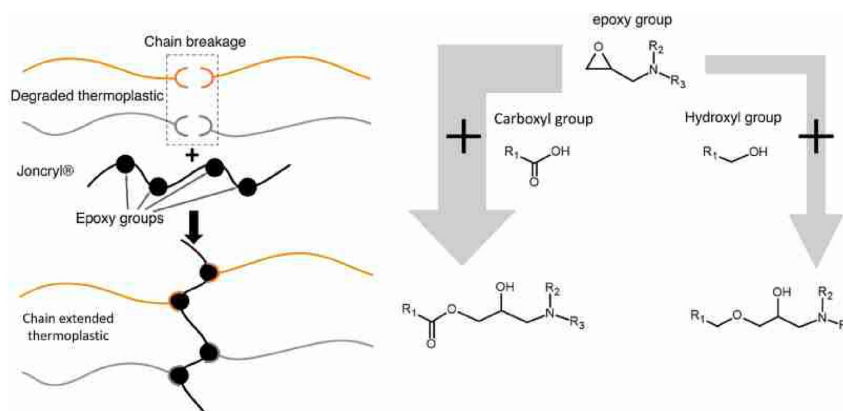

Figure 7: Schematic reaction of the chain extenders Joncryl® (Standau et al., 2022).

Ghanbari et al. (2013) and Yang et al. (2018) reported an increase in the shear-thinning behavior and an enhancement of the zero shear viscosity for PET with the addition of Joncryl® in a frequency sweep measurement of the complex viscosity in a small-amplitude oscillatory shear rheometry. Additionally, Ghanbari et al. (2013) stated in their work that the residence time in the extruder was too short for the whole Joncryl® to react in their experiment, and therefore, the complex viscosity further increased during a time sweep measurement. Ghanbari et al. (2013) used the time sweep measurement before the amplitude sweep and the frequency sweep to determine a time window for the measurement of amplitude and frequency sweep, which is necessary due to the time-dependency of PET and polyesters in general. To prove the time-independence during the frequency sweep, Ghanbari et al. (2013) did four repeats for each measurement setting, two from low to high and two from high to low angular frequency. The neat PET showed in both papers from a Newtonian behavior over the angular frequency range from 0.3 rad/s to 100 rad/s in both papers from Ghanbari et al. (2013) and Yang et al. (2018).

Kahraman et al. (2021) did frequency sweeps for amorphous and semicrystalline poly-lactic acid and added Joncryl®. They reported an increase in the zero shear viscosity of the complex viscosity and the transition point of Newtonian to shear thinning moves to lower angular frequencies.

Meng et al. (2012) also stated the increase of the complex viscosity for PLA with the addition of Joncryl® compared to neat PLA in a time sweep measurement. They also observed an increase of complex viscosity in the time sweep measurement with an increase in mixing temperature and an increase in Joncryl® concentration.

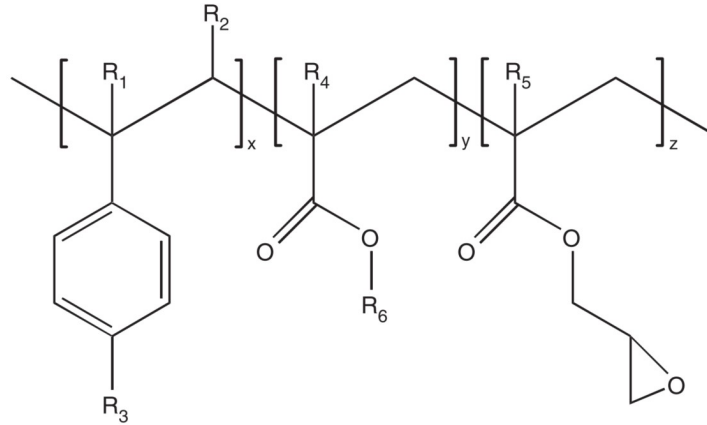*Figure 8: General chemical structure of epoxy-functionalized chain extenders; R1-R5 are H, CH₃, a higher alkyl group, or combinations of them; R6 is an alkyl group; and x,y, and z are each between 1 and 20 (Villalobos et al., 2006).*
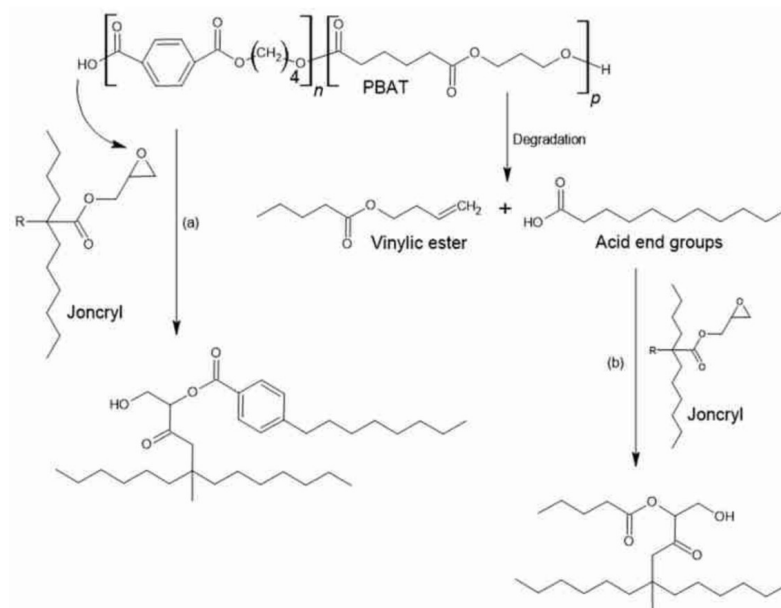

Figure 9: Reaction of Joncryl® with polyester (Standau et al., 2022). (a) reaction with carboxyl end group and (b) reaction with degraded chain.

3   Theoretical Foundations

In the following section, all measurement methods, which were used during this thesis, are briefly explained. First, for each test an overview is given, and afterward, some details of the specific measurement method are shown, which could be useful for the analysis and interpretation of the results.

3.1   Thermal Gravimetric Analysis

The aim of thermal gravimetric analysis or short TGA is to evaluate the change in mass for a specific temperature program. This includes sublimation, evaporation, decomposition, chemical reaction, and magnetic or electrical transformation. In this thesis, the main goal is to show the main decomposition temperature of PHB.

Therefore, the initial mass is determined in advance of the test and the mass is recorded over time and/or temperature during the test. A schematic TGA device can be seen in figure 10, which consists of an oven to perform the heating program, in which the pan with the sample is placed, a thermocouple to measure the sample temperature and sometimes the temperature of a reference sample (gather the heat flow during the measurement, see also DSC section 3.2), a balance to evaluate the initial mass, set the zero point according to the initial mass, and track the mass during the measurement.

The most influential factors on the TGA measurement according to Ehrenstein et al. (2004) are the specimen preparation, the pan for the sample, the specimen weight, the purge gas, the thermocouple, and the heating rate.
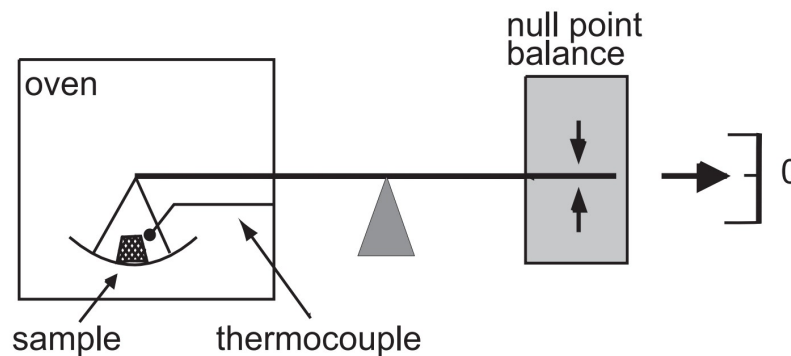
Figure 10: Schematic of TGA testing device (Ehrenstein et al., 2004).

In figure 11 a schematic TGA measurement curve can be seen. In this curve, the mass is plotted over the sample temperature or/and measurement time. Often, the residual weight is used instead of the sample mass, as in this thesis. The residual weight can be calculated by dividing the mass at each measurement point by the initial mass m_s.

Point A corresponds to the starting point or onset of the degradation process and the characteristic value is the starting point temperature T_A or onset temperature with the corresponding measurement time t_A. Point A can be determined with the intersection of the initial mass and the tangent of the maximal slope during the degradation process (maximum value of the differential thermogravimetry (DTG) curve see figure 12) (Ehrenstein et al., 2004). Point B corresponds to the end point or endset of the degradation process and the characteristic value is the end point temperature T_B at the end point

time t_B and can be determined similar to the onset, but instead of the initial mass, the end mass m_f is used. Point C is the intersection of the TGA measurement curve with a horizontal line which goes through the midpoint of points A and B (Ehrenstein et al., 2004). The corresponding temperature of point C is the midpoint temperature T_C at the midpoint time t_c.
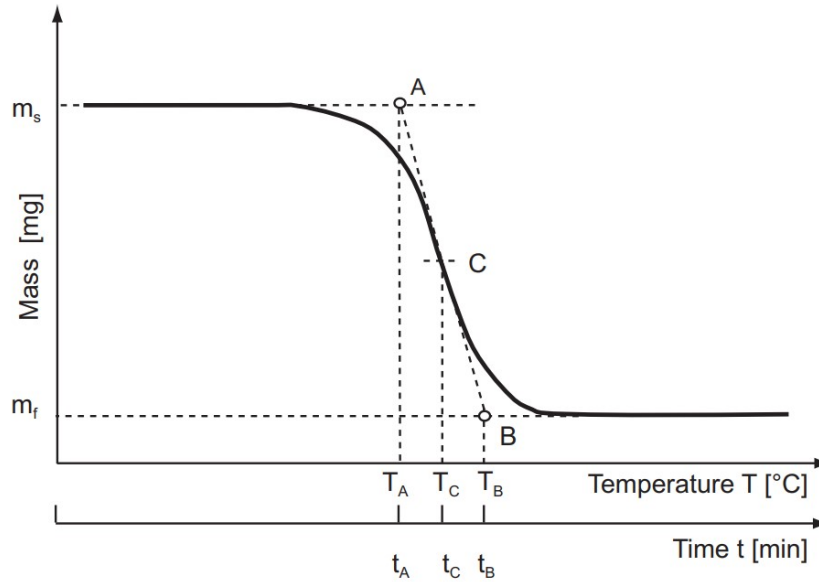
Figure 11: Schematic of a TGA measurement curve (Ehrenstein et al., 2004).

In figure 12 the DTG-signal is additionally plotted over the temperature/measurement time. The DTG-signal is the time derivative of the residual mass. The two peak temperatures T_{p1} and T_{p2} correspond to the maximal decomposition temperatures of each degradation process. M_{L1} and M_{L2} are the mass losses of each degradation process (e.g. $M_{L1} = 100 \cdot (m_s - m_i)/m_s$) (Ehrenstein et al., 2004).
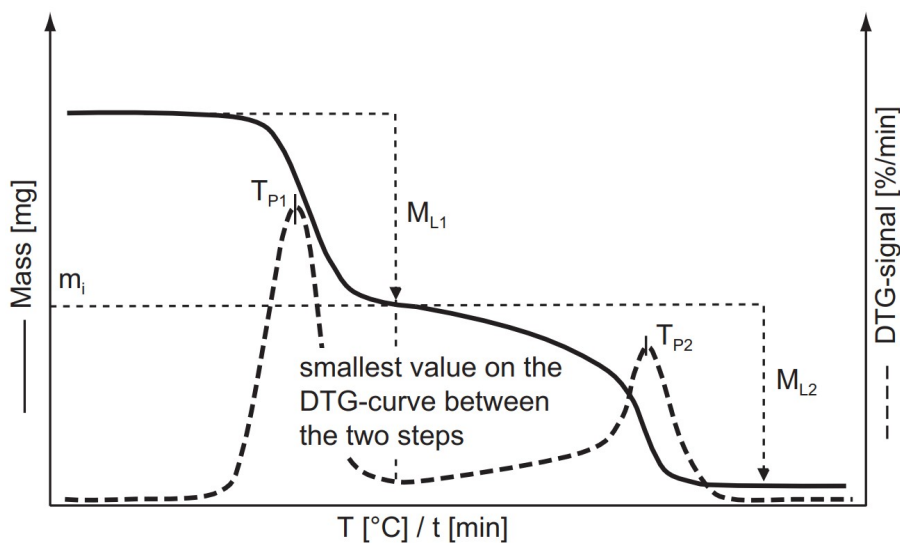
Figure 12: Schematic of a DTG-signal (Ehrenstein et al., 2004).

3.2   Differential Scanning Calorimetry

The differential scanning calorimetry is a thermal analysis, which measures the heat flow absorbed or released by a sample during heating and cooling scans. The aim of the DSC measurement is to obtain information about the physical and chemical changes that occur in a material in response to variations in temperature.

In figure 13, a schematic DSC cell is shown. This cell consists of an oven with a heating block, chromel disc and wire, a thermocouple at the chromel discs, gas purge inlet, and a thermoelectric disc made of constantan. The sample is placed into a pan and a second pan is used as a reference during the measurement. During the heating process, an equilibrium state between the heat flow into the sample $(\dot{Q}_s)$ and the heat flow into the reference $(\dot{Q}_r)$ is established, where both follow the heating program of the oven. If a transition in the sample occurs, a temperature difference between the sample and the reference is the result, due to the latent heat for the transition of the sample. This temperature difference is proportional to the heat flow into the sample $\dot{Q} \propto T_r - T_s$ with T_r as the reference temperature and T_s as the sample temperature measured at the sensors (Menczel & Prime, 2009).
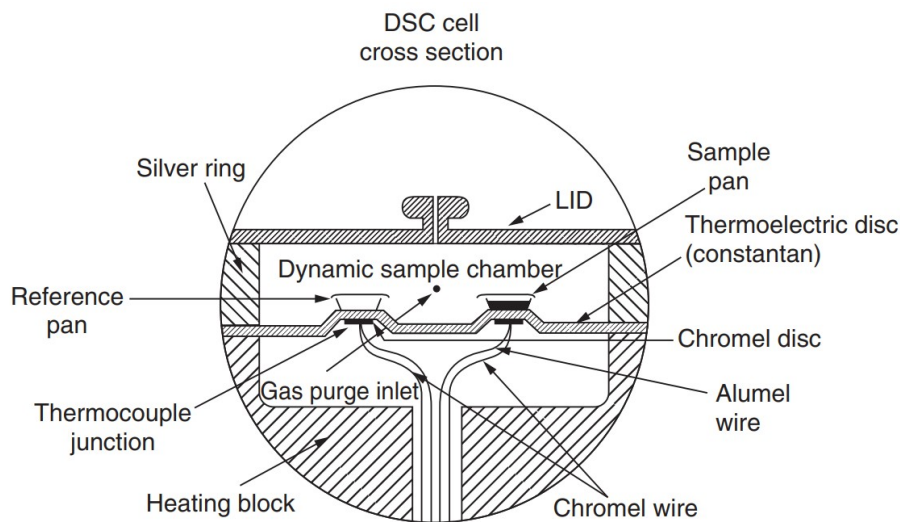
Figure 13: Cross section of a DSC cell (Menczel & Prime, 2009).

Ehrenstein et al. (2004) mention as the most important influential factors on the DSC measurement the specimen preparation, starting and end temperature of the heating program, the reference material, type of the purge gas and the volume flow rate, the heating or cooling rate, and the specimen mass. For most of these influential factors on the measurement Ehrenstein et al. (2004) provide best practice values, which are widely used and therefore are ideal for the comparison of results.

Afterward, the most important equations for the evaluation of the DSC measurement are shown. First, the enthalpy is defined in equation (1) as the sum of internal energy U and the product of the pressure p and volume V of the system (Atkins et al., 2002).

$$H \equiv U + pV \tag{1}$$

For an infinitesimal change in enthalpy of a system at constant pressure, it is possible to write equation (2) (Atkins et al., 2002).

$$dH = dU + pdV \tag{2}$$

The first law of thermodynamics for a system that only does expansion work ($W = -pdV$, $W_{ext} = 0$) can be formulated as $dU = dQ - pdV$. With this formulation it is possible to find the connection of enthalpy and heat in form of the equation (3) (Atkins et al., 2002). This equation confirms the relationship between the measured temperature difference between the sample and the reference by DSC ($\dot{Q} \propto T_r - T_s$) and the enthalpy change due to the transition of the material, if the made assumptions are not violated.

$$dH = dQ \tag{3}$$

In figure 14 the most important transitions of a polymer sample are shown. This includes the endothermic glass transition, melting or vaporization process, and the exothermic crystallization or chemical reaction (e.g. curing, cross-linking) process, and the degradation process of the sample.
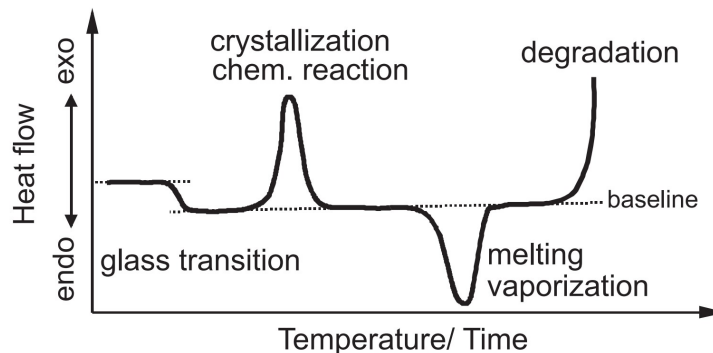
Figure 14: Schematic DSC measurement curve with possible transitions (Ehrenstein et al., 2004).

A general procedure in a DSC measurement is first to subject the sample to heat and gain information about the thermo-mechanical history or erase the history. Then the cooling process follows, which is used to gain information about the crystallization process and set a specific thermal history to compare different results. The second heating scan is used to determine the characteristic values of the material. For reactive resins, a third heating scan is used to gain information about the curing process.

The following paragraph explains the analysis of melting enthalpy, as this evaluation is utilized in this thesis. The analysis of the crystallization peak is not mentioned, because it is analogous to the analysis of the melting peak. In figure 15, an exothermic melting peak of a polymer is shown. The melting onset temperature T_{im} marks the initial deviation of the measurement curve from the baseline, while the melting end temperature T_{fm} indicates the final deviation (Ehrenstein et al., 2004). The peak melting temperature T_{pm} is the temperature at maximum heat flow during the melting process. The onset temperature T_{eim} is the intersection of the extrapolated line of the linear section of the left side of the peak with the extrapolated baseline (Ehrenstein et al., 2004). Analog is the endset

temperature T_{efm} defined for the right side of the melting peak. The melting enthalpy H_m is the absorbed energy of the sample to melt the crystalline phase. The melting enthalpy can be calculated from the area under the peak bounded by the extrapolated baseline (Frick & Stern, 2013).

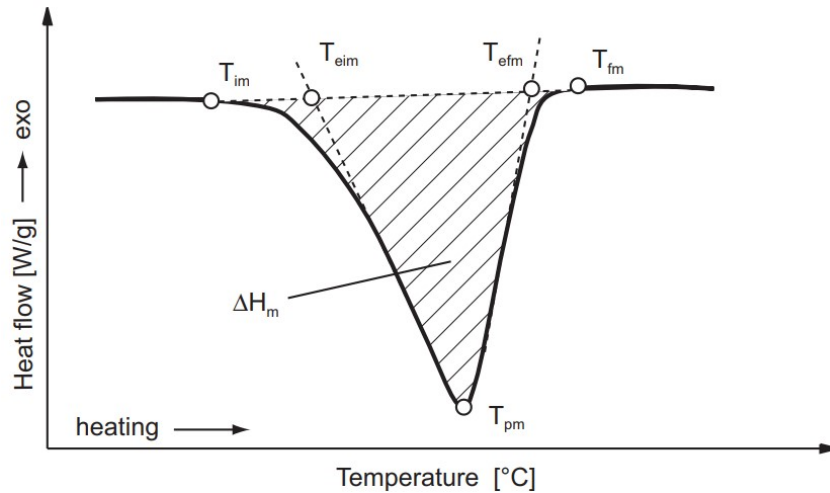*Figure 15: Characteristic values of the melting peak (Ehrenstein et al., 2004).*

The crystallinity w_c serves as a more illustrative characteristic value compared to the melting enthalpy. It represents the fraction of the crystalline structure of a sample compared to a $100\,\%$ crystalline sample (Ehrenstein et al., 2004). Therefore, the heat of fusion ΔH_m^0 is experimentally determined.

The crystallinity can be calculated with equation (4), where ΔH_m is the specific melting enthalpy of the sample, x_{fr} is the weight fraction of the polymer in the blend, and ΔH_m^0 is the heat fusion of the $100\,\%$ crystalline sample.

$$w_c = 100 \cdot \frac{\Delta H_m}{x_{fr}\Delta H_m^0} \tag{4}$$

3.3   Oscillatory Plate-Plate Rheometry

The oscillatory plate-plate rheometry is used to determine the viscosity of a material as a function of the angular frequency. The viscosity curve as a material parameter is of high interest, because it contains information about the molecular structure of the polymer and it is the main property that influences the processability of the material. With the viscosity curve, it is possible to gain information of changes in the molecular mass distribution, which is especially interesting if a chain extender is added and degradation is happening during processing.

The oscillatory shear of a sample can be modeled with a parallel connection of a spring and a dashpot as in figure 16 on the left. This model is similar to the *Kelvin-Voigt* model, but the storage and loss modulus are a function of the angular frequency in figure 16. In the *Kelvin-Voigt* model, the storage and the loss modulus are assumed as independent from the angular frequency. On the right side of figure 16, the geometric connection of the storage modulus G', the loss modulus G'', the dissipation factor $\tan\delta$, and the magnitude of the dynamic modulus $|G^*|$ is shown.
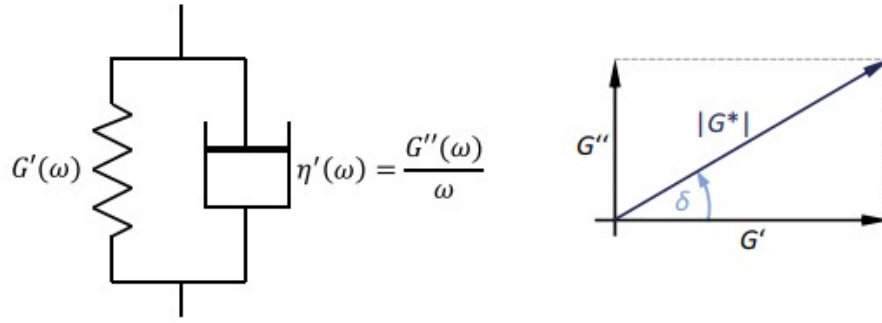
Figure 16: General viscoelasticity model (Schröder, 2020).

The shear deformation γ, the shear rate $\dot{\gamma}$, and the shear stress τ for an oscillatory test can be described with the equations (5) to (7) in which $\hat{\gamma}$ is the shear amplitude, ω the angular frequency, and t the time (Schröder, 2020).

$$\gamma = \hat{\gamma}\sin(\omega t) \tag{5}$$

$$\dot{\gamma} = \frac{d\gamma}{dt} = \hat{\gamma}\omega\cos(\omega t) \tag{6}$$

$$\tau(t) = G'\gamma + \eta'\dot{\gamma} = G'\hat{\gamma}\sin(\omega t) + \eta'\omega\hat{\gamma}\cos(\omega t) = G'\hat{\gamma}\sin(\omega t) + G''\hat{\gamma}\cos(\omega t) \tag{7}$$

Normally, in oscillatory plate-plate rheometer tests the deformation or shear is controlled and the shear stress is measured. Therefore, the shear amplitude and angular frequency are set and the response of the sample, in this case the shear stress, is measured by the measurement device. The curves of equations (5) and (7) can be seen in figure 17, in which the shear deformation γ and the shear stress τ are shown over time and have a phase shift of δ. The dissipation factor $\tan\delta$ can be determined with the equation (8) and the magnitude of the dynamic modulus $|G^*|$ can be calculated with equation (9) (Münstedt, 2016; Osswald & Rudolph, 2015). The magnitude of the complex viscosity can be obtained with the equation (10) with $\eta'' = G'/\omega$ (Münstedt, 2016).

Due to simplicity, the bars of the norm for the magnitude of the complex viscosity are often left out, and therefore, it is written η^* instead of $|\eta^*|$ (Carreau et al., 2021). This is the case in section 5.2 for the diagrams and tables.

$$\tan(\delta) = \frac{G''}{G'} \tag{8}$$

$$|G^*| = \left|G'^2 + G''^2\right|^{1/2} \tag{9}$$

$$|\eta^*| = \frac{|G^*|}{\omega} = \left|\eta'^2 + \eta''^2\right|^{1/2} \tag{10}$$
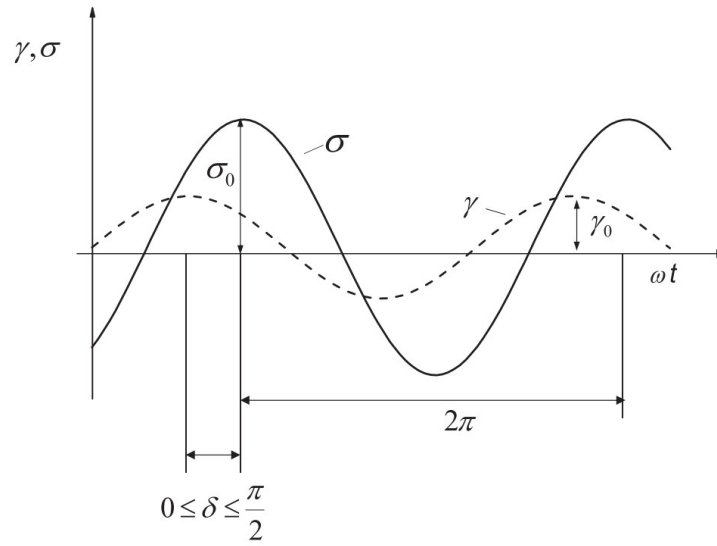
Figure 17: Schematic osciallatory plate-plate rheometry measurement curves (Münstedt, 2016). With $\sigma_0 \equiv \hat{\tau}$ and $\gamma_0 \equiv \hat{\gamma}$.

An elegant approach dealing with the equations (5) to (7) is by using *Euler's formula* $e^{ix} = \cos(x) + i\sin(x)$ and using complex numbers. This is shown in the equations (11) to (13); if only the complex parts of the equations (11) to (13) are considered, they are identical to the equations (5) to (7) (Carreau et al., 2021; Münstedt, 2016). With the shear stress and the shear rate in complex notation, the complex viscosity can be obtained as shown in equation (14).

$$\gamma = \hat{\gamma}e^{i\omega t} \tag{11}$$

$$\dot{\gamma} = i\hat{\gamma}\omega e^{i\omega t} \tag{12}$$

$$\tau = G'\gamma + \eta'\dot{\gamma} = G'\hat{\gamma}e^{i\omega t} + i\hat{\gamma}\eta'\omega e^{i\omega t} = \hat{\gamma}(G' + iG'')e^{i\omega t} = \hat{\gamma}G^*e^{i\omega t} = \hat{\gamma}|G^*|e^{i\omega t+\delta} \tag{13}$$

$$\eta^* = \frac{\tau}{\dot{\gamma}} = \frac{G^*\hat{\gamma}e^{i\omega t}}{i\hat{\gamma}e^{i\omega t}} = \frac{G' + iG''}{i\omega} = \frac{G''}{\omega} - i\frac{G'}{\omega} \tag{14}$$

An alternative way to illustrate the equations (5) and (7) is shown in figure 18 (b). In figure 18, a tensile load is used, but the evaluation is analog to the evaluation for a shear load. Figure 18 is equivalent to figure 17 and can be used to calculate storage and loss modulus.

The advantage of figure 18 compared to figure 17 is that multiple measurement curves can be shown in a clear manner and the comparison is simpler. The figure 18 is extensively used in the large amplitude oscillatory shear (LAOS) method, but for large strains the curve shows non-linear deformation.
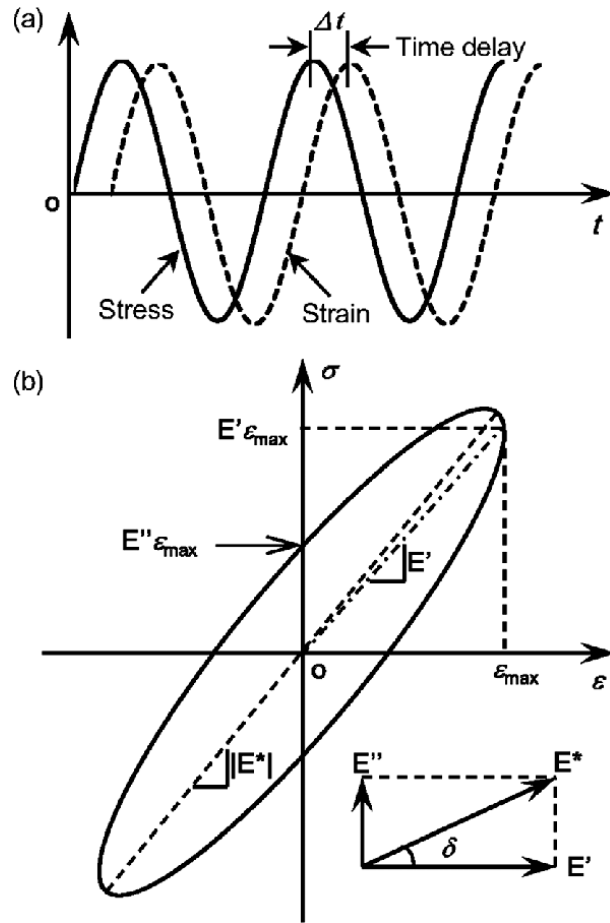
Figure 18: Evaluation of storage and loss modulus (Z. Wang et al., 2017). (a) stress and strain over time, (b) stress over strain.

In figure 19 on the left a schematic oscillatory plate plate rheometer is shown, and on the right the shear stress, shear, and the shear rate diagrams for an ideal elastic material are illustrated. Generally, for oscillatory plate-plate rheometer measurements, the shear strain profile is set and the shear stress response is measured indirectly over the torque.
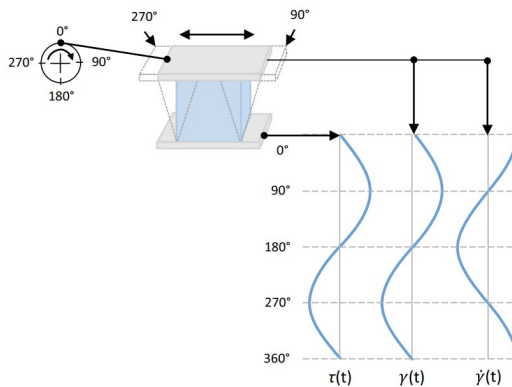
Figure 19: Schematic osciallatory plate-plate rheometry with ideal two plate model for a ideal elastic sample (Schröder, 2020).

Figure 20 shows an amplitude sweep, which is performed before the complex viscosity curve is measured. An amplitude sweep is performed with a constant angular frequency and a steady increase in the shear. The amplitude sweep is performed to find the linear visco-elastic range of the material (γ_L in figure 20).
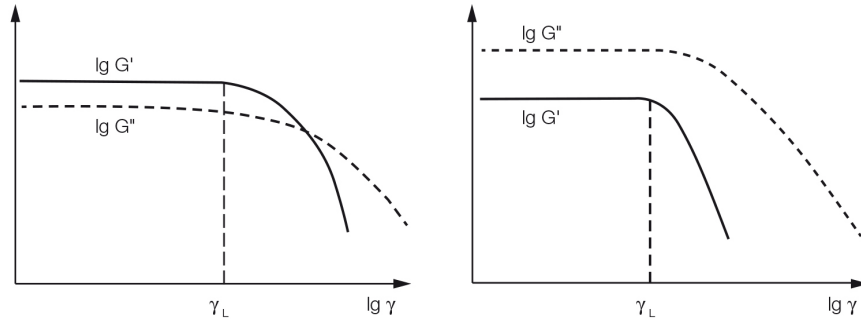
Figure 20: Amplitude sweep (Anton Paar, 2023). Left gel or solid like sample, right fluid like sample.

In figure 21 a schematic frequency sweep is shown, which is used to obtain the complex viscosity η^* of a material. Therefore, a fixed shear in the linear visco-elastic range ($\gamma < \gamma_L$) is used and the angular frequency is steadily decreased/increased in between the range of interest. As was shown in figure 16 and with the equations (11) to (13), the storage and loss modulus can be modeled as a function of the angular frequency and both can be used to determine the complex viscosity η^* with equation (14).
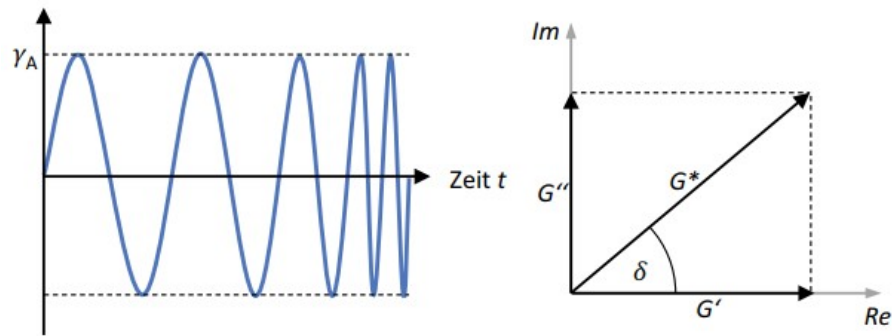
Figure 21: Frequency sweep (Schröder, 2020).

The five parameters *Bird-Carreau-Yasuda* model (Yasuda, 1979) is stated in equation (15) in its general form. If the second plateau at high shear rates η_∞, called infinity shear rate viscosity, is neglected the equation (15) can be simplified to equation (16), where η_0 is identical to A and called the zero shear viscosity. The equation (15) is shown in figure 22 and the influence of the five parameters on the curve. B is a time constant ($B = 1/\lambda$) and represents the change-over point from Newtonian to shear-thinning behavior of the material and a represents the curvature of the transition. The parameter n is the Power Law index. To fit the parameters of the *Bird-Carreau-Yasuda* model to the data for the complex viscosity, the empirical *Cox-Merz* relation (Cox & Merz, 1958) of the form $\eta(\dot{\gamma})|_{\dot{\gamma}=\omega} = |\eta^*(\omega)|$ has to be used.

$$\frac{\eta - \eta_\infty}{\eta_0 - \eta_\infty} = \left(1 + (B\dot{\gamma})^a\right)^{\frac{n-a}{a}} \tag{15}$$

$$\eta = \frac{A}{(1 + (B\dot{\gamma})^a)^{(n-1)/a}} \tag{16}$$
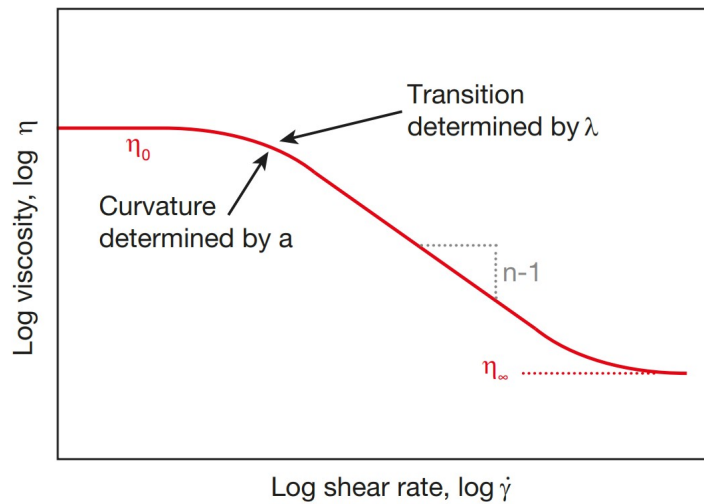
Figure 22: Schematic approximation of the Bird-Carreau-Yasuda *model on a viscosity curve (Osswald & Rudolph, 2015).*

In equation (17) the *Mark-Houwink* relation (Houwink, 1940; Mark, 1938) can be seen, in which α and k represent material constants, $[\eta]$ is the intrinsic viscosity, and $\bar{M}_V$ is the viscosity average molecular weight. This connection between the intrinsic viscosity and the viscosity average can be used for the zero shear viscosity of a polymer and its molecular mass, as in figure 23 illustrated. The linear relationship between viscosity and molecular mass is also known as *Staudinger's rule* (Staudinger & Heuer, 1930) and results of friction between chains. At higher molecular masses, a power law relationship is the result of entanglements between chains.

$$[\eta] = k\bar{M}_V^{\alpha} \tag{17}$$
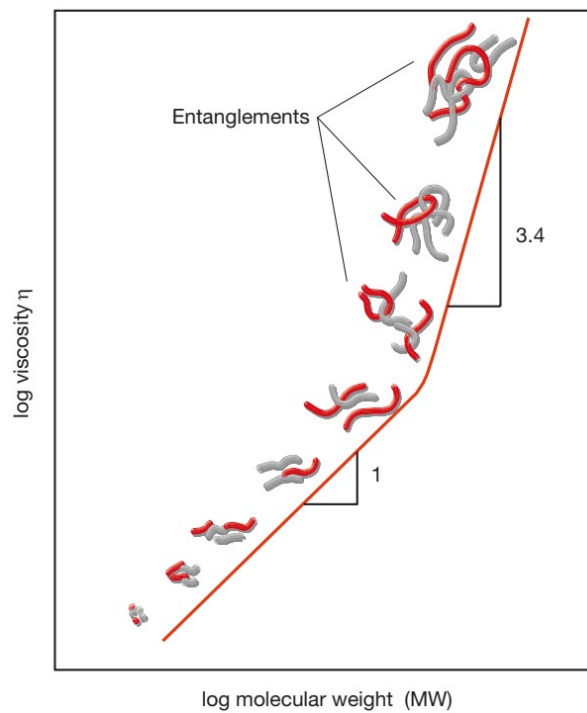
Figure 23: Schematic Mark-Houwink *relation (Osswald & Rudolph, 2015).*

3.4   Tensile Test

The tensile test is a quasi-static testing procedure used to evaluate the characteristic mechanical properties of the material. It involves unidirectional loading that increases over time (can be force or deformation controlled; in the case of polymers, deformation-controlled tensile tests are more common). The tensile test is especially an interesting testing procedure to gain information about the material's tangent modulus, the ultimate tensile strength (UTS), and the elongation at break. These values are especially of high importance for materials that undergo a multi-stage recycling process, because these values can alter during the recycling process.

In figure 24, the most important parameters for the tensile test are shown. This includes the initial measurement length L_0, the change in length during the measurement ΔL, the initial cross-section A_0, the engineering stress σ, and the speed of the traverse v_T.
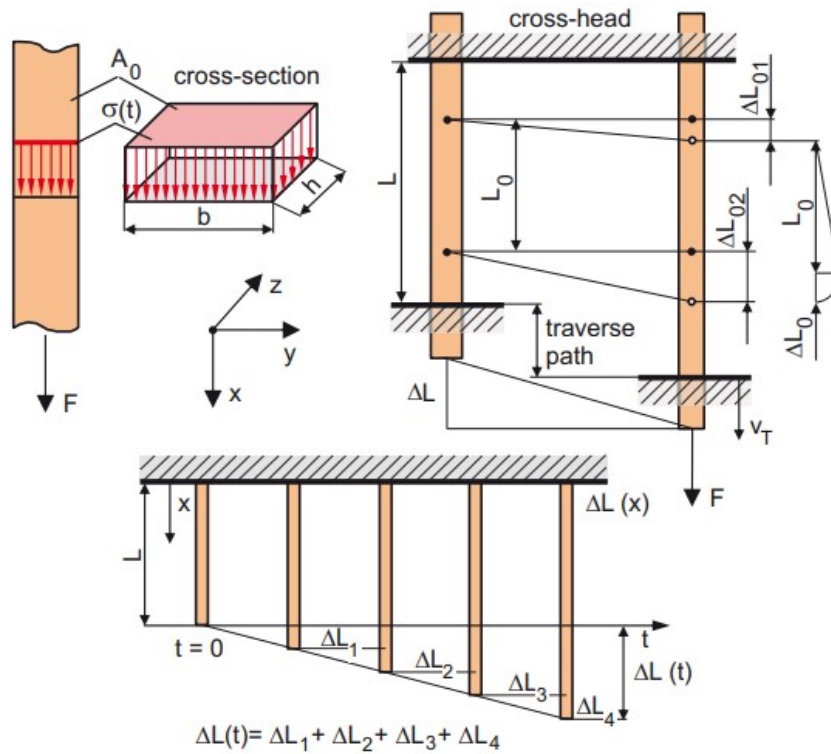
Figure 24: Tensile test (Grellmann & Seidler, 2022).

Generally, the tensile test is traverse speed controlled, this means that the nominal strain rate is controlled during the measurement with $\dot{\varepsilon}_T = \frac{v_T}{L_0}$. The response of the material to the strain is a stress, which is then measured by a measurement device (e.g. load cell). The nominal strain is calculated with the traverse speed as in equation (18) and the normative elongation is determined with a measurement device (e.g. strain gauge) on the tensile specimen and determined with equation (19).

$$\varepsilon_T = \frac{1}{L_0} \int_0^{\tilde{t}} v_T dt \tag{18}$$

$$\varepsilon = \frac{\Delta L}{L_0} \tag{19}$$

The difference of both strains can be seen in figure 25. Both strains are per se engineering strains, because every strain point in the stress-strain-curve is referenced on the initial length L_0. The engineering stress is evaluated with the equation (20) and as for the engineering strain every point in the stress-strain-curve is referenced on the initial cross-section of the specimen. With each elongation step ΔL_i the length of the specimen changes ($L_0 + \sum_i \Delta L_i$, compare with figure 24) and the cross-section decreases (if *Poisson's* ratio $\nu > 0$), this is not considered in the determination of the engineering stress and strain. Therefore, the true stress is higher compared to the engineering stress (if $\nu > 0 \Rightarrow$ necking) and the true strain is smaller compared to the engineering strain ($\varepsilon_{true} = \ln(1 + \varepsilon)$ with ε_{true} as the true strain).

$$\sigma = \frac{F}{A_0} \tag{20}$$
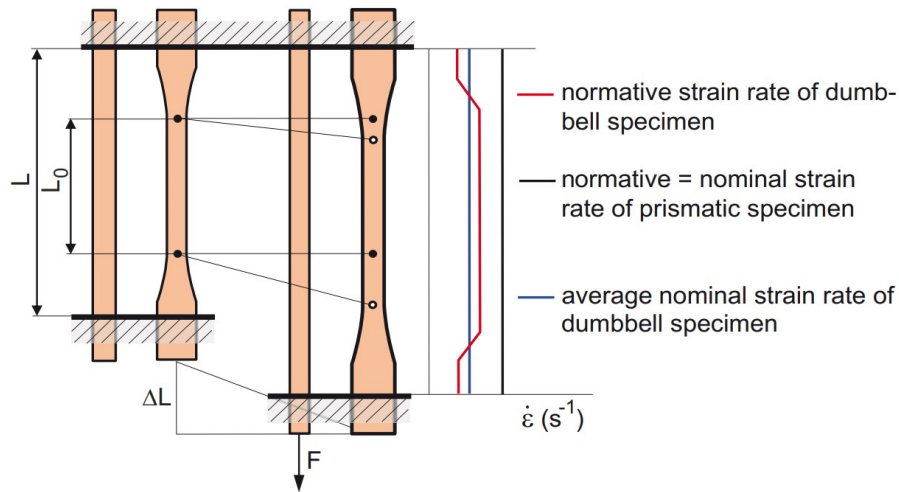
Figure 25: Difference between nominal and normative strain for dumbbell and prismatic specimen (Grellmann & Seidler, 2022).

In figure 26 stress-strain curves are shown for different polymers with ε_y as the strain at yield, σ_y stress at yield, ε_B strain at break, σ_b stress at break, ε_M ultimate strain, σ_M ultimate stress. The material a in figure 26 is a brittle polymer, b and c are tough polymers with a significant yield point, d is a tough polymer without a significant yield point, and e is a hyper-elastic polymer (Grellmann & Seidler, 2022).

The tangent modulus E_t can be evaluated with different methods; according to DIN EN ISO 527-1, the tangent modulus should be determined between an engineering strain of 0.05 % and 0.25 %. In equation (21) the calculation according to DIN EN ISO 527-1 is shown.

$$E_t = \frac{\sigma_2 - \sigma_1}{\varepsilon_2 - \varepsilon_1} = \frac{F_2 - F_1}{0.2 A_0} \tag{21}$$
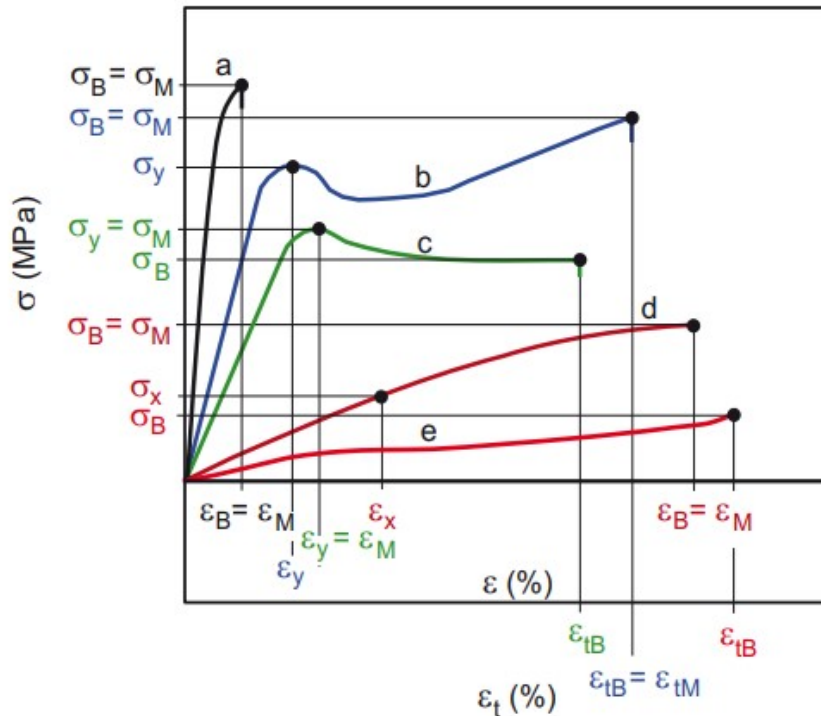
Figure 26: Stress-strain-curves for different polymers (Grellmann & Seidler, 2022).

The *Poisson's* ratio in width ν_b and thickness ν_h can be acquired with the addition of an extensometer or with a digital image correlation system. For the calculation, the following equations (22) and (23) are used, where ε_b is the elongation in width and ε_h the elongation in thickness (Grellmann & Seidler, 2022).

$$\nu_b = \left| \frac{\varepsilon_b}{\varepsilon} \right| = \left| \frac{\Delta b L_0}{\Delta L_0 b_0} \right| \tag{22}$$

$$\nu_h = \left| \frac{\varepsilon_h}{\varepsilon} \right| = \left| \frac{\Delta h L_0}{\Delta L_0 b_0} \right| \tag{23}$$

Figure 27 shows on the left the evaluation of the tangent modulus from the stress-strain or force-displacement curve. The tangent modulus can be determined with ΔF and the initial cross-section according to equation (21). On the right, the determination of the *Poisson's* ratio is shown, therefore, the equations (22) and (23) are used and the data of the geometry.
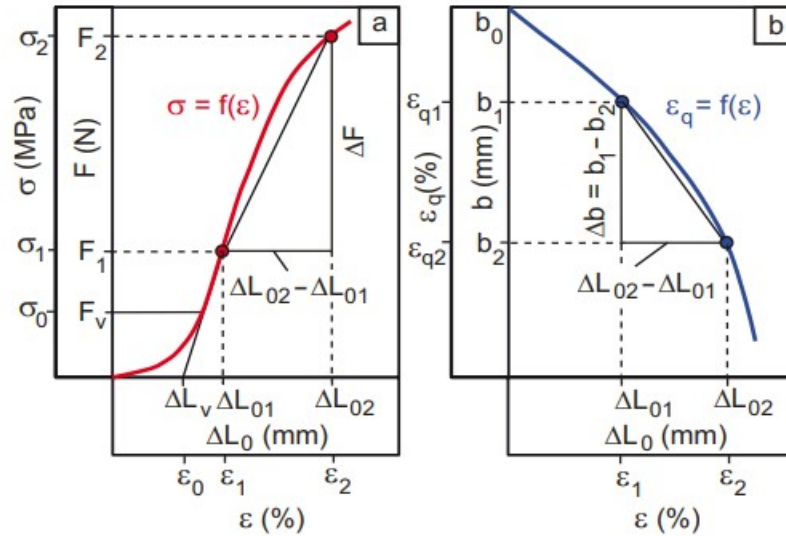
Figure 27: Evaluation of material parameters from tensile test (Grellmann & Seidler, 2022). (a) Stress-Strain and force-displacement diagram, (b) transverse strain-strain and displacement-displacement diagram.

3.5   Notched Charpy Impact Test

The notched Charpy impact test is a widely employed testing procedure to assess the toughness of polymers at high strain rate. The notch introduces a multiaxial stress state at the notch's bottom, this results in a more brittle material response additionally to the high strain rates. The evolution of the notched Charpy impact strength parallel to a multi-stage recycling process is of high interest, because it provides information about the changes in the absorbed energy during an impact loading case.

In figure 28, a schematic drawing of an impact device is visible. It consists of a pendulum, a scale for the energy, and anvils for the specimen. The height difference $(h_a - h_b)$, seen in the figure 28, represents the loss of potential energy, which is consumed to deform or destroy the specimen. In figure 29, two different testing arrangements are shown. For the Charpy arrangement the specimen is notched. Generally, the Charpy arrangement is more commonly used compared to the IZOD arrangement. The notched impact strength a_{cN} is measured with a notched specimen and calculated according to the equation (24), in which W_c represents the necessary potential energy to break or deform the specimen $(W_c = mg(h_a - h_b)$ with m as the pendulum weight and g the gravitational acceleration), b_N the remaining notched specimen width, h the specimen height (Grellmann & Seidler, 2022).

$$a_{cN} = \frac{W_c}{b_N h} \tag{24}$$
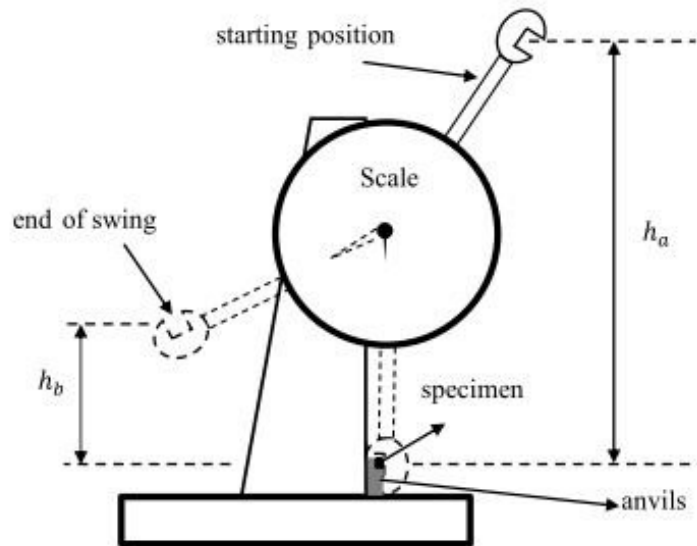
Figure 28: Schematic impact testing device (Bozkurt et al., 2017).
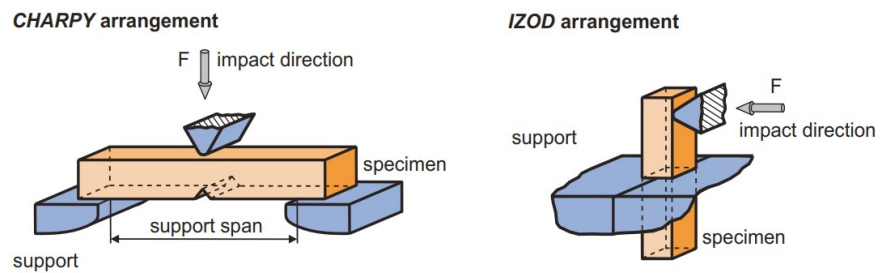
*Figure 29: Charpy and IZOD arrangements for impact load testing (Grellmann &
Seidler, 2022).*

It is crucial to bear in mind, if notched impact strength values are compared, that the notched impact strength is an integrated value, which concentrates a functional relationship of force and displacement into a scalar value. This can be seen in figure 30, which shows force-displacement curves for two different materials from instrumented notched Charpy measurements. Both curves result in roughly the same notched impact strength, but it is easy to detect that the material behavior varies significantly from each other. The first material is considerably stiffer and also more brittle compared to the second material.
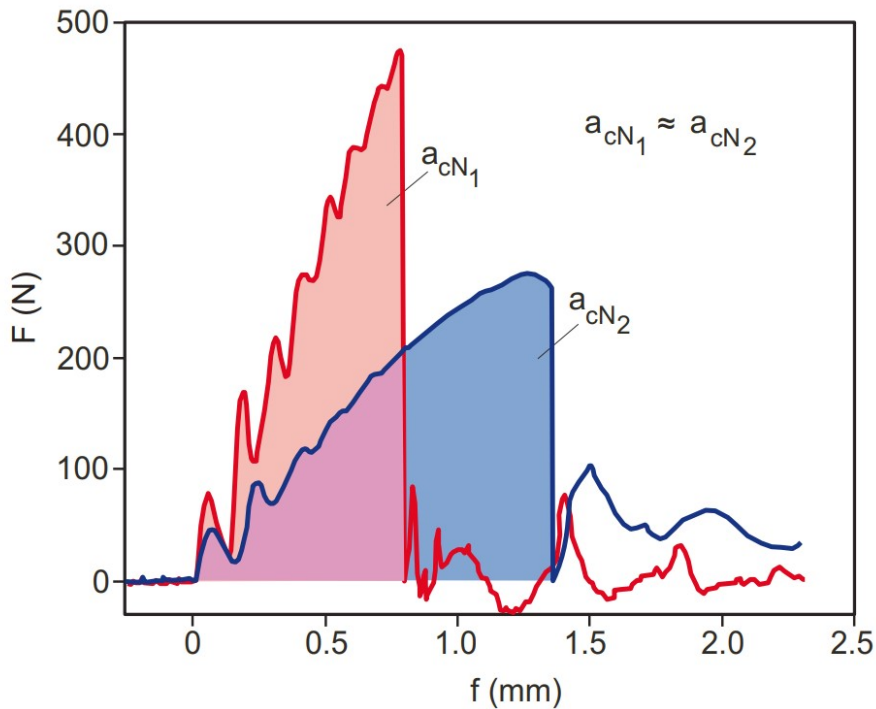
Figure 30: Difficulty in the comparison of notched Charpy impact strength a_{cN} (Grellmann & Seidler, 2022).

4   Experimental

In the following section, the sample nomenclature, the used materials including all additives, the processes which were used to induce thermo-mechanical loading into the material, and the used testing methods with the settings for characterizing the samples are described.

First, in section 4.1 the used polymer PHB will be introduced in detail, then the additives and the producers of the materials are mentioned. Then all the Python libraries and their version numbers are shown. Following, the sample nomenclature will be explained. Afterward, in section 4.4 all relevant processing steps and the settings will be discussed to make the processing steps and the thermo-mechanical loading of the material as reproducible as possible. In section 4.5 the procedure for the plate-plate rheological testing is shown and the measurement settings are presented. In section 4.6, the testing procedures for the DSC and TGA testing and the used settings for each are shown. In the last section of the experimental part (section 4.7), all necessary settings and standards for the tensile test and the notched Charpy impact test are defined.

4.1   Material and Additives

The used PHB P263 injection molding grade was manufactured by Biomer (Schwalbach, Germany) and provided in pellet form. Biomer provides a blend with 89.8 wt% PHB (Biomer GmbH, 2023) and the heat fusion of PHB is 146.6 J/g according to Barham et al. (1984). The chain extenders were obtained from BASF in flake form and are marketed under the name Joncryl®. In this thesis, two types of Joncryl® were used, the Joncryl® 4400 and 4468. These two types differ in weight-average molecular weight and epoxy equivalent weight, both are measured in units of g/mol. The Joncryl® 4400 has a weight-average molecular weight of 7100 g/mol and the Joncryl® 4468 of 7250 g/mol. The epoxy equivalent weight is 485 g/mol for the Joncryl® 4400 and 310 g/mol for the Joncryl® 4468. The addition of Joncryl® to the processed PHB is expected to increase the mechanical and rheological properties, which decline during the processing. For further information see Appendix A starting at page 71 for the data sheets of PHB and Appendix B starting at page 75 for the data sheets of the two Joncryl® grades.

4.2   Software Used in this Thesis

For data analysis and visualization Python 3.9 (Van Rossum & Drake Jr, 1995), Numpy 1.21.2 (Harris et al., 2020), Pandas 1.5.3 (pandas development team, 2020), Matplotlib 3.7.1 (Hunter, 2007), and SciPy 1.10.1 (Virtanen et al., 2020) were used.

4.3   Nomenclature of Samples

In this section, the nomenclature of the different samples will be explained. Generally, there are two different kinds of naming conventions for the samples; first the nomenclature for change in Joncryl® concentration at the stage of E2, and second the nomenclature of multiple addition of Joncryl® for E3 to E4.

Common ground for both naming convention is the "E" with a corresponding number, the corresponding number represent the compounding (extrusion) processing cycles the sample has undergone (e.g. E2 was extruded two times). Then for both naming conventions after the count of processing cycles (e.g. E2), the part how often a concentration was added follows (e.g. 1x0.2% means that to the sample E1 0.2 wt% of Joncryl® was added). For the nomenclature of change in Joncryl® concentration and type of Joncryl®, there is only Joncryl® added at the stage of E1, therefore it is always 1x the concentration (see figures 31 and 32). The last number of the nomenclature for both naming conventions represents the used type of Joncryl® mentioned in section 4.1.
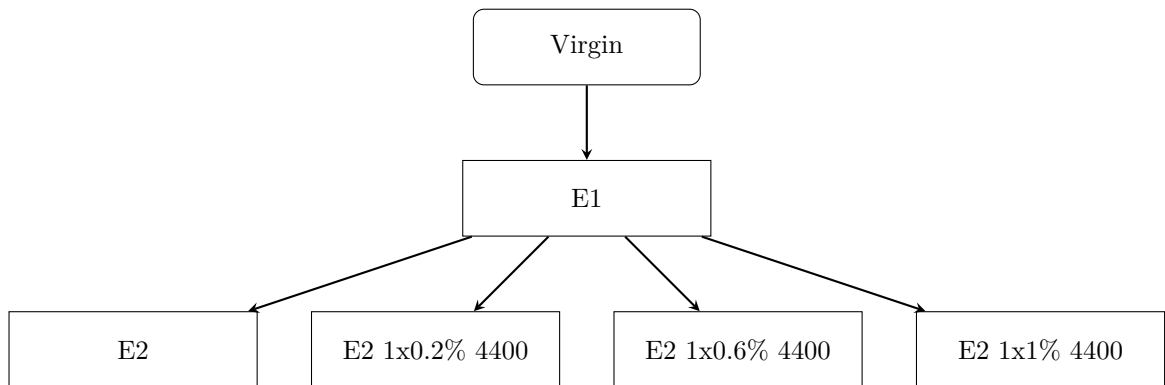
Figure 31: Nomenclature of samples with different Joncryl® 4400 concentration.
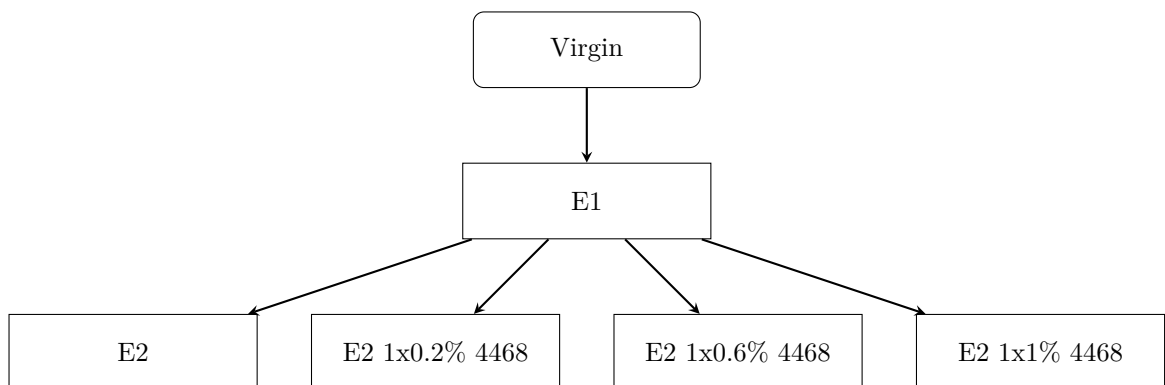
Figure 32: Nomenclature of samples with different Joncryl® 4468 concentration.

For the naming convention of the multiple addition of Joncryl® 4468, the 1 wt% was added at different stages and this is represented by the number before the x, which means times in this case (times added concentration). Starting point for the naming convention is the sample E2 1x1% 4468, as we can see in figure 33, it is possible to create the samples E3 1x1% and E3 2x1% out of the sample E2 1x1%. To produce the sample E3 1x1% the sample E2 1x1% gets processed, and to generate the sample E3 2x1% out of E2 1x1%, we first have to add 1 wt of Joncryl® 4468 to the sample E2 1x1% and then process it. For the sample E3 1x1%, there is Joncryl® added once at the stage of E1, and for the sample E3 2x1%, there is added Joncryl® twice at the stage of E1 and E2 (sample E2 1x1%). The naming convention for stage E4 is analogous to the E3 stage.

For clarity, a summary of the naming convention of multiple addition of Joncryl® is provided. If the sample at multiple addition is called 1x1%, Joncryl® was added to E1 and processed as many times as the number after E expresses. For 2x1% Joncryl® was added to the samples E1 and E2 1x1%, and for 3x1% Joncryl® was added to the samples E1, E2 1x1%, and E3 2x1%. To prevent confusion, the %-symbol in the nomenclature stands for wt% and concentration of Joncryl® always means weight percent in this thesis.

The E2 samples were processed only once and this was done in the set of the samples of the Joncryl® 4468.
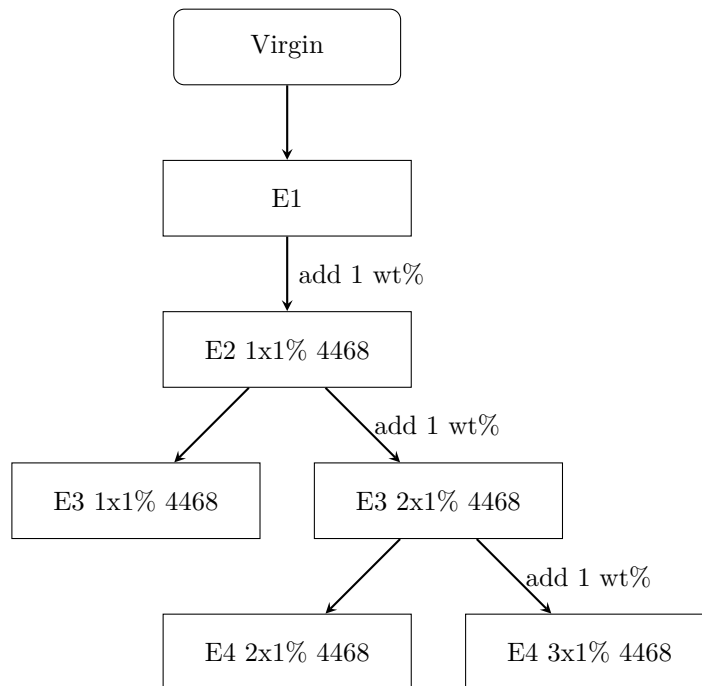
Figure 33: Nomenclature of multiple addition of Joncryl® 4468 at different processing stages.

4.4   Processing and Testing Procedure

In figure 34 the processing and testing procedure is shown. First, the steps from figure 34 will be explained. The processing and testing steps are as follows (the steps below are highlighted in figure 34 with (x), where x is the step number from below):

1. Prepare the E1 sample by processing the virgin material according to the settings for E1 in table 2 (second column).

2. Decide if Joncryl® has to be added to the sample. Yes → Step 3, No → Step 5.

3. If Joncryl® has to be added, supplement the specified amount to the sample and premix it before processing it again.

4. Process the material and use the processing settings from table 2 for E2, E3, and E4 (third column), then continue with step 2.

5. If it is decided in step 2, that no Joncryl® has to be added, decide if further processing is required. Yes → Step 4, No → Step 6.

6. If no further processing is necessary, continue with essential material tests.

7. After the testing of the sample is finished, the processing and testing cycle for the sample is finished.
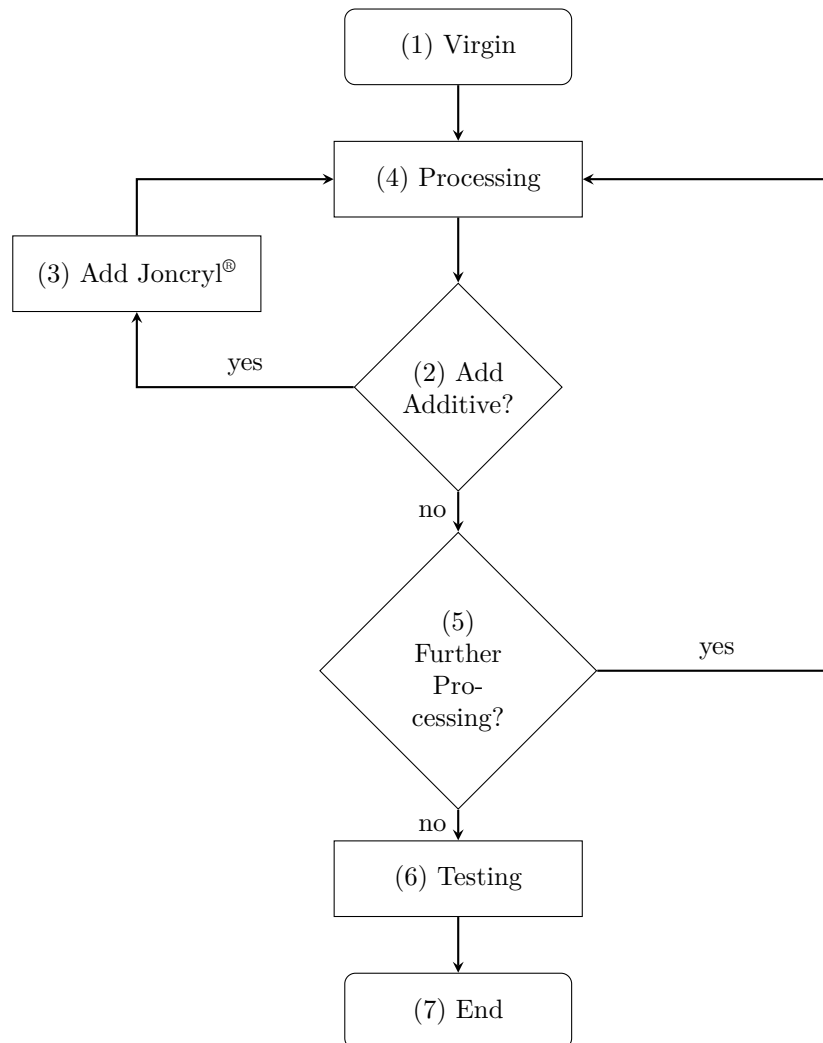
Figure 34: Flow-diagram of processing and testing cycle for one sample.

4.4.1 Compounding

For the compounding process of the samples, a Compounder ZSE 18HP-48D (Leistritz Extrusionstechnik GmbH, Germany) was used as a co-rotating twin screw extruder. The compounding process was used to simulate the recycling process and introduce thermo-mechanical loading into the material, generate a homogenous mixture of PHB and Joncryl®, and initiate the Joncryl® reaction with PHB. In table 2 the relevant processing parameters for the compounding parameters are illustrated. For the preparation of the E1 sample, the virgin material was processed with the settings of the second column with the column label "E1". For the samples after E1, the settings in the third column with the column label "E2, E3, and E4" were used. The change in settings was caused by the need for a longer residence time of the PHB and Joncryl® mixture, to ensure sufficient time for the Joncryl® to react with PHB.

Table 2: Relevant process parameters of the compounding process.

Parameter	E1	E2, E3, and E4
Screw speed in rpm	500	100
Feed rate in kg/h	5	1
T1 in °C	50	50
T2 in °C	100	100
T3 in °C	160	160
T4 in °C	180	180
T7 in °C	170	170
T9 in °C	160	160

4.4.2 Injection Molding

The samples for the mechanical tensile test and notched Charpy impact test (see section 5.3) were produced on an injection molding machine 320 C 500 -100 (ARBURG GmbH + Co KG, Germany) with the processing parameters of table 3. The samples virgin, E1, E2 1x0.6% 4468 were produced with different settings due to filling problems of the specimens during the injection molding process.

Table 3: Relevant process parameters of the injection molding process.

Parameter		Virgin	E1	E2	Concentration 4400			Concentration 4468			E3 4468		E4 4468	
					0.2 %	0.6 %	1%	0.2 %	0.6 %	1 %	1x1%	2x1%	2x1%	3x1%
	Hopper	35	35	35	35	35	35	35	35	35	35	35	35	35
Cylinder temperature in °C	C1	185	185	185	185	185	185	185	185	185	185	185	185	185
	C2	180	180	180	180	180	180	180	180	180	180	180	180	180
	C3	175	175	175	175	175	175	175	175	175	175	175	175	175
	C4	170	170	170	170	170	170	170	170	170	170	170	170	170
	Nozzle	165	165	165	165	165	165	165	165	165	165	165	165	165
Mold temperature in °C		38	38	38	38	38	38	38	38	38	38	38	38	38
Injection speed in cm^3/s		15	15	15	15	15	15	15	15	15	15	15	15	15
Back pressure in bar		30	30	30	30	30	30	30	30	30	30	30	30	30
Holding pressure in bar		900	900	900	900	900	900	900	900	900	900	900	900	900
Holding pressure time in s		11	13	9	9	9	9	9	11	9	9	9	9	9
Holding pressure switchover point in cm^3		11	11	11.5	11.5	11.5	11.5	11.5	11	11.5	11.5	11.5	11.5	11.5
Cooling time in s		30	30	30	30	30	30	30	30	30	30	30	30	30
Cycle time in s		48.13	50.15	46.13	46.13	46.13	46.13	46.13	48.13	46.13	46.13	46.13	46.13	46.13

4.5   Rheological Testing

To measure the complex viscosity as a function of the angular frequency, a Modular Compact Rheometer MCR702 TD (Anton Paar GmbH, Austria) was used. The relevant measurement data is provided in table 4 (for the settings of the amplitude sweep see Appendix D).

Two different types of settings were used. The reason for the change in settings was the significant thermal and thermo-mechanical degradation before and during the measurement. The changes between the two settings are the reversed measurement of the angular frequency for the new settings and the omission of values below 1 rad/s angular frequency. The reversed measurement made sure, that the least time-consuming measurements are performed first and the exclusion of angular frequencies below 1 rad/s removed the most time-consuming measurements. The exclusion of angular frequencies below 1 rad/s resulted in a decrease in measurement time of around 12 min. The second major change was the reduction of the preparation time, which led to a higher temperature variation during the measurement because the rheometer had not had enough time to stabilize the temperature. The preparation time represents the time amount from inserting the sample into the rheometer to the start of the measurement.

The strain was changed from the old settings to the new settings from 10 % to 3 %, because some samples of the multiple addition with a deformation of 10 % were close to the linear viscoelastic range determined with amplitude sweeps (see Appendix D).

The old settings were used for the change in concentration for both Joncryls®, and both settings were used in the multiple addition of Joncryl®. For the frequency sweeps in the figures 43, 45 and 47, the old settings were used and for figures 49 and 51 the new settings were used. The value after the + symbol at the temperature row shows the maximal appeared temperature during the measurement, caused by the decrease in preparation time.

The samples for the rheology measurements were produced with a vacuum press P200PV (Dr. Collin GmbH) with the settings of table 5. The temperature profile of the vacuum press was set according to the measurement temperature in the rheological tests. For each sample, three repeats were measured.

Table 4: Relevant testing parameters of the frequency sweep in dynamic oscillatory rheology measurement.

Parameter	Old settings	New settings
Preparation time in min	~10	~2
Plate diameter in mm	25	25
Gap in mm	1	1
Temperature in °C + max. value	190+0.5	190+3
Angular frequency in rad/s	0.1 to 500	500 to 1
Measurement time in min	~16	~3.7
Strain in %	10	3

Table 5: Settings vacuum press for rheology sample production.

	Phase 1	Phase 2	Phase 3	Phase 4	Phase 5
Time in min	10	2	2	2	15
Pressure in bar	1	50	75	100	100
Temperature in °C	190	190	190	190	30

4.6   Thermal Testing

In the following section, the testing parameters for the TGA and DSC measurements will be explained.

4.6.1   TGA

For the evaluation of the thermal stability and main degradation temperature of PHB, a thermogravimetric analysis (TGA) on a TGA/DSC 3+ STARe System (Mettler-Toledo LLC, United States of America) was carried out. The samples were heated from room temperature to 600 °C with a heating rate of 10 K/min under a nitrogen atmosphere. The weight loss of the samples was recorded as a function of the sample temperature. A ceramic crucible was used and the nitrogen flow rate was set to 50 ml/min. For each sample, three repeats were measured to ensure the reproducibility of the results.

4.6.2   DSC

The evaluation of a change in melting and crystallization behavior for the different samples was done with Differential Scanning Calorimeter (DSC 1, Mettler-Toledo LLC, United States of America). The range of temperature was chosen from 20 °C to 220 °C. The first and second heating processes were performed with a heating rate of 10 K/min and the cooling process at a cooling rate of 20 K/min. The samples were annealed for 10 min in between the first heating process and the cooling phase at 220 °C, and between the cooling phase and the second heating process at 20 °C. The DSC measurements were carried out under a nitrogen atmosphere with a volume flow rate of 50 mL/min and a sample size of approximately 8 ±1 mg. To ensure an accurate testing procedure, the heating rate and sample weight was chosen as suggested by Ehrenstein et al. (2004), only the cooling rate was chosen differently. Three repeats were recorded for each sample.

4.7   Mechanical Testing

The mechanical properties of the various samples were analyzed with a notched Charpy impact testing and tensile testing. For the notched Charpy impact test, a non-instrumented test was used, the pendulum energy was 0.5 J, and the support length was 64 mm. The notched Charpy impact tests were carried out on an impact testing pendulum CEAST Resil 25 (Instron GmbH, United States of America) according to DIN EN ISO 179. The tensile tests were executed according to DIN EN ISO 527-1 on a Tensile/Compression universal testing machine type Z010 (ZWICK/ROELL GmbH & Co. KG, Germany). For both tests, multipurpose test specimens type 1A, as defined by DIN EN ISO 3167, were produced by injection molding (see section 4.4.2). The multipurpose test specimens type

1A were mechanically processed and notched to create the notched impact specimens, as required by DIN EN ISO 179. For each sample, five repeats were recorded to estimate the most significant mechanical properties. The tests were performed three to four weeks after the production, to increase the reproducibility.

5   Results

In this section, the experimental data are presented in the form of diagrams and tables and the respective results are analyzed. The results section is substructured into thermal testing (TGA and DSC), rheological testing, and mechanical testing in the same order as mentioned. This sequence was chosen, because the thermal and rheological results are necessary for the interpretation of the results of the mechanical tests.

In each subsection, first the results of the change in concentration and then the results of the multiple addition of Joncryl® 4468 at multiple processing steps are shown. At the end of each testing group (e.g. thermal testing), a summary and conclusion of the obtained results will be presented.

First, the results of the TGA testing are shown and afterward, the measurement results for the DSC are presented. In the section 5.1.1, the TGA results are presented in two figures; these diagrams show the effect of the added Joncryl® on the degradation temperature of PHB. For the DSC measurements in section 5.1.2 the most important characteristic values like the crystallinity of the second heating scan and the peak temperatures are compared in box-plot-diagrams.

In the section 5.2, the frequency sweeps for the Joncryl® 4400 and 4468 and the multiple addition of 4468 are shown. In this section also the complex viscosity is plotted over the measurement time to show the time-dependency of the measurement. The amplitude sweeps can be seen in the Appendix D.

The results of the DSC and rheology measurements are important for the interpretation of the results of mechanical testing in section 5.3. Therefore, these results are discussed last. The change in crystallinity and a change in the complex viscosity are indications of a change in the morphology of the polymer and have a direct effect on the mechanical properties of tangent modulus, ultimate tensile strength, elongation at break, and notched impact strength, which are the analyzed mechanical values.

For the DSC results and for the mechanical properties a linear regression model was built for the different Joncryl® concentration, to show the significance of the change in properties with the change in concentration and to get a rough estimation of the magnitude of the effect. The E2 samples were not included in the regression model and are only used as reference and compared to the intercept of the model (for the ANOVA with the E2 for both Joncryl® see Appendix C).

For the multiple addition of Joncryl® the 4468 was chosen, because of the greater effect on the complex viscosity with change in concentration.

5.1   Thermal Testing

In the following section, the effect of Joncryl® on the degradation process will be investigated with TGA measurements. Therefore, the maximum decomposition rate temperature, onset temperature, and total weight loss will be considered. To investigate changes in morphology and especially in the crystalline structure, DSC measurements were performed. From the DSC measurements, the peak melting temperature and crystallinity of the second heating scan, and the peak crystallization temperature will be discussed. At the end of this section, a summary of the main findings will be provided.

5.1.1   TGA

The figure 35 shows the TGA-curves (average curves of three repeats and standard deviations as error bars) for the Joncryl® 4400 in the left column and the 4468 in the right column. The first row shows the residual weight over the sample temperature and the second row shows the time deviation of the residual weight over the sample temperature.

For both Joncryl there is not a significant change with Joncryl® concentration on the onset temperature, maximum decomposition rate temperature, and the total weight loss detectable. The error bars for all samples except of the sample E2 1x1% 4468 overlap, therefore no significant effect can be detected for most of the samples. The trend for the sample E2 1x1% 4468 was not detected for the multiple addition, see next paragraph and figure 36.
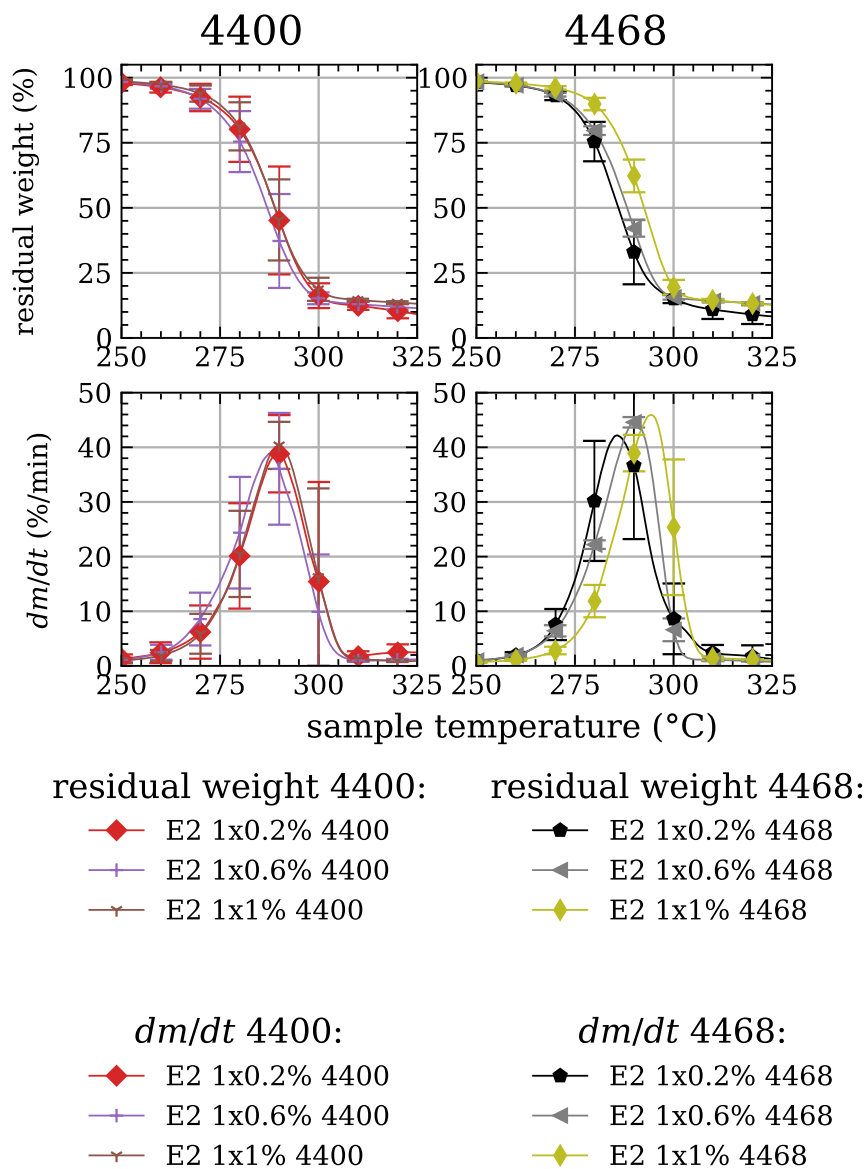
Figure 35: TGA-Curves for different Joncryl® and Joncryl® concentration.

In figure 36 the TGA-curves (average curves of three repeats and standard deviations as error bars) for the multiple addition of Joncryl at different process steps are shown. In the first row the residual weight is plotted over the sample temperature and in the second row the time derivate of the residual weight is plotted over the sample temperature. There is not an effect of the addition of Joncryl or degradation due to processing on the onset temperature, maximum decomposition rate temperature, and the total weight loss detectable.
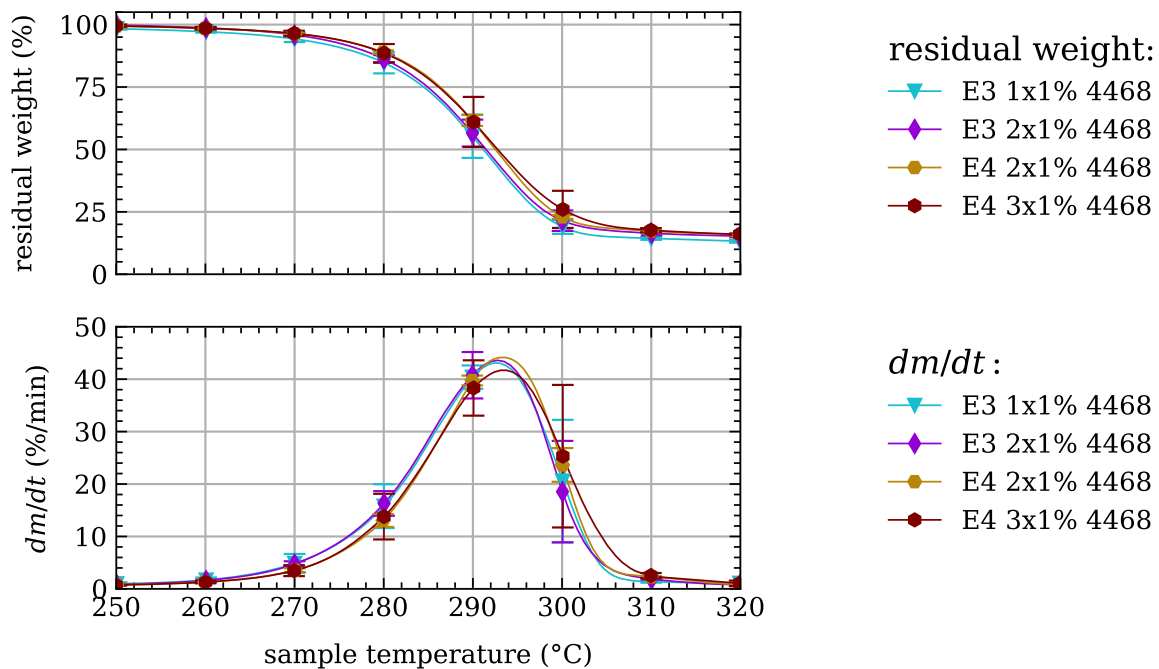
Figure 36: TGA-Curves for multiple addition of Joncryl® 4468 at different processing steps.

5.1.2 DSC

The DSC measurements are used to investigate the effect of Joncryl® on the crystallization and melting behavior. Therefore, the peak crystallization temperature, the crystallinity, and the peak melting temperatures of the second heating scan are considered. For the crystallinity, the added Joncryl® concentration is considered in the calculation and the added additives from Biomer are not considered in the calculation.

First, multiple box-plot diagrams for the characteristic values crystallinity of second heating scan, peak melting temperature of the second heating scan, and peak crystallization temperature are presented and these characteristic values are interpreted. Then, linear regression models with the most important statistical values are provided in table form. The linear regression models are used to demonstrate the statistical significance of the effects with a change of the independent variable. The virgin and E2 results are used as a reference in the diagrams for the change of type of Joncryl® and concentration and for the addition of Joncryl® at multiple processing steps. The DSC measurements are the same and were recorded alongside the multiple addition of Joncryl® at multiple processing

steps. They are used as a reference in all of the diagrams. The E2 was processed alongside the samples with a change in concentration of Joncryl® 4468, and therefore, fits better in the trend of the Joncryl® 4468.

5.1.2.1   Effect of Different Types of Joncryl® and Change in Concentration

In figure 37, the peak melting temperature T_{pm} over the different samples is shown. The samples show a variation in processing steps, kind of Joncryl®, and Joncryl® concentration. The measurement results for the peak melting temperature stretch from around 161.7 °C to 164.3 °C, this results in a difference of around 2.5 K. The Joncryl® 4468 shows an increase in melting temperature with higher concentration of Joncryl®, which is against the trend for the peak crystallization temperature and the expected trend of a decrease in peak melting temperature with the degree of branching and cross-linking (Duangphet et al., 2014; Ehrenstein et al., 2004; Ehrenstein, 2012). For the Joncryl® 4400, this trend is not as clear.
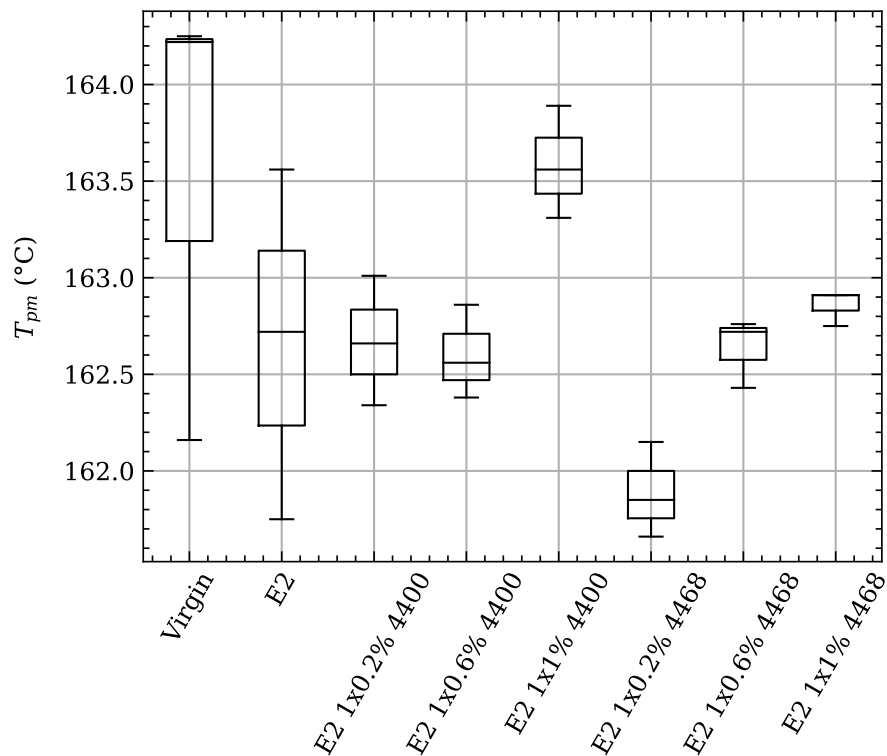
Figure 37: Peak melting temperature of second heating scan for different Joncryl® types and concentrations.

The figure 38 shows the peak crystallization temperature T_{pc} over the different samples. The measurement stretches from around 96.8 °C to 101.8 °C, which results in a range of 5 K. The range of the peak crystallization temperature is around 2 K higher than the peak melting temperature. Additionally, the peak crystallization temperature shows a decline for both types of Joncryl® with an increase in concentration in wt% and declines with processing from virgin to E2.
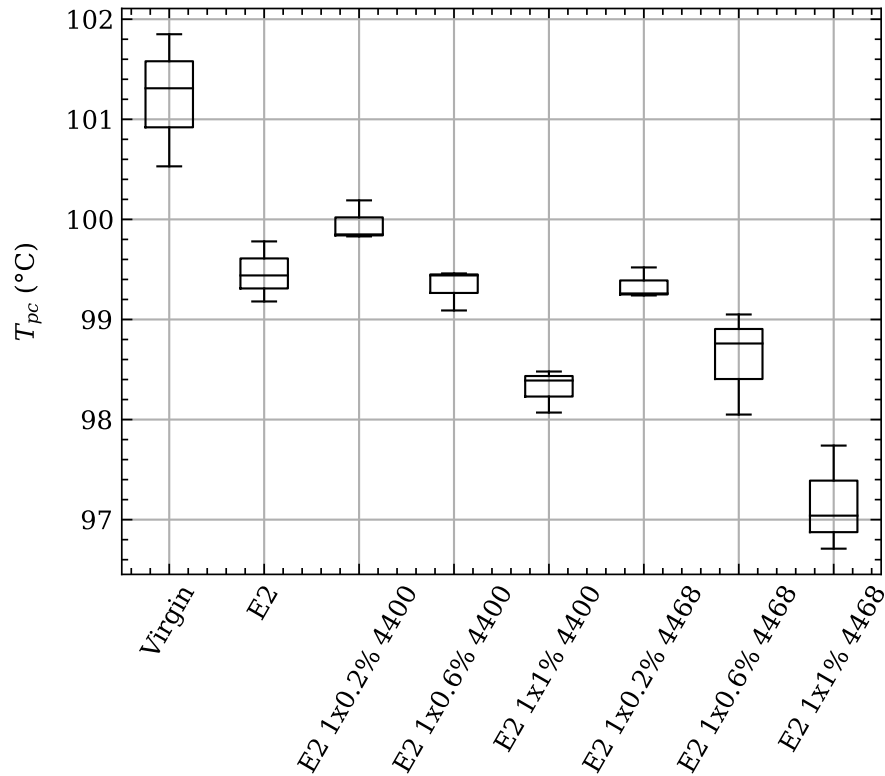
Figure 38: Peak crystallization temperature for different Joncryl® types and concentrations.

For the crystallinity of the second heating scan over the different samples in figure 39 a range of around 49 % to 53.8 % can be detected. As for the peak crystallization temperature, the crystallinity of the second heating scan decreases with an increase in Joncryl® concentration. This trend is better visible for the Joncryl® 4400 than for the 4468. For the Joncryl® 4468, the measurements of the sample with 0.6 wt% do not show a decline of the crystallinity of the second heating scan compared to the measurements with 0.2 wt%. The decline of around 3 % in the median of the crystallinity of the second heating scan of the virgin material compared to the sample E2 1x1% 4468 is the first indication of cross-linking and side-branching reactions of the Joncryl® with PHB. Cross-linking and side-branching result in an increase of the amorphous fraction in a semi-crystalline polymer, and therefore, the crystallinity declines.
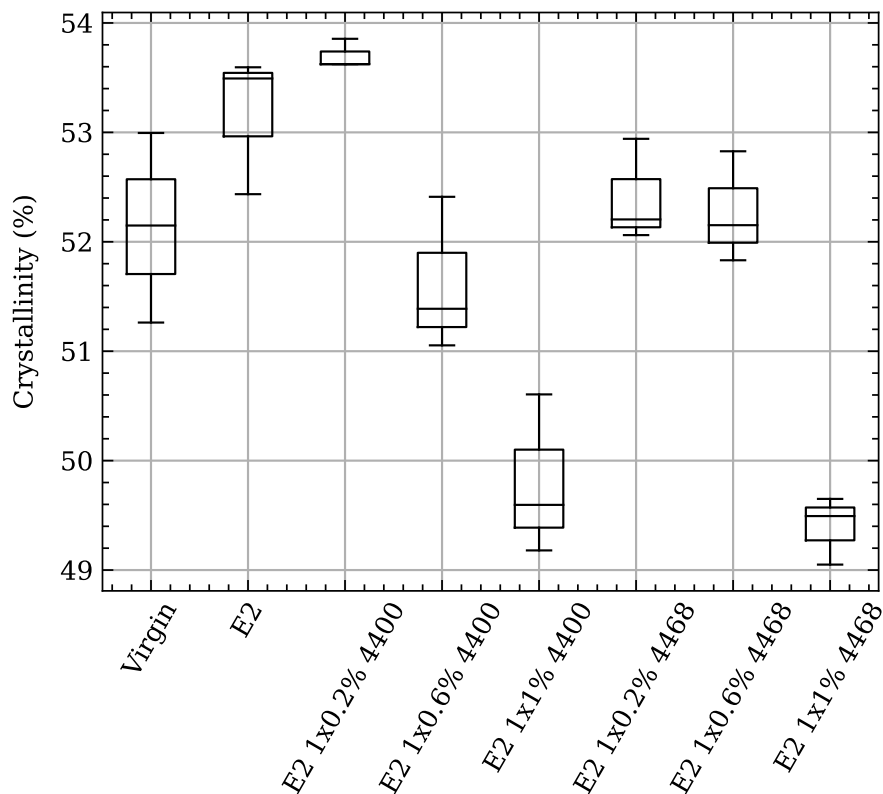
Figure 39: Crystallinity of the second heating scan for different Joncryl® types and concentrations.

In the tables 6 and 7 the statistical analyses of the figures 38 and 39 for both Joncryl® 4400 and Joncryl® 4468 are shown. For the analysis, the samples for the weight percentage of 0.2, 0.6, and 1 wt% for both Joncryls® were used. In the regression model, the weight percentage is considered as the independent variable and T_{pc} or w_c is considered as the dependent variable. This analysis includes the normality test after *Shapiro-Wilk*, the slope and the intercept with the 95 % confidence interval (CI), the r-value of the linear regression model, and the p-value of the *Wald* test with a null hypothesis of a slope of zero.

According to the *Shapiro-Wilk* test, the residuals of the regression model are normally distributed, and therefore, methods that assume a dataset with normally distributed measurements can be used. The confidence intervals for the intercepts of the 4468 Joncryl® for the peak crystallization temperature and the crystallinity of the Joncryl® 4400 include the median of the sample E2; the confidence interval of the intercepts for the peak crystallization temperature for the regression model of the Joncryl® 4400 do not. All of the confidence intervals of the linear regression parameters overlap, therefore it cannot be assumed, that the regression parameters are different. The largest discrepancy between the measured data and the linear regression model is observed for the crystallinity of Joncryl® 4468, as indicated by the r-value in table 7. The p-values of the *Wald* tests lead to the conclusion that the Joncryl® concentration affects w_c and T_{pc} of PHB. Comparing both types of Joncryl® it is possible to detect an effect on the slope of the linear regression model of the peak crystallization temperature. The steeper slope for the Joncryl® 4468

means that the peak crystallization temperature declines more rapidly with an increase in the weight percentage of Joncryl® 4468 compared to the Joncryl® 4400. The regression model for the crystallinity would predict a decrease of 4.9 % with 1 wt% Joncryl 4400, this is a change of 8.97 % considering the intercept of the model.

Table 6: Linear regression coefficients and r-value for peak crystallization temperature for both Joncryl® types at different concentrations with Shapiro-Wilk *test and* Wald *test.*

	Unit	T_{pc} for 4400	T_{pc} for 4468
p-value *Shapiro-Wilk* test	-	0.544	0.636
slope	K/wt%	-2.1	-2.8
lower bound 95 % CI of the slope	K/wt%	-2.6	-3.9
upper bound 95 % CI of the slope	K/wt%	-1.5	-1.8
intercept	°C	100.4	100.1
lower bound 95 % CI of the intercept	°C	100.1	99.4
upper bound 95 % CI of the intercept	°C	100.8	100.8
r-value	-	-0.961	-0.923
p-value *Wald* test	-	0.000	0.000

Table 7: Linear regression coefficients and r-value for the crystallinity for second heating scan for both Joncryl® types at different concentrations with Shapiro-Wilk *test and* Wald *test.*

	Unit	w_c for 4400	w_c for 4468
p-value Shapiro-Wilk test	-	0.499	0.365
slope	%/(gwt%)	-4.9	-3.8
lower bound 95 % CI of the slope	%/(gwt%)	-6.2	-5.8
upper bound 95 % CI of the slope	%/(gwt%)	-3.5	-1.7
intercept	%/g	54.6	53.6
lower bound 95 % CI of the intercept	%/g	53.7	52.2
upper bound 95 % CI of the intercept	%/g	55.5	55.0
r-value	-	-0.956	-0.857
p-value Wald test	-	0.000	0.003

5.1.2.2   Effect of Multiple Addition of Joncryl® 4468 at Different Processing Steps

In figure 40 the peak melting temperature is plotted over the different samples with change of processing steps and addition of 1 wt% Joncryl® 4468 at multiple processing steps. As for the addition of different Joncryl® concentration and different kinds of Joncryl® in figure 37, there is not a clear trend for the addition of Joncryl® at multiple processing steps in peak melting temperature detectable.
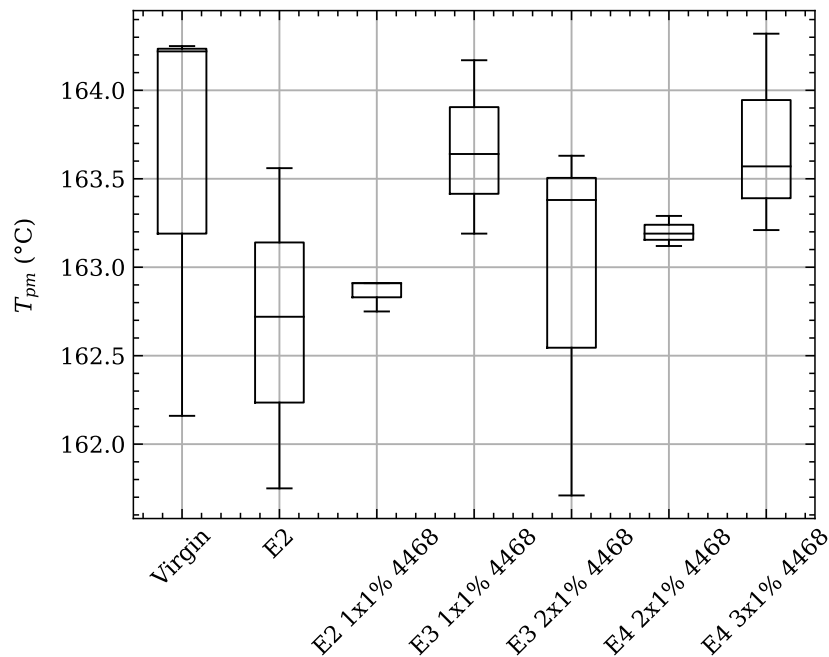
Figure 40: Peak melting temperature of second heating scan for multiple addition of Joncryl® 4468 at different processing steps.

The peak crystallization temperature in figure 41 is again plotted over the different samples for the multiple addition of Joncryl® 4468 at multiple processing steps. The peak crystallization temperature changes from around 101 °C for the virgin material to approximately 90 °C to 91 °C for the sample E4 3x1% 4468.

The peak crystallization temperature declines from virgin to E2 by around 2 K. If the samples E2 1x1% 4468 and E3 1x1% 4468, E3 2x1% 4468 and E4 2x1% 4468 are compared there is not an effect due to processing noticeable. Generally, processing leads to degradation of the polymer, this results in a decrease of molecular mass and change of the distribution (Dos Santos et al., 2018; Melik & Schechtman, 1995; Pachekoski et al., 2013). There is a negative effect distinguishable for the addition of Joncryl® 4468, if the samples E2 and E2 1x1%, E3 1x1% and E3 2x1%, and E4 2x1% and E4 3x1% are set against each other. The reduction of the peak crystallization temperature and crystallinity is an indication for cross-linking reaction and side chain creation of the reaction of Joncryl® 4468 with PHB (Duangphet et al., 2014; Ehrenstein et al., 2004; Ehrenstein, 2012). The decline of peak crystallization temperature with the increase of Joncryl concentration fits the trend of figure 38 and the regression model in table 6.

In figure 42 the crystallinity of the second heating scan is plotted over the different samples as in the two figures before. The change from virgin to E4 3x1% 4468 in median of the crystallinity of the second heating scan is around 11 %, which is a significant physical decline of the crystallinity.

The trend considering processing steps and addition of Joncryl® 4468 is similar to the peak crystallization temperature, but the effect is not as clear as for the peak crystallization temperature. This is due to the higher variation of the data compared to the effect of the addition of Joncryl®. The formation of cross-linking and side chains in the polymer structure reduce the crystallinity.
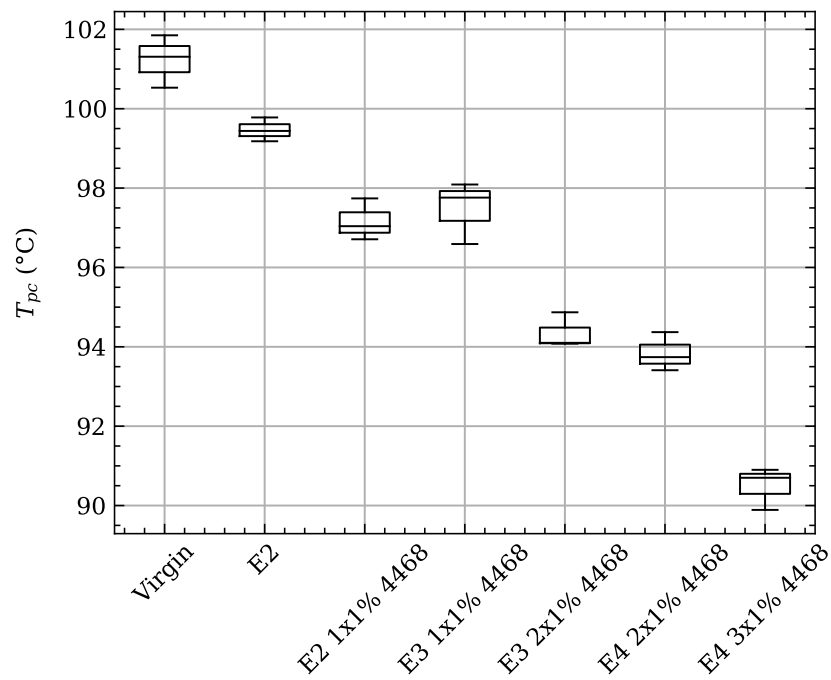
Figure 41: Peak crystallization temperature for multiple addition of Joncryl® 4468 at different processing steps.
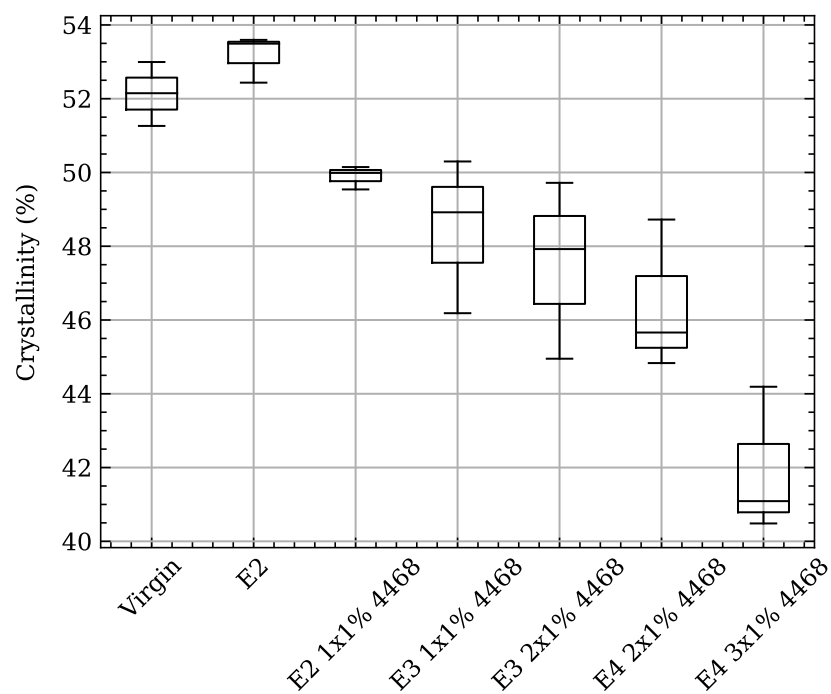
Figure 42: Crystallinity for the second heating scan for multiple addition of Joncryl® 4468 at different processing steps.

5.1.3 Summary of Thermal Testing

The TGA measurements revealed no significant effect on the maximum decomposition rate temperature, onset temperature, or total weight loss with a change in concentration of Joncryl® 4400 and 4468 and also for the multiple addition of Joncryl® 4468 no clear trend can be observed.

The change of Joncryl® concentration and the multiple addition of Joncryl® 4468 results in a decline of the peak crystallization temperature and crystallinity. The decrease of peak crystallization temperature and crystallinity are consequences of the formation of cross-linking and side chains due to the reaction of Joncryl® with PHB. The decline of the crystallinity with an increase in Joncryl® affects the mechanical properties, especially the tangent modulus, and elongation at break.

In the next section, the rheology of the different samples will be discussed. As the DSC measurements indicate, there is a reaction of Joncryl® happening and this should be also detectable in the complex viscosity curves, especially in the zero shear viscosity and the transition point from Newtonian to shear thinning.

5.2   Rheology

The results of the rheology tests are shown and discussed here. This includes the measurements for the change in concentration at the E2 stage for both Joncryl® 4400 and 4468 and the multiple processing of virgin PHB and addition of 4468 at multiple processing stages. The different samples were tested in a frequency sweep with the oscillatory rheometry and afterward, the complex viscosity η^* was calculated with the applied deformation on the specimen and the stress response due to the deformation. For all samples in advance, the assumption of linear viscoelastic material behavior was tested with amplitude sweeps (for the results see Appendix D). The complex viscosity is shown as a function of the angular frequency first and then the complex viscosity is presented over the measurement time. The figures of complex viscosity over measurement time of the frequency sweep measurements show the time-dependency of the samples during the measurement. The time-dependency of the measurement significantly influences the result of the frequency sweep. In the table 8 the measurement times and the corresponding angular frequencies for the different settings from table 4 are shown. For the figures 43, 45 and 47 the old settings were used and for figure 49 the new settings were used, according to table 4.

5.2.1   Frequency Sweep

In the following section, the frequency sweeps of the oscillatory rheometry are presented. The frequency sweeps were measured with two different settings, in which the main difference is the reversed measurement in figures 49 and 51 from 500 rad/s to 1 rad/s and the reduction of the preheating time.

Figure 43 shows the complex viscosity over the angular frequency for the Joncryl® 4400 at different weight percentages. For each concentration, three repeats were measured. The repeats show a high variability; for example, the spread for the measurements of the sample E2 1x0.2% 4400 at an angular frequency of 0.1 rad/s is roughly 10 Pa s, whereas the lowest repeat is approximately 10 Pa s. The complex viscosity of the sample E2 1x0.2% 4400 is significantly lower compared to the other samples. For the other three samples, it is not possible to detect any significant effect of the Joncryl® concentration on the complex viscosity due to the high variability of the repeats for each sample. The high variability of the repeats is a result of the temperature stabilizing process of the rheometer, which is needed to make sure that the temperature is constant during the whole measurement. This time depends on the temperature drop when the sample is inserted into the rheometer and needs circa ten minutes for the old settings (see table 4). During the temperature stabilizing process, the material starts degrading. Changes in time to stabilize the temperature directly affect the complex viscosity curve and as a result, the reproducibility of the repeats is insufficient. A comparison of the needed preheating time and measurement time for both settings is shown in table 4.

In figure 44, the complex viscosity for the measurement points of the frequency sweep of figure 43 is plotted over the measurement time. The angular frequency for each point increases with measurement time, e.g. the angular frequency for the measurement time 190 s is 0.1 rad/s, and the angular frequency for the measurement time of 775 s is 0.84 rad/s (see also table 8 left). Figure 44 demonstrates an exponential decline of the complex viscosity in the semi-logarithmic diagram with the beginning of the measurement (0.1 rad/s) until approximately 800 s (roughly 1 rad/s). This result is similar to the time sweeps done

by Lajewski et al. (2021), Park et al. (2001), and Plavec et al. (2022). Below 1 rad/s the decline in complex viscosity in figure 43 is primarily due to the time-dependent thermo-mechanical degradation. With an increase in angular frequency, the measurement time for each point decreases and, as a consequence, the time-dependent degradation decreases and the shear-thinning becomes more dominant. The measurement time per point can be estimated with the distance of two measurement points (markers in figure 44) and is shown in table 8 for both settings. Above a measurement time of 800 s (roughly 1 rad/s) in figure 44, the complex viscosity declines more rapidly. This indicates a non exponential decline due to shear thinning (compare with figure 49). Summarized, the viscosity curves of the samples are highly time-dependent, and therefore, the functional connection $\eta^* = f(\omega)$ is true when the measurement time is negligible. Otherwise, the connection of the complex viscosity during the measurement has to be modeled with a function of the form $\eta^* = f(\omega, t)$, where t is the measurement time.

For most polymers it can be assumed that the complexe viscosity is independent of time during the measurement, but this assumption is not valid for PHB, due to degradation.

Table 8: Relationship of angular frequency and measurement time. Left old and right new settings from table 4.

Angular frequency in rad/s	Time in s	Angular frequency in rad/s	Time in s
0.10	189.18		
0.14	344.04		
0.20	472.20		
0.29	579.12		
0.41	664.80	500.00	5.76
0.59	728.40	361.00	10.54
0.84	774.60	260.00	15.39
1.20	809.40	187.00	20.17
1.71	834.60	135.00	25.03
2.44	853.20	97.40	30.11
3.48	867.60	70.30	35.27
4.96	879.60	50.70	40.66
7.07	889.80	36.50	46.66
10.10	898.80	26.30	52.91
14.40	906.00	19.00	59.98
20.50	913.80	13.70	67.74
29.20	919.80	9.87	76.62
41.70	925.20	7.12	86.94
59.50	930.00	5.13	98.88
84.80	935.40	3.70	112.80
121.00	940.20	2.67	130.02
172.00	945.00	1.92	152.88
246.00	949.80	1.39	183.18
351.00	954.60	1.00	223.26
500.00	960.60		

Figure 43: Freqeuncy sweep for different concentration of Joncryl® 4400.

Figure 44: Complex viscosity for measurement points of frequency sweep of figure 43 over measurement time.

As mentioned for the samples of the Joncryl® 4400, the variability of the complex viscosity for the Joncryl® 4468 in figure 45 is high compared to the effect of change in concentration of Joncryl® 4468. In figure 45, the viscosity for the sample E2 1x1% 4468 is considerably higher compared to E2 and the concentration of 0.2 wt% and 0.6 wt%. For the samples E2, E2 1x0.2% 4468, E2 1x0.6% 4468 no significant difference can be detected as a result of the variability of the repeats of each sample. As for Joncryl® 4400, the complex viscosity of the frequency sweep measurements in figure 45 are plotted

over the measurement time in figure 46 to see the degradation during the measurement. Figure 46 shows the exponential decline of the complex viscosity over the measurement time until approximately 800 s (roughly 1 rad/s) for the frequency sweeps in the semi-logarithmic plot similar to the measurement for Joncryl® 4400.
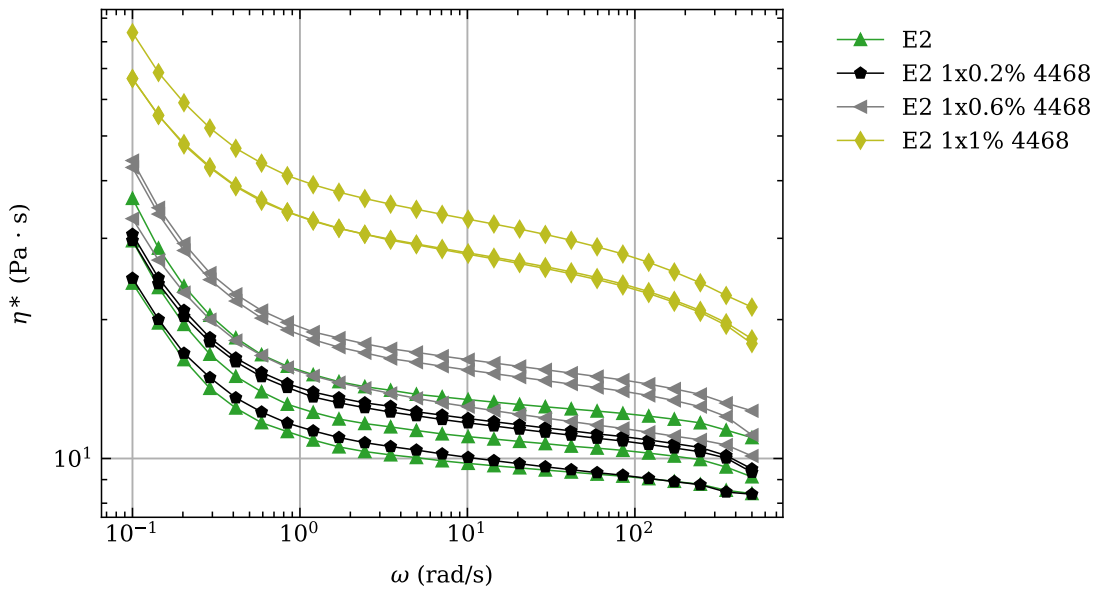
Figure 45: Freqeuncy sweep for different concentration of Joncryl® 4468.
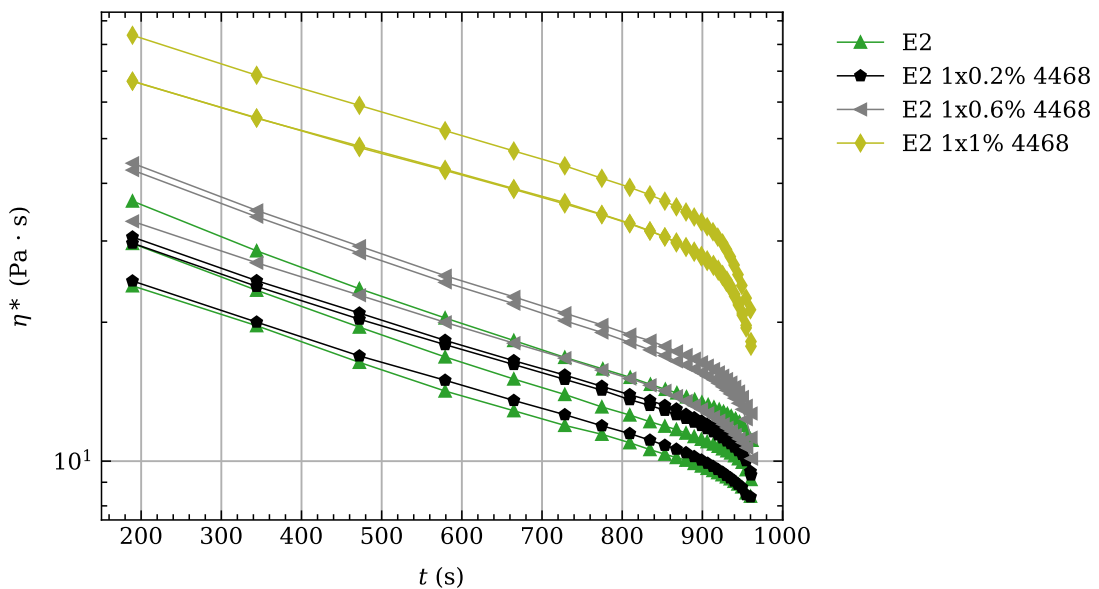
Figure 46: Complex viscosity for measurement points of frequency sweep of figure 45 over measurement time.

For the multiple addition of Joncryl® and multiple processing of the material, the frequency sweep in figure 47 was performed with the same settings as in the figures 43 and 45 (see old settings in table 4). The effect of the addition of Joncryl® can be detected,

if the sample E3 1x1% 4468 is compared to E3 2x1% 4468, and the sample E4 2x1% 4468 is contrasted with E4 3x1% 4468. As in the figures 44 and 46, the complex viscosity is plotted over the measurement time for the frequency sweep measurements of figure 47 in figure 48 in a semi-logarithmic diagram. As for the previous diagrams (figures 44 and 46), the complex viscosity declines exponentially with time till 800 s (approximately 1 rad/s) in the semi-logarithmic diagram.

Figure 47: Frequency sweep for multiple addition of Joncryl® 4468 at different processing steps with old settings.

Figure 48: Complex viscosity for measurement points of frequency sweep of figure 47 over measurement time.

In the figures 49 to 51, the measurement was started immediately when the temperature reached 190 °C and the measurement was performed from 500 rad/s to 1 rad/s. This procedure was chosen, because of the time-dependent thermo-mechanical degradation of PHB below a time of 800 s shown in the figures 44, 46 and 48. The immediate start after reaching 190 °C reduces the preheating time from approximately 10 min to around 2 min, but therefore, the temperature reaches 192 °C to 193 °C during the measurement. The reversed measurement from 500 rad/s to 1 rad/s has the advantage, that the most time-consuming measurement points are proceeded last, and therefore, the measurement points are less affected by the degradation during testing (minimization of the overall thermo-mechanical history of the measurement points).

The addition of Joncryl® at the additional processing step between samples (E3 1x1% 4468 to E3 2x1% 4468, E4 2x1% 4468 to E4 3x1% 4468) enhances the zero shear viscosity in figure 49. The additional processing step without the addition of Joncryl®4468 decreases the zero shear viscosity, which can be seen for the sample E2 1x1% 4468 compared to E3 1x1% 4468, and E3 2x1% 4468 compared to E4 2x1% 4468.

In figure 50, the complex viscosity is plotted over the measurement time for the frequency sweep of figure 49. It has to be considered, if the measurement points of the figures 49 and 50 are compared, that the measurement points are reversed. Specifically, the measurement points in figure 50 from left to right correspond to the measurement points in figure 49 from right to left (e.g. the first measurement point in figure 49 at 1 rad/s is the last measurement point in figure 50 at 223.3 s). The complex viscosity in figure 50 increases with a longer measurement time (decrease of angular frequency) and then settles at a plateau. This plateau is the zero shear viscosity of the material. Only for the virgin material, a significant exponential decline for the complex viscosity with longer measurement time is visible.
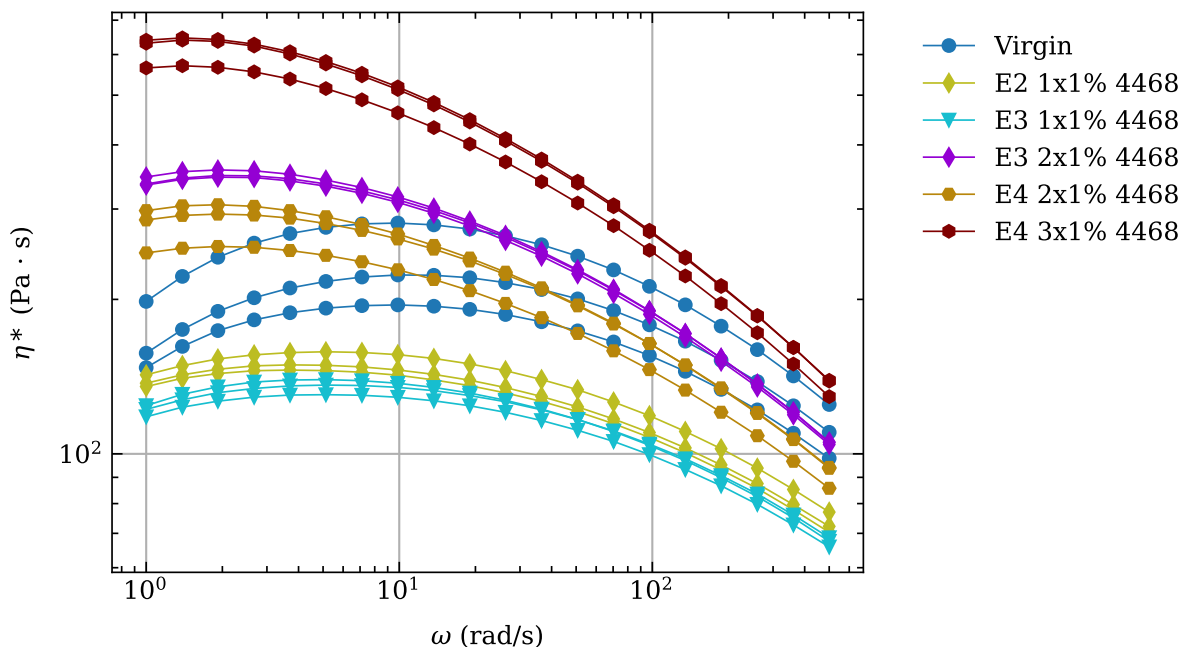
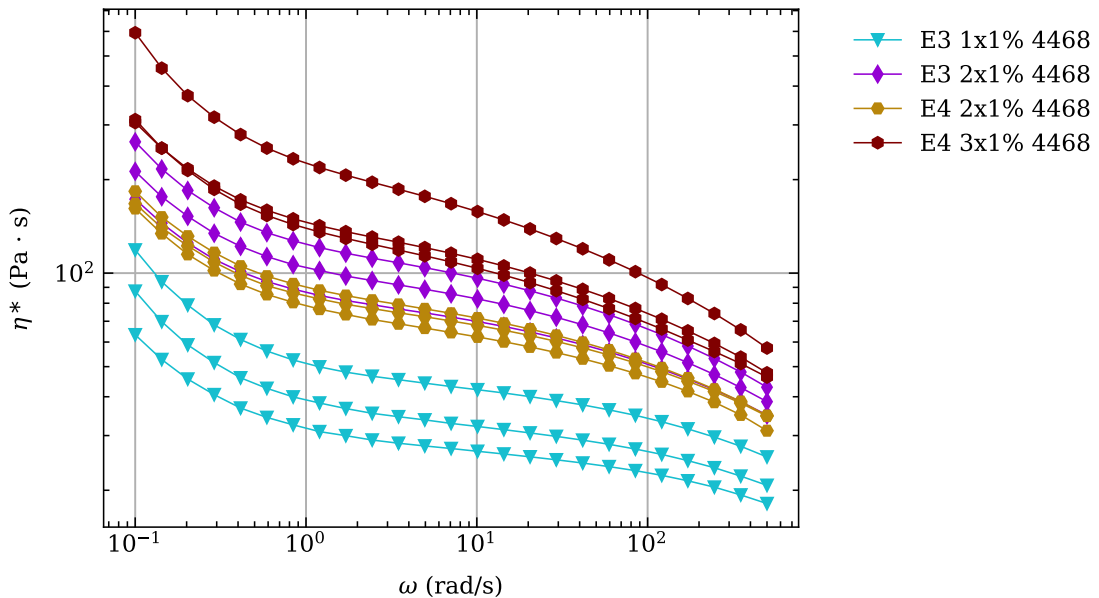Figure 49: Frequency sweep for multiple addition of Joncryl® 4468 at different processing steps with new settings.

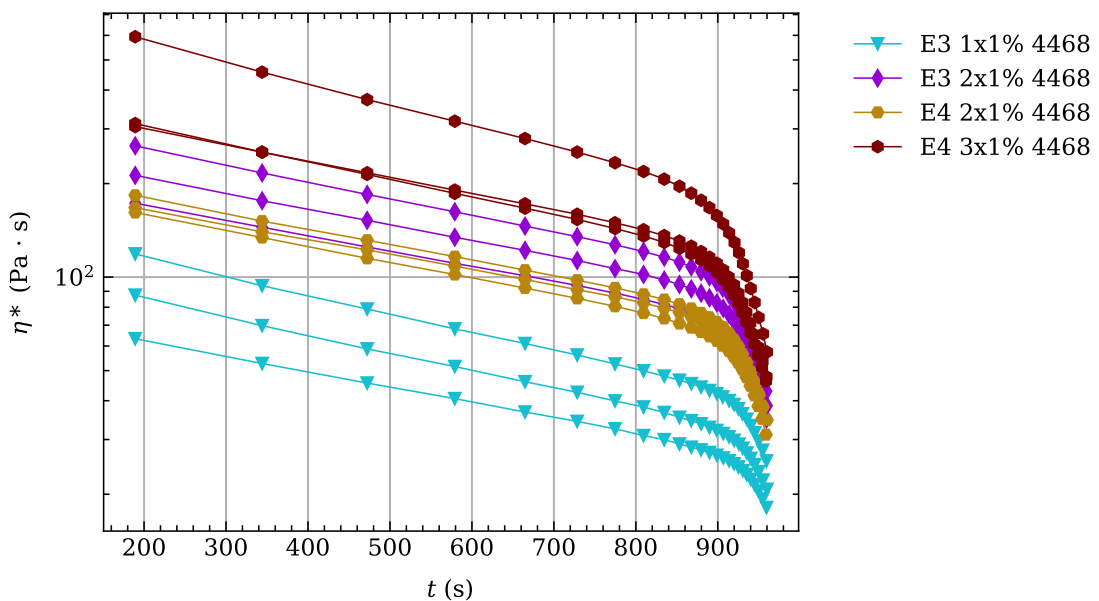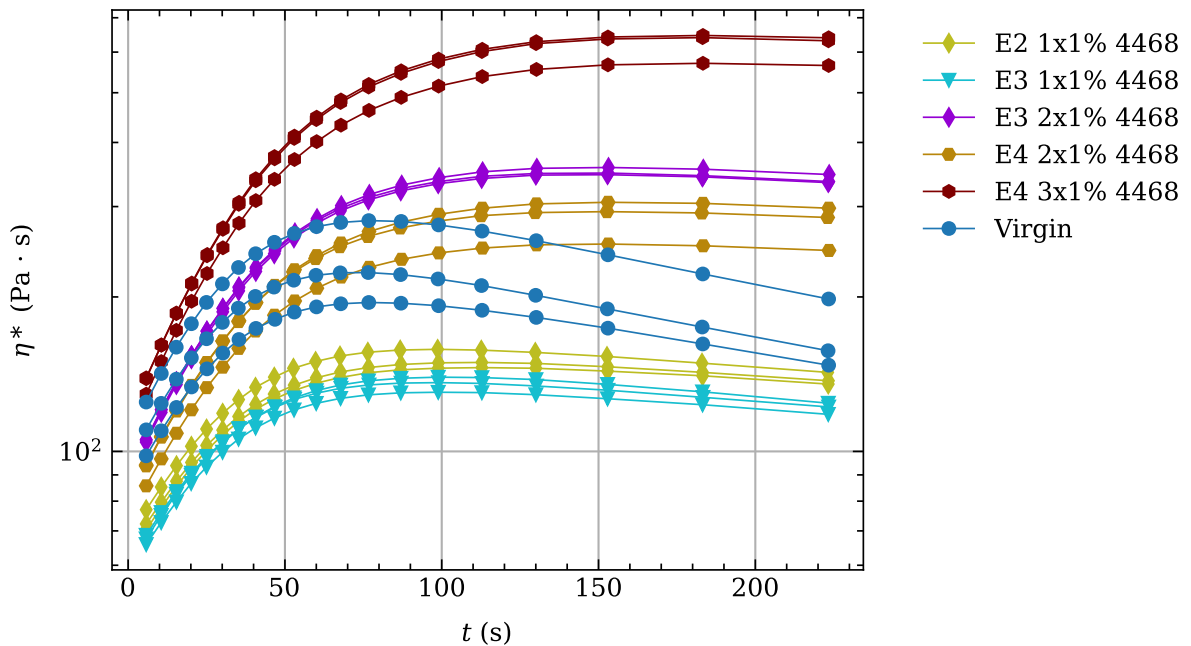*Figure 50: Complex viscosity for measurement points of freqency sweep of figure 49 over measurement time.*

The *Bird-Carreau-Yasuda* equation fits the measurement data well in between an angular frequency of 1 rad/s to 500 rad/s, which can be seen in figure 51. The viscosity curve of the virgin material is not considered in figure 51, because the virgin material shows a high tendency of degradation below an angular frequency of 10 rad/s, and therefore, the *Bird-Carreau-Yasuda* equation cannot be fitted accordingly. In table 9, the fitted parameters of the *Bird-Carreau-Yasuda* equation are shown. The equation (16) is repeated below to make it easier to interpret the change in parameters for the different samples in figure 51 and table 9.

Comparing the fitted parameters from table 9, it is possible to detect an effect of degradation and addition of Joncryl® on the zero shear viscosity, and most probably the addition of Joncryl® has an effect on the transition point of Newtonian to shear-thinning behavior of the material. For the samples E2 1x1% 4468 and E3 1x1% 4468, there is a decline of the zero shear viscosity of roughly 16 Pa s due to processing and for the samples E3 2x1% 4468 and E4 2x1% this decline is approximately 65 Pa s. If the addition of 1 wt% of Joncryl® is considered, it is possible to detect an effect on the zero shear viscosity for the samples E3 1x1% 4468 and E3 2x1% 4468 of roughly 220 Pa s and for the samples E4 2x1% 4468 to E4 3x1% 4468 there is an effect of approximately 360 Pa s.

It is possible that the addition of Joncryl® shifts the transition from Newtonian to shear-thinning behavior to lower angular frequencies. This can be observed in the difference in the fitting parameter B of the *Bird-Carreau-Yasuda* equation. If the parameter B for the samples E3 1x1% 4468 and E3 2x1% 4468 is compared, there is a change of 0.035 s, and for the samples E4 2x1% 4468 to E4 3x1% 4468 an increase of 0.036 s. The parameter B is reciprocally proportional to the angular frequency at the transition point of Newtonian to shear-thinning behavior, therefore an increase of B results in a decrease in shear rate or angular frequency for the transition of Newtonian behavior to shear thinning.

The parameter n significantly declines with each addition of Joncryl® 4468 and each additional processing step; this can be seen for the samples E2 1x1% 4468 to E3 2x1% 4468 with a decrease of approximately 0.09, and between the samples E3 2x1% 4468 to E4 3x1% 4468 with a decline of approximately 0.05. For the parameter a no clear trend is visible due to processing and the addition of Joncryl® 4468.
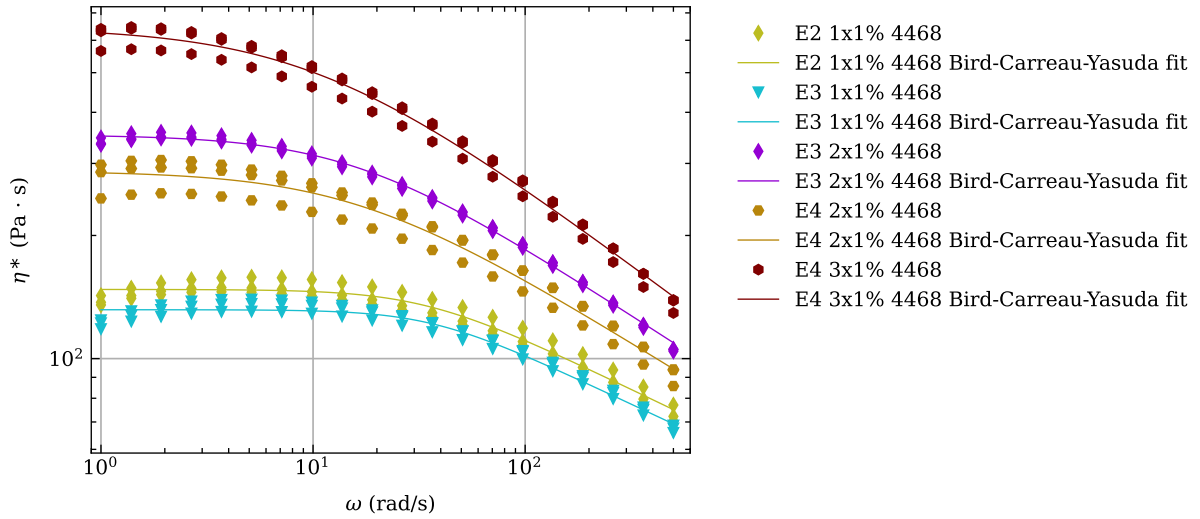
Figure 51: Frequency sweep for multiple addition of Joncryl® 4468 at different processing steps for new settings with Bird-Carreau-Yasuda fit.

$$\eta = \frac{A}{(1 + (B\dot{\gamma})^a)^{(n-1)/a}} \qquad \text{(repeat (16))}$$

Table 9: Fitted parameters of the Bird-Carreau-Yasuda equation for the frequency sweep for multiple addition of Joncryl® 4468 at different processing steps for the new settings.

	Unit	E2 1x1% 4468	E3 1x1% 4468	E3 2x1% 4468	E4 2x1% 4468	E4 3x1% 4468
A	Pa s	147.6	131.7	352.5	287.4	645.0
B	s	0.030	0.028	0.063	0.061	0.097
a	-	1.926	2.182	1.295	1.170	1.042
n	-	0.750	0.756	0.662	0.676	0.611

5.2.2 Summary of Rheology

In the following section, the results of the rheological tests will be summarized and the most important results will be discussed. This should give an overview of the most important results and the impact on the overall properties of the material.

For the measurements in figures 43, 45 and 47, which were proceeded from 0.1 rad/s to 500 rad/s the longest measurements were performed first, and therefore, the latest measurements already had a certain extent of thermo-mechanical history. This is the reason why in the figures 43, 45 and 47 the viscosity declines from 0.1 rad to 1 rad/s and then either ends in a plateau (figures 43 and 45) or reaches an inflection point at approximately 10 rad/s for figure 47. Lajewski et al. (2021), Park et al. (2001), and Plavec et al. (2022) have performed time sweeps on PHB, which shows a significant exponential decline of the complex viscosity under five minutes. As an example, the measurement for the angular frequencies of 0.1 rad/s to 1.2 rad/s needs approximately 13.5 minutes. Therefore, for measurements below 1 rad/s, the measurement points are more dependent on the measurement time than on the angular frequency. This is shown in the figures 44, 46, 48 and 50, where the complex viscosity is plotted over the measurement time and the exponential decline resulting from random chain scission can be observed (Kervran et al., 2022; Melik & Schechtman, 1995). The diagram of the complex viscosity over the angular frequency is only proper to use, if the decline due to thermo-mechanical degradation is minor compared to the change due to the variation of the angular frequency.

For the multiple addition of Joncryl® at multiple processing steps, it was possible to detect a positive effect of Joncryl® on the zero shear viscosity and a decrease to lower angular frequencies of the change over point from Newtonian to shear thinning. Thermo-mechanical degradation due to processing resulted in a decline of the zero shear viscosity. For the new settings, the *Bird-Carreau-Yasuda* equation could be fitted to the measurement data and the change due to the addition of Joncryl and thermo-mechanical degradation could be shown in changes of the fitted parameters. The thermo-mechanical loading due to the processing steps resulted in a decrease in the zero shear viscosity (Dos Santos et al., 2018; Pachekoski et al., 2013; Plavec et al., 2022; Rivas et al., 2017). The thermo-mechanical loading of PHB leads to random chain scission of the ester groups in PHB (Dos Santos et al., 2018; Hablot et al., 2008). This random chain scission reduces the mean molecular weight, and therefore, has as a consequence the decline of the zero shear viscosity. The reaction of Joncryl® with PHB and the formation of cross-linking and side-chains results in a change in the molecular mass distribution, which affects the rheological properties; this can be observed in an increase of the zero shear viscosity and a decrease in the transition shear rate between Newtonian and shear-thinning behavior of the material (Osswald & Rudolph, 2015; Schröder, 2020).

5.3   Mechanical Tests

For the evaluation of the mechanical properties of the different samples, tensile tests and notched Charpy impact tests were performed. These tests were used to provide information on the change of the tangent modulus, ultimate tensile strength, elongation at break, and notched impact strength with change in concentration of Joncryl® 4400 and 4468 and the effect of multiple processing of PHB with multiple addition of Joncryl® 4468.

5.3.1   Tensile Test

In this section, the results of the tensile tests will be discussed. The tensile tests were used to investigate the tangent modulus E_t, ultimate tensile strength σ_m, and elongation at break ε_b. As in the section 5.1.2 this part is separated into two sections, first the change in concentration of the two Joncryl® 4400 and 4468 and second the multiple addition of Joncryl® 4468. The tangent modulus, the ultimate tensile strength, and the elongation at break are plotted into box-plot diagrams over the different samples, as in section 5.1.2. Linear regression models were used to evaluate the effect of the different Joncryl® types, the effect of Joncryl® concentration, and to analyze the significance of the Joncryl® concentration. Therefore, the Joncryl® concentration is used as the independent variable and the dependent variables are the tangent modulus, ultimate tensile strength, and elongation at break.

5.3.1.1   Effect of Different Types of Joncryl® and Change in Concentration

In figure 52 the tangent modulus is plotted over the different samples for different types of Joncryl® and change in concentration. The tangent modulus enhances from virgin to E2 of around 300 MPa. A decline in tangent modulus with increasing Joncryl® concentration is visible for both Joncryl® types. In table 10 the linear regression model is shown, which assumes the tangent modulus as the dependent variable and the Joncryl® concentration as the independent variable. The p-value in table 10 for the *Shapiro-Wilk* test for the tangent modulus with a change in concentration of the Joncryl® 4400 and 4468 is above 0.05. For that reason, it is possible to assume, that the residuals for both regression models are normally distributed.

For the regression model of the Joncryl® 4468 the p-value for the *Wald* test is above 0.05 and the confidence interval for the slope stretches over zero, which leads to the conclusion, that the slope could be equal to zero. This is due to the high variation of the sample E2 1x0.6% 4468, without this sample, the p-value for the *Wald* test is 0.001. As mentioned in the section 4.4.2, the specimens of the sample E2 1x0.6% 4468 were produced with different injection molding settings.

The slope for the regression model of the Joncryl® 4400 is unequal to zero, according to the confidence interval and the p-value of the *Wald* test in table 10. For the Joncryl® 4400, the effect on the tangent modulus is negative with an increase of the wt% of Joncryl®. The confidence interval for the intercept of the regression of the Joncryl® 4468 includes the median of the sample E2, but the confidence interval of the intercept for the Joncryl® 4400 does not include the median. This could be caused by the fact that the samples virgin, E1, E2, and the samples of Joncryl® 4468 were processed and tested together. The

r-values for the linear regression models for both Joncryl® are small; however, the primary aim of the regression analysis was to demonstrate the statistical significance.
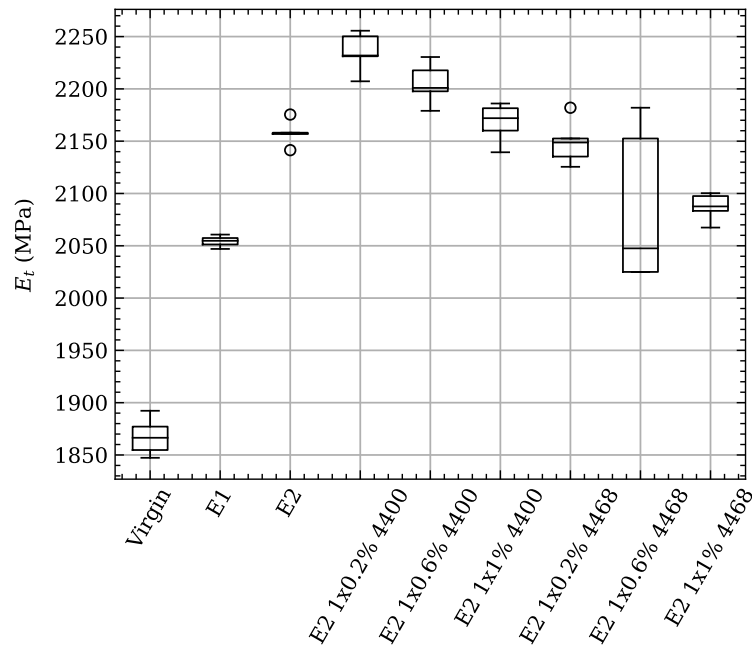
Figure 52: Tangent modulus for different Joncryl® types and concentrations.

Table 10: Linear regression for tangent modulus E_t at different Joncryl® concentrations and different kinds of Joncryl®.

	Unit	Et 4400	Et 4468
p-value *Shapiro-Wilk* test	-	0.259	0.177
slope	MPa/wt%	-84	-77
lower bound 95 % CI of the slope	MPa/wt%	-113	-157
upper bound 95 % CI of the slope	MPa/wt%	-54	3
intercept	MPa	2253	2154
lower bound 95 % CI of the intercept	MPa	2232	2099
upper bound 95 % CI of the intercept	MPa	2274	2208
r-value	-	-0.852	-0.500
p-value *Wald* test	-	0.000	0.058

In figure 53 the ultimate tensile strength is plotted over the samples with different Joncryl® types and concentrations as in the previous diagram. The same as for the ultimate tensile strength was done for the elongation at break in figure 54.

In figure 53 no trend for the ultimate tensile strength can be observed. For the elongation at break in figure 54 there is a sharp decline from virgin material to E1 of around 10 %, then a small decline of approximately 1 % from E1 to E2, and then the elongation at break increases slightly with an increase in Joncryl® concentration for both Joncryl® types.

The elongation at break for the virgin material is high compared to results of 1 % to 15 % reported by various authors (Bugnicourt et al., 2014; Keskin et al., 2017; Rajan

et al., 2019). This could be a result of the short ageing time at room temperature, which can result in a change of 50 % of elongation at break for freshly molded PHB to 5 % of elongation at break for several weeks aged material at room temperature as reported by Hobbs and Barham (1999).
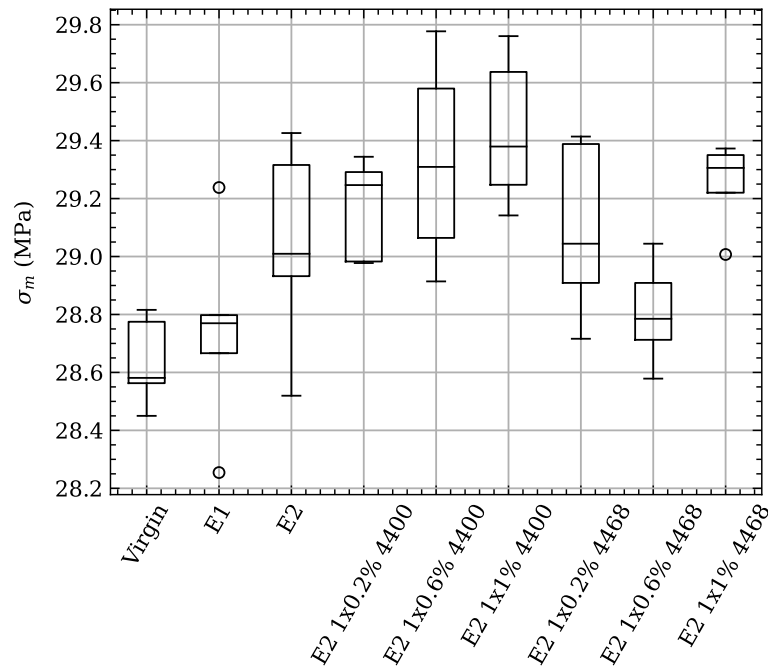
Figure 53: Ultimate tensile strength for different Joncryl® types and concentrations.
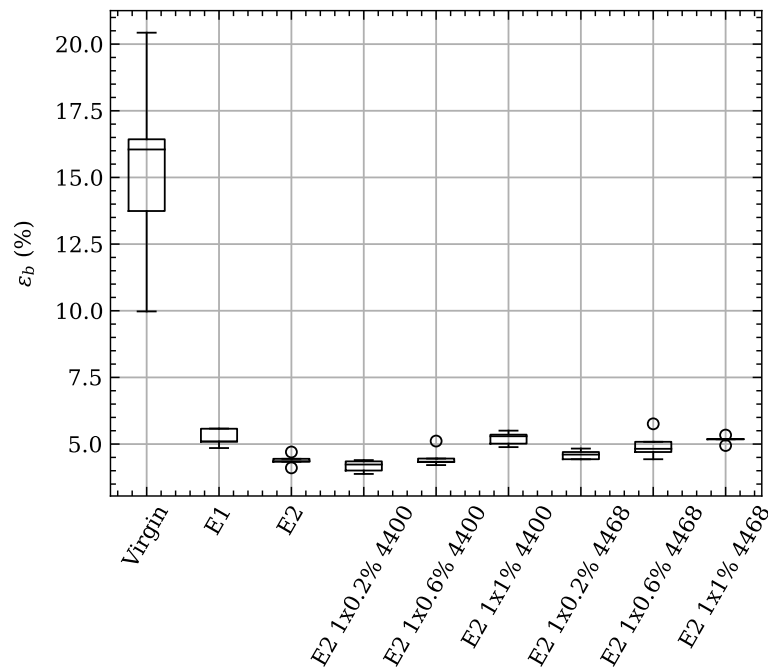
Figure 54: Elongation at break for different Joncryl® types and concentrations.

As for the tangent modulus, a linear regression model was built for the elongation at break and the ultimate tensile strength as dependent variables, and the concentration of either Joncryl® 4400 or 4468 as the independent variable. The summary of the statistical analysis of the data of the figures 53 and 54 is provided in the tables 11 and 12.

The median of the sample E2 is included in the 95% confidence interval of the intercept of the ultimate tensile strength for both Joncryl® types. If the slope of the linear model of the ultimate tensile strength in table 11 is considered, the p-value of the *Wald* test and the 95% confidence interval lead to the conclusion, that there is not an effect on the ultimate tensile strength with a change in Joncryl® concentration for both Joncryl® types.

On the other hand, both Joncryl® types reveal a positive correlation between Joncryl® concentration and elongation at break in table 12. The 95% confidence interval of the intercept for the elongation at break for the Joncryl® 4400 does not include the median of the sampe E2 but the regression model for the Joncyl 4468 does include the median. For the Joncryl® 4468, the p-value for the *Shapiro-Wilk* test is below the significance level of 5 %. Although it cannot be assumed that the residuals of the linear regression are distributed normally, the confidence intervals were calculated for the intercept and the slope. For the interpretation of the result, it has to be considered, that those two intervals are prone to error, because of the violation of the assumption of normally distributed data.

Table 11: Linear regression for ultimate tensile strength σ_m at different Joncryl® concentrations and different kinds of Joncryl®.

	Unit	σ_m 4400	σ_m 4468
p-value *Shapiro-Wilk* test	-	0.637	0.936
slope	MPa/wt%	0.3	0.2
lower bound 95 % CI of the slope	MPa/wt%	-0.1	-0.3
upper bound 95 % CI of the slope	MPa/wt%	0.8	0.7
intercept	MPa	29.1	28.9
lower bound 95 % CI of the intercept	MPa	28.8	28.6
upper bound 95 % CI of the intercept	MPa	29.4	29.3
r-value	-	0.404	0.237
p-value *Wald* test	-	0.120	0.395

*Table 12: Linear regression for elongation at break ε_b at different Joncryl®
concentrations and different kinds of Joncryl®.*

	Unit	ε_b 4400	ε_b 4468
p-value *Shapiro-Wilk* test	-	0.239	0.032
slope	%/wt%	1.31	0.71
lower bound 95 % CI of the slope	%/wt%	0.84	0.18
upper bound 95 % CI of the slope	%/wt%	1.78	1.24
intercept	%	3.84	4.48
lower bound 95 % CI of the intercept	%	3.51	4.12
upper bound 95 % CI of the intercept	%	4.17	4.84
r-value	-	0.849	0.627
p-value *Wald* test	-	0.000	0.012

5.3.1.2 Effect of Multiple Addition of Joncryl® 4468 at Different Processing Steps

In the following section, the mechanical properties of the tensile tests for the multiple addition of Joncryl® 4468 at multiple processing steps will be discussed. This includes, as in the previous section, the tangent modulus E_t, the ultimate tensile strength σ_m, and the elongation at break ε_b. The influences of multiple processing steps and the addition of Joncryl® at multiple processing steps will be discussed. The samples virgin E1, E2, and E2 1x1% 4468 are used as a reference and were not processed and tested again (results used from the previous section). The three-times processed samples and the four-times processed samples were processed and tested in separate sets on different days.

In figure 55 the tangent modulus is shown over the different samples of the multiple addition of Joncryl® 4468 and multiple processing steps. As in the previous section, the tangent modulus increases with each additional processing step. This can be seen in the change from virgin to E2, the change from E2 1x1% 4468 to E3 1x1% 4468, and the increase in tangent modulus from E3 2x1% 4468 to E4 2x1% 4468. With the addition of Joncryl® the tangent modulus decreases, which can be seen, if the samples E2 to E2 1x1% 4468, E3 1x1% 4468 to E3 2x1% 4468, and E4 2x1% 4468 to E4 3x1% 4468 are compared. For the samples E4 2x1% 4468 to E4 3x1% 4468 the box plots of the samples overlap, therefore the effect is not for sure significant.

In figure 56, the ultimate tensile strength is plotted over the different samples for the multiple addition of Joncryl®. For the samples from virgin to E3 2x1% 4468 (left to right), there is no clear trend. The four times extruded samples (E4 2x1% 4468, E4 3x1% 4468) show a significant increase in ultimate tensile strength. This increase for the two E4 samples does not fit into the trend of the other samples in figure 55, and the results of the change in concentration of Joncryl® in figure 53 do not suggest this result either. The E4 samples were processed and tested on separate days compared to the E3 samples, which could be a reason for the significant difference in ultimate tensile strength.
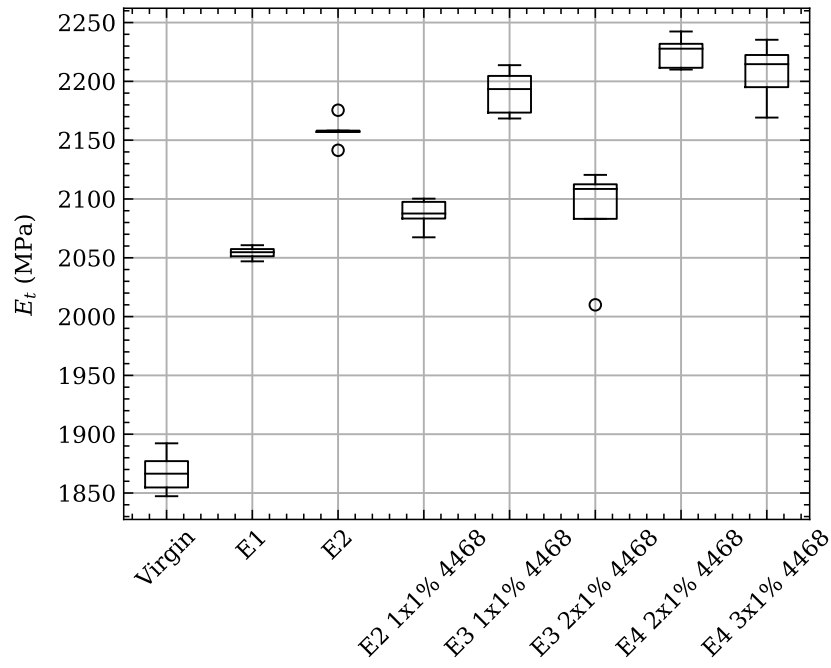
Figure 55: Tangent modulus for multiple addition of Joncryl® 4468 at different processing steps.
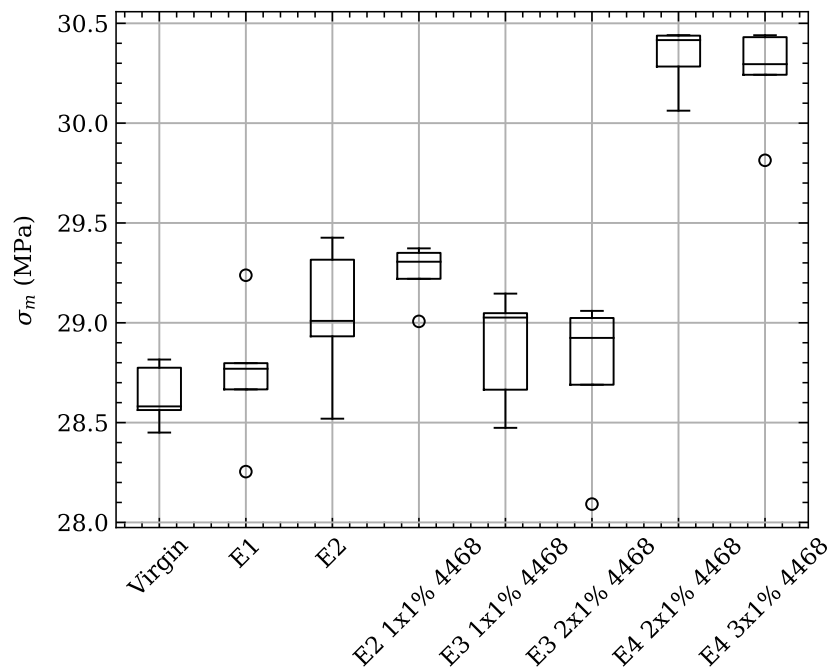
Figure 56: Ultimate tensile strength for multiple addition of Joncryl® 4468 at different processing steps.

For the elongation at break over the different samples in figure 57, the trend does not fit the results of the change in concentration as well as the tangent modulus does. The decline of elongation at break with processing can be detected between the samples virgin to E2, E2 1x1% 4468 and E3 1x1% 4468. Between E3 2x1% 4468 and E4 2x1% 4468, there is not a significant decline of the elongation at break due to processing. The addition of Joncryl® leads to an enhancement in elongation at break for the samples E2 to E2 1x% 4468, E3 1x1% 4468 and E3 2x1% 4468. If the samples E4 2x1% 4468 and E4 3x1% 4468 are considered, there is a small decline in elongation at break with addition of Joncryl® 4468.
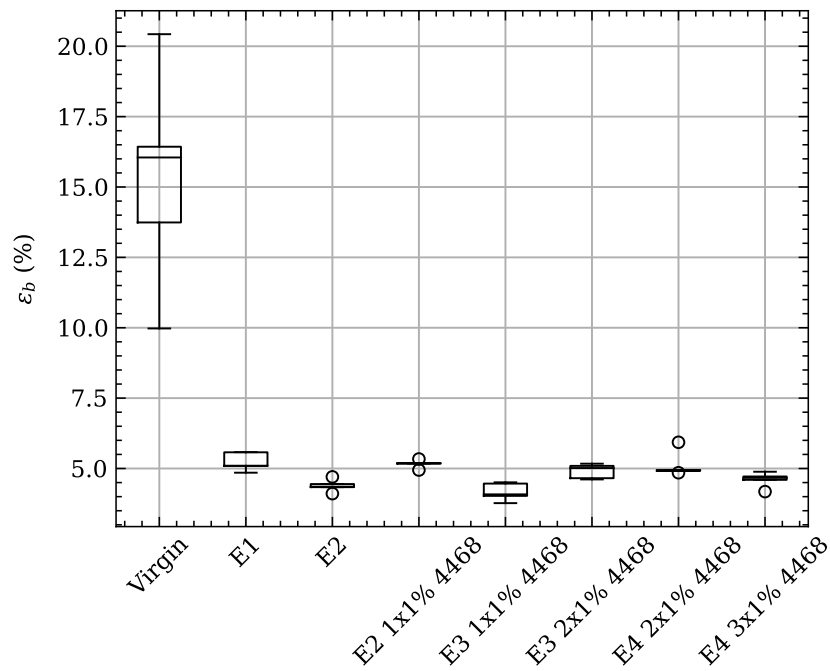
Figure 57: Elongation at break for multiple addition of Joncryl® 4468 at different processing steps.

5.3.2   Notched Charpy Impact Test

The notched Charpy impact results will be discussed in this section; this test was performed to investigate the effect of degradation through processing and the impact of Joncryl® on the notched impact strength. Therefore, the notched impact strength a_{cN} is plotted into a box-plot diagram over the different samples, as in the section for DSC (section 5.1.2) and in the previous section of tensile testing. In figure 58 the notched impact strength is plotted over different Joncryl® concentrations and the two Joncryl® types 4400 and 4468 and also the degradation path is shown from virgin over E1 to E2. In figure 59 the notched impact strength over the multiple addition and multiple processing samples is shown, and the samples virgin, E1, E2, and E2 1x1% 4468 are used as a reference.

The notched impact strength declines rapidly from virgin to E2 by around 2 J/m² due to processing in figures 58 and 59. For the change in Joncryl® concentration for both Joncryl® 4400 and 4468 a linear regression model (table 13) was used as an evaluation of a significant effect of the concentration or difference in kind of Joncryl® on the notched impact strength. Considering the statistical values in table 13, there is a significant negative effect (p-value *Wald* test of 0.004) with a change in Joncryl® concentration of Joncryl® 4400; for the Joncryl® 4468, there is not a significant effect (p-value *Wald* test of 0.313) with a change in Joncryl® concentration. The intercepts of both Joncryl® types can be considered equal (overlap of confidence intervals), but both do not include the median of sample E2. The r-values for both linear regression models are small, which is a result of the high variance of the samples (especially the samples of 4468 and E2 1x0.6% 4400) and the absence of a clear relationship of Joncryl® concentration and notched impact strength.
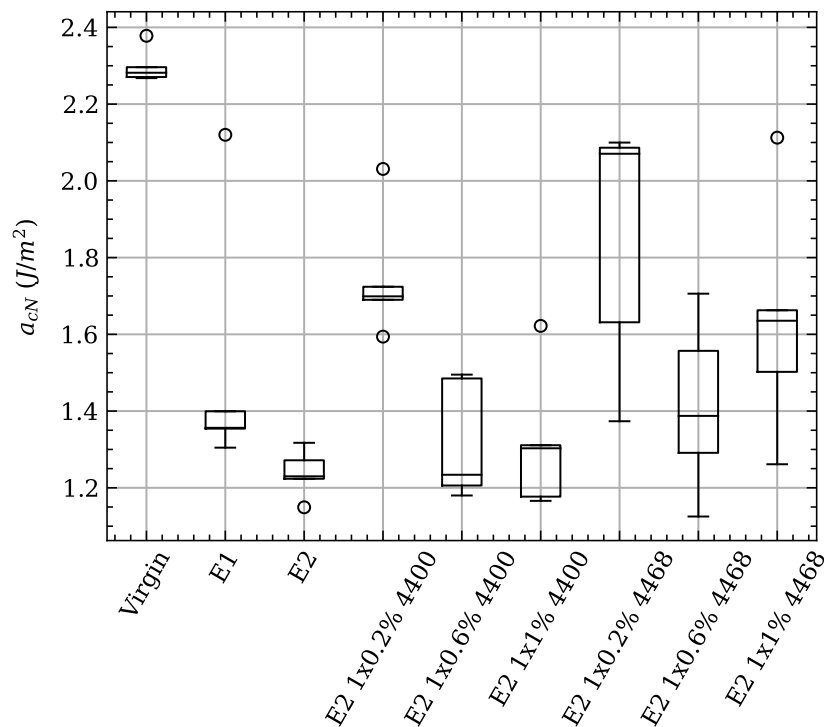
Figure 58: Notched Charpy test for for different Joncryl® types and Joncryl® concentration.

Table 13: Linear regression for notched chapry impact a_{cN} at different Joncryl®
concentrations and different kinds of Joncryl®.

	Unit	a_{cN} 4400	a_{cN} 4468
p-value *Shapiro-Wilk* test	-	0.097	0.885
slope	J/(m² wt%)	-0.54	-0.27
lower bound 95 % CI of the slope	J/(m² wt%)	-0.87	-0.83
upper bound 95 % CI of the slope	J/(m² wt%)	-0.21	0.29
intercept	J/m²	1.79	1.80
lower bound 95 % CI of the intercept	J/m²	1.56	1.414
upper bound 95 % CI of the intercept	J/m²	2.01	2.18
r-value	-	-0.697	-0.279
p-value *Wald* test	-	0.004	0.313

In figure 59 notched impact strength over the samples for multiple addition of Joncryl®
at different processing steps is shown. For the multistage processing with multiple addition
of Joncryl®, the notched impact strength declines rapidly from virgin to E2 by around
2 J/m², and then the notched impact strength decreases with each additional processing
step and addition of Joncryl® 4468.
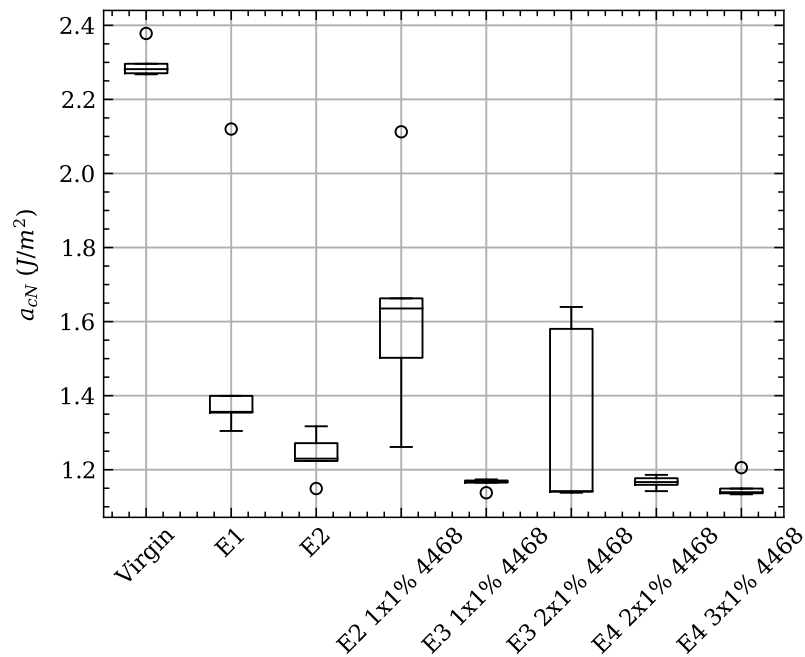
Figure 59: Notched impact strength for multiple addition of Joncryl® 4468 at different
processing steps.

5.3.3 Summary of Mechanical Testing

In the following paragraphs, the main results for the tensile tests and the notched Charpy impact tests are summarized and discussed. This includes the tangent modulus, ultimate tensile strength, elongation at break, and notched impact strength.

With each additional processing step, the tangent modulus increases and the elongation at break and the impact strength decrease. This can especially be observed in the change between the samples virgin, E1, and E2, which were only processed and no Joncryl® was added. For the ultimate tensile stress, there is not a clear relationship to degradation or Joncryl® detectable for all samples. The addition of Joncryl® has a positive effect on the elongation at break and a negative effect on the tangent modulus. For the elongation at break, only the samples E4 2x1% and E4 3x1% do not fit this pattern. To get an estimation of the effect of the Joncryl® on the tangent modulus and the elongation at break, the slope and the intercept of the regression models of the tables 10 and 12 are compared ($100 \cdot |slope|/intercept$ in percent). For the tangent modulus, this comparison results in an change of 3.7 % for the 4400 and 3.6 % for the 4468 for the addition of 1 wt% Joncryl®. These changes are small compared to the degradation from approximately 1860 MPa for the virgin to a loss of roughly 300 MPa to E2 compared to the slope of -84 MPa/wt% for the Joncryl® 4400. As for the tangent modulus, the slope and intercept of the elongation at break of the linear regression model in table 12 are compared. For the Joncryl® 4400 there is a change of 34.2 %/wt%, and for the 4468 of 15.8 %/wt%. These are significant effects, but the elongation at break declines from virgin to E2 approximately by 10 %, the slope for the Joncryl® as a comparison is 1.31 %/wt%.

The addition of Joncryl® does not reverse the impact of the thermo-mechanical degradation due to processing completely, but there is a positive effect on the elongation at break. The elongation at break is critical, because PHB is a brittle polymer, and therefore, a further decline of the elongation at break due to processing would further restrict the fields of applications.

6   Summary and Outlook

In this thesis, the effect of Joncryl® 4400 and 4468 on the thermal, rheological, and mechanical properties of PHB was investigated. This effect was first tested with a change in Joncryl® concentration and in the second step, a multiple recycling process was simulated and Joncryl® 4468 was added multiple times.

The change in Joncryl® concentration decreased the peak crystallization temperature, decreased the crystallinity, enhanced the zero shear viscosity, moved the transition from Newtonian to shear-thinning to lower angular frequencies, declined the tangent modulus, and increased the elongation at break. This trend continued for the multiple addition of Joncryl® at different processing steps, but for these samples also the additional processing had an impact on the properties. Each additional processing step declined the zero shear viscosity, enhanced the tangent modulus, decreased the elongation at break, and reduced the notched impact strength. This thesis showed that Joncryl® has a positive effect on the properties of PHB, and therefore, can improve the recyclability of the material, despite the fast decline of the properties due to thermal degradation. Especially the elongation at break showed an increase with the addition of Joncryl®, and therefore, the material is more ductile compared to PHB without the addition of Joncryl®.

The trends mentioned above were not as consistent as they could be, the E2 samples do not fit in many of the regression models. The E2 should represent the $0\,\mathrm{wt\%}$ sample, but this is not the case for all regression models. The observed trends from the peak crystallization temperature and crystallinity could not be detected in the peak melting temperature. This could be due to the double melting peak of PHB in the second heating process. The samples after the fourth processing cycle (E4 2x1% 4468 and E4 3x1% 4468) showed some set difference for the ultimate tensile strength. For the TGA test Duangphet et al. (2014) used the method of *Flynn-Wall-Ozawa* to investigate the activation energy of the degradation process and found a stabilizing effect of Joncryl®. In this work we were not able to find a significant effect of Joncryl® on the TGA results, this could be improved in further works by also considering the method of *Flynn-Wall-Ozawa* for the evaluation of the TGA results. The effect of the concentration of Joncryl® on the complex viscosity could not be detected consistently due to the high time-dependency of PHB. Therefore, the settings were changed for the multiple addition of Joncryl®, then the effect of processing and Joncryl® were detectable in the measurements. The measurements still showed a high variation and the temperature deviation during the measurement influenced the quality of the results, therefore there is still room for improvement of the complex viscosity measurements. The tensile test measurements for the virgin material showed a high elongation at break compared to values reported by various authors (Bugnicourt et al., 2014; Keskin et al., 2017; Rajan et al., 2019).

The addition of Joncryl® impacts the properties of PHB, but the decline compared to the virgin is still huge. Especially with each additional processing step, the material got more brittle and reduced the application fields for recycled material further. A common practice for PET is to use a combination of stabilizers and chain extenders (Maier & Schiller, 2016; Murphy, 2001; Schyns & Shaver, 2021), but stabilizers have not shown a significant improvement and there are different results from different groups on the effect of stabilizers on PHB (Arza et al., 2015; Tocháček et al., 2021; L. Wang et al., 2008). Therefore, either new additives have to be developed to stabilize PHB, a chain

extender which exhibits optimal reaction times in the processing window of PHB, or the residence time or the processing window has to be reduced significantly. Also, a combination of stabilizers and chain extenders could be investigated. The combination of stabilizers and chain extenders is common practice in the recycling of PET, which shares analogous degradation mechanisms with PHB and polyesters in general (Maier & Schiller, 2016; Murphy, 2001; Schyns & Shaver, 2021). Future research efforts can center on developing new additives, especially chain extenders and stabilizers. Moreover, exploring the potential of commercially available additives that have not been previously blended with PHB could provide valuable insights.

References

Anton Paar. (2023). Amplitude sweeps :: Anton Paar Wiki [Accessed on August 23, 2023]. https://wiki.anton-paar.com/en/amplitude-sweeps/

Arza, C. R., Jannasch, P., Johansson, P., Magnusson, P., Werker, A., & Maurer, F. H. (2015). Effect of additives on the melt rheology and thermal degradation of poly [(r)-3-hydroxybutyric acid]. *Journal of Applied Polymer Science*, *132*(15).

Atkins, P., Atkins, P. W., & de Paula, J. (2002). *Atkins' physical chemistry*. Oxford university press.

Barham, P., Keller, A., Otun, E., & Holmes, P. (1984). Crystallization and morphology of a bacterial thermoplastic: Poly-3-hydroxybutyrate. *Journal of Materials Science*, *19*, 2781–2794.

Biomer GmbH. (2023). Composition of virgin PHB [Accessed on August 23, 2023]. https://www.biomer.de/IndexD.html

Bordes, P., Hablot, E., Pollet, E., & Avérous, L. (2009). Effect of clay organomodifiers on degradation of polyhydroxyalkanoates. *Polymer Degradation and Stability*, *94*(5), 789–796.

Bousfield, G. (2014). *Effect of chain extension on rheology and tensile properties of phb and phb-pla blends* [Doctoral dissertation, École Polytechnique de Montréal].

Bozkurt, Ö. Y., Özbek, Ö., & Abdo, A. R. (2017). The effects of nanosilica on charpy impact behavior of glass/epoxy fiber reinforced composite laminates. *Periodicals of Engineering and Natural Sciences*, *5*(3).

Bugnicourt, E., Cinelli, P., Lazzeri, A., & Alvarez, V. A. (2014). Polyhydroxyalkanoate (pha): Review of synthesis, characteristics, processing and potential applications in packaging.

Carreau, P. J., De Kee, D. C., & Chhabra, R. P. (2021). *Rheology of polymeric systems: Principles and applications*. Carl Hanser Verlag GmbH Co KG.

Choi, J. Y., Lee, J. K., You, Y., & Park, W. H. (2003). Epoxidized polybutadiene as a thermal stabilizer for poly (3-hydroxybutyrate). ii. thermal stabilization of poly (3-hydroxybutyrate) by epoxidized polybutadiene. *Fibers and Polymers*, *4*, 195–198.

Cox, W., & Merz, E. (1958). Correlation of dynamic and steady flow viscosities. *Journal of Polymer Science*, *28*(118), 619–622.

Delva, L., Van Kets, K., Kuzmanovic, M., Demets, R., Hubo, S., Mys, N., De Meester, S., & Ragaert, K. (2019). Mechanical recycling of polymers for dummies. *Capture-Plastics to Resource*.

Dos Santos, A. J., Oliveira Dalla Valentina, L. V., Hidalgo Schulz, A. A., & Tomaz Duarte, M. A. (2018). From obtaining to degradation of phb: A literature review. part ii. *Ingeniería y Ciencia*, *14*(27), 207–228.

Duangphet, S., Szegda, D., Song, J., & Tarverdi, K. (2014). The effect of chain extender on poly (3-hydroxybutyrate-co-3-hydroxyvalerate): Thermal degradation, crystallization, and rheological behaviours. *Journal of Polymers and the Environment*, *22*, 1–8.

Ehrenstein, G. W., Riedel, G., & Trawiel, P. (2004). *Thermal analysis of plastics: Theory and practice*. Carl Hanser Verlag GmbH Co KG.

Ehrenstein, G. W. (2012). *Polymeric materials: Structure, properties, applications*. Carl Hanser Verlag GmbH Co KG.

Endres, H.-J., & Siebert-Raths, A. (2011). Engineering biopolymers. *J. Eng. Biopolym.*, *71*(1), 3–15.

Frick, A., & Stern, C. (2013). *DSC-Prüfung in der Anwendung*. Carl Hanser Verlag GmbH Co KG.

Ghanbari, A., Heuzey, M., Carreau, P., & Ton-That, M. (2013). A novel approach to control thermal degradation of pet/organoclay nanocomposites and improve clay exfoliation. *Polymer*, *54*(4), 1361–1369.

Grellmann, W., & Seidler, S. (2022). *Polymer testing*. Carl Hanser Verlag GmbH Co KG.

Hablot, E., Bordes, P., Pollet, E., & Avérous, L. (2008). Thermal and thermo-mechanical degradation of poly (3-hydroxybutyrate)-based multiphase systems. *Polymer Degradation and Stability*, *93*(2), 413–421.

Hamad, K., Kaseem, M., & Deri, F. (2013). Recycling of waste from polymer materials: An overview of the recent works. *Polymer degradation and stability*, *98*(12), 2801–2812.

Hamilton, L. A., & Feit, S. (2019). Plastic & climate: The hidden costs of a plastic planet.

Harris, C. R., Millman, K. J., Van Der Walt, S. J., Gommers, R., Virtanen, P., Cournapeau, D., Wieser, E., Taylor, J., Berg, S., Smith, N. J., et al. (2020). Array programming with numpy. *Nature*, *585*(7825), 357–362.

Hobbs, J., & Barham, P. (1999). The fracture of poly (hydroxybutyrate) part iii fracture morphology in thin films and bulk systems. *Journal of materials science*, *34*, 4831–4844.

Hopewell, J., Dvorak, R., & Kosior, E. (2009). Plastics recycling: Challenges and opportunities. *Philosophical Transactions of the Royal Society B: Biological Sciences*, *364*(1526), 2115–2126.

Houwink, R. (1940). Zusammenhang zwischen viscosimetrisch und osmotisch bestimmten Polymerisationsgraden bei Hochpolymeren. *Journal für praktische Chemie*, *157*(1-3), 15–18.

Hundertmark, T., Mayer, M., McNally, C., Simons, T. J., & Witte, C. (2018). How plastics waste recycling could transform the chemical industry. *McKinsey & Company*, *12*, 1–1.

Hunter, J. D. (2007). Matplotlib: A 2d graphics environment. *Computing in Science & Engineering*, *9*(3), 90–95. https://doi.org/10.1109/MCSE.2007.55

Janigová, I., Lacík, I., & Chodák, I. (2002). Thermal degradation of plasticized poly (3-hydroxybutyrate) investigated by DSC. *Polymer Degradation and Stability*, *77*(1), 35–41.

Kahraman, Y., Özdemir, B., Kılıç, V., Goksu, Y. A., & Nofar, M. (2021). Super toughened and highly ductile PLA/TPU blend systems by in situ reactive interfacial compatibilization using multifunctional epoxy-based chain extender. *Journal of Applied Polymer Science*, *138*(20), 50457.

Kervran, M., Vagner, C., Cochez, M., Poncot, M., Saeb, M. R., & Vahabi, H. (2022). A review on thermal degradation of polylactic acid (PLA)/polyhydroxybutyrate (PHB) blends. *Polymer Degradation and Stability*, 109995.

Keskin, G., Kızıl, G., Bechelany, M., Pochat-Bohatier, C., & Öner, M. (2017). Potential of polyhydroxyalkanoate (PHA) polymers family as substitutes of petroleum based polymers for packaging applications and solutions brought by their composites to form barrier materials. *Pure and Applied Chemistry*, *89*(12), 1841–1848.

Kolahchi, A. R., & Kontopoulou, M. (2015). Chain extended poly (3-hydroxybutyrate) with improved rheological properties and thermal stability, through reactive modification in the melt state. *Polymer degradation and stability*, *121*, 222–229.

Lajewski, S., Mauch, A., Geiger, K., & Bonten, C. (2021). Rheological characterization and modeling of thermally unstable poly (3-hydroxybutyrate-co-3-hydroxyvalerate)(phbv). *Polymers*, *13*(14), 2294.

Longé, L. F., Michely, L., Gallos, A., Rios De Anda, A., Vahabi, H., Renard, E., Latroche, M., Allais, F., & Langlois, V. (2022). Improved processability and antioxidant behavior of poly (3-hydroxybutyrate) in presence of ferulic acid-based additives. *Bioengineering*, *9*(3), 100.

Maier, R.-D., & Schiller, M. (2016). *Handbuch kunststoff additive*. Carl Hanser Verlag GmbH Co KG.

Mark, H. (1938). Der feste Körper. *Hirzel, Leipzig*, *103*, 391–456.

McAdam, B., Brennan Fournet, M., McDonald, P., & Mojicevic, M. (2020). Production of polyhydroxybutyrate (PHB) and factors impacting its chemical and mechanical characteristics. *Polymers*, *12*(12), 2908.

Melik, D., & Schechtman, L. (1995). Biopolyester melt behavior by torque rheometry. *Polymer Engineering & Science*, *35*(22), 1795–1806.

Menczel, J. D., & Prime, R. B. (2009). *Thermal analysis of polymers: Fundamentals and applications*. John Wiley & Sons.

Meng, Q., Heuzey, M.-C., & Carreau, P. J. (2012). Control of thermal degradation of polylactide/clay nanocomposites during melt processing by chain extension reaction. *Polymer Degradation and Stability*, *97*(10), 2010–2020.

Messerli, P., Murniningtyas, E., Eloundou-Enyegue, P., Foli, E. G., Furman, E., Glassman, A., Hernández Licona, G., Kim, E. M., Lutz, W., Moatti, J.-P., et al. (2019). Global sustainable development report 2019: The future is now–science for achieving sustainable development.

Münstedt, H. (2016). *Rheological and morphological properties of dispersed polymeric materials: Filled polymers and polymer blends*. Carl Hanser Verlag GmbH Co KG.

Murphy, J. (2001). *Additives for plastics handbook*. Elsevier.

Nizamuddin, S., Boom, Y. J., & Giustozzi, F. (2021). Sustainable polymers from recycled waste plastics and their virgin counterparts as bitumen modifiers: A comprehensive review. *Polymers*, *13*(19), 3242.

Osswald, T., & Rudolph, N. (2015). Polymer rheology. *Carl Hanser, München*.

Pachekoski, W. M., Dalmolin, C., & Agnelli, J. A. M. (2013). The influence of the industrial processing on the degradation of poly (hidroxybutyrate)-PHB. *Materials Research*, *16*, 237–332.

pandas development team, T. (2020, February). *Pandas-dev/pandas: Pandas* (Version latest). Zenodo. https://doi.org/10.5281/zenodo.3509134

Park, S., Lim, S., Shin, T., Choi, H., & Jhon, M. (2001). Viscoelasticity of biodegradable polymer blends of poly (3-hydroxybutyrate) and poly (ethylene oxide). *Polymer*, *42*(13), 5737–5742.

PlasticsEurope. (2022). Plastics - the facts 2022 • Plastics Europe [An analysis of European plastics production, demand, conversion and end-of-life management]. Retrieved May 6, 2023, from https://plasticseurope.org/knowledge-hub/plastics-the-facts-2022-2/

Plavec, R., Horváth, V., Hlaváčiková, S., Omaníková, L., Repiská, M., Medlenová, E., Feranc, J., Kruželák, J., Přikryl, R., Figalla, S., et al. (2022). Influence of multiple thermomechanical processing of 3d filaments based on polylactic acid and polyhydroxybutyrate on their rheological and utility properties. *Polymers*, *14*(10), 1947.

Przybysz, M., Marć, M., Klein, M., Saeb, M. R., & Formela, K. (2018). Structural, mechanical and thermal behavior assessments of PCL/PHB blends reactively compatibilized with organic peroxides. *Polymer Testing*, *67*, 513–521.

Rajan, K. P., Thomas, S. P., Gopanna, A., & Chavali, M. (2019). Polyhydroxybutyrate (PHB): A standout biopolymer for environmental sustainability. *Handbook of ecomaterials*, 2803–2825.

Rivas, L. F., Casarin, S. A., Nepomuceno, N. C., Alencar, M. I., Agnelli, J. A. M., Medeiros, E. S. d., Wanderley, A. d. O., Oliveira, M. P. d., Medeiros, A. M. d., & Santos, A. S. F. (2017). Reprocessability of PHB in extrusion: ATR-FTIR, tensile tests and thermal studies. *Polímeros*, *27*, 122–128.

Rosenboom, J.-G., Langer, R., & Traverso, G. (2022). Bioplastics for a circular economy. *Nature Reviews Materials*, *7*(2), 117–137.

Schröder, T. (2020). *Rheologie der Kunststoffe: Theorie und Praxis*. Carl Hanser Verlag GmbH Co KG.

Schyns, Z. O., & Shaver, M. P. (2021). Mechanical recycling of packaging plastics: A review. *Macromolecular rapid communications*, *42*(3), 2000415.

Standau, T., Nofar, M., Dörr, D., Ruckdäschel, H., & Altstädt, V. (2022). A review on multifunctional epoxy-based joncryl® adr chain extended thermoplastics. *Polymer Reviews*, *62*(2), 296–350.

Staudinger, H., & Heuer, W. (1930). Über hochpolymere Verbindungen, 33. Mitteilung: Beziehungen zwischen Viscosität und Molekulargewicht bei Poly-Styrolen. *Berichte der deutschen chemischen Gesellschaft (A and B Series)*, *63*(1), 222–234.

Tocháček, J., Přikryl, R., Menčík, P., Melčová, V., & Figalla, S. (2021). The chances of thermooxidation stabilization of poly (3-hydroxybutyrate) during processing–a critical evaluation. *Journal of Applied Polymer Science*, *138*(27), 50647.

Turco, R., Santagata, G., Corrado, I., Pezzella, C., & Di Serio, M. (2021). In vivo and post-synthesis strategies to enhance the properties of PHB-based materials: A review. *Frontiers in Bioengineering and Biotechnology*, *8*, 619266.

Van Rossum, G., & Drake Jr, F. L. (1995). *Python tutorial* (Vol. 620). Centrum voor Wiskunde en Informatica Amsterdam, The Netherlands.

Villalobos, M., Awojulu, A., Greeley, T., Turco, G., & Deeter, G. (2006). Oligomeric chain extenders for economic reprocessing and recycling of condensation plastics. *Energy*, *31*(15), 3227–3234.

Virtanen, P., Gommers, R., Oliphant, T. E., Haberland, M., Reddy, T., Cournapeau, D., Burovski, E., Peterson, P., Weckesser, W., Bright, J., van der Walt, S. J., Brett, M., Wilson, J., Millman, K. J., Mayorov, N., Nelson, A. R. J., Jones, E., Kern, R., Larson, E., … SciPy 1.0 Contributors. (2020). SciPy 1.0: Fundamental Algorithms for Scientific Computing in Python. *Nature Methods*, *17*, 261–272. https://doi.org/10.1038/s41592-019-0686-2

Wang, L., Zhu, W., Wang, X., Chen, X., Chen, G.-Q., & Xu, K. (2008). Processability modifications of poly (3-hydroxybutyrate) by plasticizing, blending, and stabilizing. *Journal of Applied Polymer Science*, *107*(1), 166–173.

Wang, Z., Schmitt, D. R., & Wang, R. (2017). Modeling of viscoelastic properties of nonpermeable porous rocks saturated with highly viscous fluid at seismic frequencies at the core scale. *Journal of Geophysical Research: Solid Earth*, *122*(8), 6067–6086.

Weinmann, S., & Bonten, C. (2019). Thermal and rheological properties of modified polyhydroxybutyrate (PHB). *Polymer Engineering & Science*, *59*(5), 1057–1064.

World Economic Forum, Ellen MacArthur Foundation, & McKinsey & Company. (2016). The new plastics economy – rethinking the future of plastics.

Yang, Z., Xin, C., Mughal, W., Li, X., & He, Y. (2018). High-melt-elasticity poly (ethylene terephthalate) produced by reactive extrusion with a multi-functional epoxide for foaming. *Journal of Applied Polymer Science*, *135*(8), 45805.

Yasuda, K. (1979). *Investigation of the analogies between viscometric and linear viscoelastic properties of polystyrene fluids* [Doctoral dissertation, Massachusetss Institute of Technology].

Zheng, J., & Suh, S. (2019). Strategies to reduce the global carbon footprint of plastics. *Nature Climate Change*, *9*(5), 374–378.

A   Data Sheets PHB produced by Biomer®

A.1   Processing Data Sheet

Processing of Biomer®PHB

Melting behavior

Being highly crystalline and absolutely linear (60-70% crystallinity) Biomer polyesters liquify when heated and freeze when cooled. Crystallization speed is fast between 80°C and 100°C. Below 60°C or above 130°C the speed of crystallization is rather slow. The material then remains amorphous and sticky for hours.

Don't use barrier screws because of the temperature profile!

Consequences

The sharp transition fluid/solid can be used to achieve very fast processing speeds. To obtain this it is best to melt the material right behind the filling zone and to lower its temperature towards the die (see temperature profile on the reverse side). The material then has a viscosity similar to PP of a high MFI, eg. Ducor 110.

Pre-cleaning screw and barrel

As most materials left over in the machine after the last run have high viscosity at 130°C, they will not be displaced by the low viscous PHB. Such materials can be replaced by setting all zones to 180-185°C and purging with a colored batch of a low melting polymer such as PCL (polycaprolactone) or a high MFI PP.

Drying (only thin parts!)

As all polyesters PHB based resins contain bound water (not only surface bound one!). In spite of this drying is recommended only for thin parts (0,1 mm or less). Best results are obtained in dry air dryers: >2 hours at max. 60°C (not higher!). Please note that the pellets regain the original humidity within 30 minutes if they are removed from the dryer.

Getting the set points:

Crystallization speed depends on many (local) factors. We recommend to find the set points by following these steps:

Start conditions:

- Cooling time 20 seconds (keep fixed till the end of the optimization).
- Temperature profile of 185°C (hopper) to 165°C (die, see temperature profiles below).On large machines start the temperature profile only in zone 2 to not to expose the resins to excess thermal heath.

- Set mold temperature to 45°C.

Optimization:

- Cool barrel in 5°C steps at the tip (and zones in front of tip accordingly, but keep zone 1 at 185°C) till the form no longer is filled. Increase the temperature by 5°C.
- Vary the mold temperature by 5°C up or down so that the melt temperature is cooled to about about 90°C.
    - Reduce cooling time till the article sticks to die. Increase time in 1 – 2 second steps.

Temperatures:

Screw diameter <40 mm numbers in °C					hopper ↓
Grade	Tip	Zone n-1		Zone 1	
P226	145	155	165	180	
P209	140	150	160	180	
P316	140	150	160	175	
P310	140	155	165	188	
Hot runners	150	150			

Screw diameter >40 mm Values in °C						Hopper ↓
Grade	Tip	Zone n-1			Zone 1	
P226	145	155	165	180	60	
P209	140	150	160	180	60	
P316	140	150	160	175	60	
P310	140	155	165	188	60	
Hot runners	150	150	150			

optimal Tool Temperature:

Set tool temperature in such a way that the melt cools to 90°C:

45-55 °C at wall thickness under 1 mm

30-45 °C at wall thickness over 2 mm

A.2 Mechanical Data Sheet

Mechanical properties*)

Type	Biomer® P209/P209E	Biomer® P226/P226E	Biomer® P263/P263E
Modulus (MPa)(1mm/min)	840-1200/830	1140-1900/1240	1730-1760/1820-1860
Tensile strength (MPa)(50 mm/min)	15-20/18,7	24-27/25,5	28-29
Elongation (%)(50 mm/min)	8-15/16	6-9/8,5	5,4/3,7-4,3
Flexural strength (N/mm2)	18	35	-
Deformation at bending break (%)	4,7	6,6	-
Flexural strength at 3,5% (N/mm2)	16	29	-
Impact strength 23°C (KJ/m) (ISO 179/1eU)	no break/111,8	no break/82,9	-
Impact strength -30°C KJ/m2 (ISO 179/1eU)	70	30	-
Notched impact strength 23°C (ISO 179/1eA)	4,7/6,2	2,7/6,6	2,5/2,4
Notched impact strength -30°C (ISO 179/1eA)	3,4	1,4	-
MFR 180°C	10 (2,16 kg)	10 (5 kg)	-
MVR 180°C	10 (2,16 kg)	9,5 (5 kg)	-
Vicat temperature °C (ISO 306/A/120)	134;54 (B/50)	147	-
HDT °C (ISO 75/A)	50	59	-
Density (g/cm3)	1,20	1,25	1,3
Moisture absorption (%)	0,75	0,4	-
Hardness (Shore D)	57	67	-
Shrinkage (%)	1,2-1,3	1,2-1,3	1,2-1,3

*) means of tests done at least 4 weeks after preparing test specimens
Werte Data for most parts from University of Applied Sciences Hannover: P304, P209, P209E, and P226E single values

Comparison

Polymer	Tensile strength	Elongation	Modulus
Biomer®P226	24-27	6-9	1140-1900
PP	22	12-20	600-1200
Biomer®P209	15-20	8-15	600-1200
PE-LD	15-20	600	150-450
PE-HD	25-32	600-900	700-1200

B   Data Sheets Joncryl®

B.1   Joncryl® ADR 4400

Technical Information	**Joncryl®**
TI / EV/BX 001 e March 2014	**Functional Additives**
Page 1 of 6	

□ · BASF
The Chemical Company
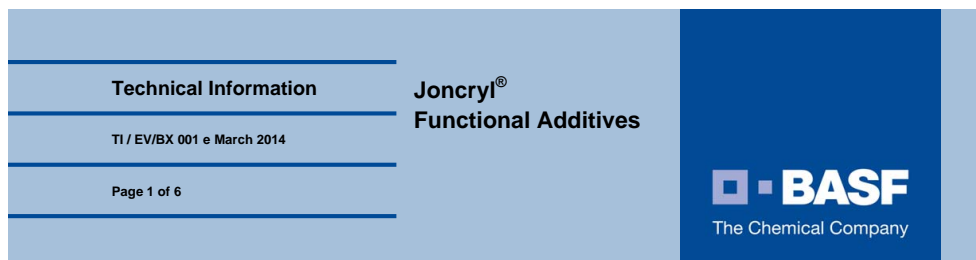
Joncryl® is a registered
trademark of
BASF Corporation

Joncryl® ADR 4400

Polymeric Chain Extender for Food Contact Applications

Joncryl® ADR 4400 is a patented, multi-functional reactive polymer with an improved thermal stability versus earlier chain extenders, making it a better additive for specific food contact applications based on polycondensation polymers (e.g. PET and PLA). It can also be used for the modification of other thermoplastics such as PBT, TPU, PC, PC/ABS, etc.

Joncryl ADR4400 is a polymeric chain extender with a medium epoxy equivalent weight (= medium number of epoxy groups per chain) that reacts with the chain ends of polycondensates and effectively increases their melt viscosity.

Joncryl® ADR 4400 can be used during processing to increase the melt strength of polycondensates, to improve the processing during extrusion of films, sheets, foams, paper coatings, and blow-molded objects.
For food contact notification, see BASF Regulatory Information Sheet.

Key Features & Benefits

- Reacts and modifies polycondensation polymers
- Increases molecular weight and melt strength
- Improves hydrolytic stability
- Improved processability and accelerated polycondensation reaction

Appearance	Solid flakes
Specific gravity, 25° C	1.08
Mw	7100
T_g (°C)	65
Non-volatile by GC (%)	>99
Epoxy equivalent weight (g/mol)	485

These typical values should not be interpreted as specifications

1. Product Form

Form	Particle Size [1]/ Physical Characteristics	Description
ADR 4400 (Flakes)	2.5 – 4.0 mm mean <2% (w/w) smaller than 0.15 mm	Efficient for dry blending with cold plastics pellets of flake, or for separate feeding
Pre-compounded masterbatch (supplied by recommended masterbatcher)	Appearance will depend on pelletization and carrier resin.	Masterbatches are recommended for single screw extrusion or injection molding applications where mixing is limited.

[1] *Particle size distribution may shift toward smaller particle sizes with handling due to the brittle nature of this additive.*

2. Recommended dosage for Joncryl® ADR 4400

Every chain extension problem is unique and you may consult our technical service team should you need help with determining the right dosage for your specific operation. In general, the recommended initial trial dosage should be 0.2%. You may increase or decrease the dosage after your initial trial depending on the outcome and your target requirements in the following applications for different type of resins:

Resin Types
Polyesters (PET, PETG, PBT, PLA, etc.)
Polycarbonates (PC, PC/ABS)
Others (TPU, etc.)

Applications
Fibers, like staple, spun bond, etc.
Injection molding (compound of recycled polycondensates)
Extrusion (film, sheet, tape, strap profile)
Blow molding (extrusion blow molding, ISBM of recycled polyesters)
Hydrolytic stabilization

3. Feeding Method

Dry-Blending

Procedure

a) Flake or masterbatch can be dry-blended with pre-dried and cold (<40ºC) plastic pellets or flakes with the aid of low shear mixer such as tumble mixer or conical mixer.

b) All solid forms of Joncryl® ADR 4400 can be mixed with other materials in a high shear mixer such as a Henschel mixer below 50ºC. Cold mixing may be aided with 0.2% of Joncryl® ADP-1200, acrylic plasticizer.

Feeding of Joncryl® ADR 4400 on a single screw extruder, twin screw extruder or kneader

a) Dry-blends prepared as in (1) can be volumetrically, gravimetrically or flood fed directly into the mixing zone of the extruder (see temperature recommendations in the Processing Conditions in Section 4.)

b) Gravimetric feed metering systems can be used to feed any solid product form in a parallel stream with the plastic directly into the feeding zone of the extruder. Belt and disc feeders are particularly recommended for the flake form.

- Single Screw Feeders – clearance of 3 to 5 mm (0.76 – 1.27 in) between the screw and the tube recommended.

- Twin-Screw Feeders – non-intermeshing spiral screw with 6 mm (1.52 in) clearance between the screw and the tube recommended. Eliminate agglomeration at the throat or feed zone by maintaining tube temperature below 80 °C.

c) Volumetric Feeders: Well calibrated feeders with variation of less than 0.5% are recommended. Clearance of 3 to 5 mm (0.76 – 1.27 in) between the screw and tube is also required to reduce fines.

Eliminate agglomeration at the throat or feed zone by maintaining tube temperature below 80 °C.

d) Side feed systems and other types of forced dosing extruders may be employed with all solid product forms, except for fine powder, to feed the products downstream. Residence time recommendations are given below in reference to downstream feeds.

e) Direct gravimetric/volumetric addition of the chain extender in any form to the plastic melt may be carried out through any suitable downstream venting or degassing port.

4. Processing Method

Procedure

Pre-drying

Pre-dry the base plastic at manufacturer's recommended conditions.
In some instances small amounts of Joncryl® chain extenders can compensate for poor/incomplete drying, thus bringing robustness and savings to your operations. For example in polyesters, degradation brought about by 100 ppm of moisture can be compensated by 0.2 % of Joncryl® ADR 4400
Hygroscopicity: there is no evidence of bulk absorption of moisture over extended periods of time for Joncryl® ADR 4400.

- At normal conditions of temperature and relative humidity (i.e. 25°C and 50% RH) its surface reaches equilibrium saturation through adsorption at less than 0.25% moisture.

- At extreme conditions (i.e. fine powder at 35°C and 100 % RH) its surface reaches equilibrium saturation at less than 0.50 % of moisture.

Therefore, Joncryl® ADR 4400 can generally be processed without any drying, even after long exposure to drastic conditions bringing no more than 5 ppm moisture per every 0.1% used.
In systems where moisture sensitivity is extreme, Joncryl® ADR 4468 can be dried in a desiccant dryer at 30°C for 1 hour, prior to use
Masterbatches of Joncryl® ADR 4400 should not be dried above 120°C to prevent pre-reaction within the masterbatch from happening.

Extruder Temperature Profile

When feeding solid Joncryl® ADR 4400 into the 1st zone of the extruder or injection molder, we recommend operating this zone at 20°C to 40°C lower temperature than normal. This will prevent early melting and agglomeration of the additive.

Refer to masterbatch suppliers' directions for additional information and instructions regarding how to use chain extender masterbatches.

All other zones should employ normal processing conditions as recommended by the plastic's manufacturer.

Additive Thermal Stability

Neat Joncryl® ADR 4400 has a better thermally stable than Joncryl® ADR 4300-F / ADR 4300-S. Therefore Joncryl® ADR 4400 has better chances for more strict food contact approvals.

Residence Time

Joncryl® ADR 4400 reacts quickly. Its reaction will be over 99% complete if at least 120 sec residence time is provided at 200°C in a well-mixed system. Alternatively, 30 sec residence time at 280°C will provide 99% completion. These limits accommodate most extrusion processes for the recommended thermoplastics and applications.

Maximum Process Temperature

Joncryl® ADR 4400 should not be processed at temperatures higher than 320°C (see Thermal Stability in Section 4)

Extruder pressure effects

The use of Joncryl® ADR 4400 in reactive extrusion operations produces significant increases in molecular weight of the plastic being modified. This increase in molecular weight raises the melt viscosity, which in turn raises the pressure observed in the equipment.

It is important that operators be aware of these expected pressure changes. Alarms, automatic shut-offs, screen purging set-points, and other operation variables should be adjusted to accommodate these normal and expected pressure increases.

Instantaneous pressure variations and spikes are due to large instantaneous changes in melt viscosity. At constant temperature, changes in melt viscosity are often due to variable feed rate and/or poor mixing

Fluctuations in the feed rate of Joncryl® ADR 4400 larger than 10% of the target value may cause large instantaneous extruder pressure spikes. To attain steady and consistent pressure, homogenous dry blends or robust co-feed systems are essential.

Finer screen mesh will produce even higher pressures during chain extension process.

5. Troubleshooting

In case of unexpectedly high pressure:

1. Decrease the feed rate of Joncryl® ADR 4400

2. Decrease the RPM. This decreases pressure on single screw extruders and flood-fed twin-screw extruders, and will decrease heating on starve-fed twin- screw extruders

3. Slowly increase the temperature, starting from the die and then from the last to the zone.

4. In a typical extruder with an L/D >24 normally most of the extension reaction takes place in the first half of the extruder length. In-creasing the temperature in the zones of the final half of the extruder will generally result in lower viscosity and pressure.

5. With pressure under control, increase the Joncryl® ADR 4400 feed slowly.

6. For steady operation follow recommendations given in the section 5 above.

7. Keep in mind that chain extension will always result in higher pres-sure at constant extruder settings.

8. In case extruder stopped on high torque caused by overdosing of Joncryl® ADR 4400, increase barrel temperature up to 320°C and purge the extruder with raw material.

6. Note

The data contained in this publication are based on our current knowledge and experience. In view of the many factors that may affect processing and application of our product, these data do not relieve processors from carrying out their own investigations and tests; nei-ther do these data imply any guarantee of certain properties, nor the suitability of the product for a specific purpose. Any descriptions, drawings, photographs, data, proportions, weights, etc. given herein may change without prior information and do not constitute the agreed contractual quality of the product. It is the responsibility of the recipient of our products to ensure that any proprietary rights and existing laws and legislation are observed.

It is the responsibility of those to whom we supply our products to en-sure that any proprietary rights and existing laws and legislation are observed. Some uses of Joncryl® and products obtained by use of Joncryl® are subject of intellectual property rights. Purchase of Joncryl® does not entitle the buyer or any third party to produce, offer or use any blends protected under property rights and all their equiva-lents as listed here: EP-B 1656423 and EP-B 1838784

EV/BX, Rev. March 2014   Page 6 of 6   Joncryl® ADR 4400

Europe, Africa and Middle East
BASF Nederland B.V.
Innovatielaan 1
8467 SN Heerenveen
The Netherlands
Tel: 31-513-619619
Fax: 31-513-619600

US and Canada
BASF Corporation
100 Campus Dr.
Florham Park,
NJ 07932
USA
Tel: (973) 245-7829

Latin and South America
BASF Mexicana, S.A. de C.V.
Av. Insurgentes Sur #975
Col. Ciudad de los Deportes
C.P. 03710, Mexico. D.F.
Tel: (52-55) 5325-2787
        (52-55) 5325-2687
Fax: (52-55) 5611-4897

Asia / Pacific Rim:
BASF East Asia Regional Headquarters Limited
45th Floor, Jardine House
No. 1 Connaught Place
Central, Hong Kong
Tel: (852) 2731-4316
Fax: (852) 2731-5633

B.2   Joncryl® ADR 4468

Joncryl®
Functional Additives

BASF
The Chemical Company

Joncryl® is a registered
trademark of
BASF Corporation

Joncryl® ADR 4468

Polymeric Chain Extender for Food Contact Applications

Joncryl® ADR 4468 is a patented, multi-functional reactive polymer with an improved thermal stability versus earlier chain extenders for specific food contact applications polycondensation polymers (e.g. PET and PLA). It can also be used for the modification of other thermoplastics such as PBT, TPU, PC, PC/ABS ect.

It is a polymeric chain extender with low epoxy equivalent weight (= high number of epoxy groups per chain) that reacts with the chain ends of polycondensates and effectively increases their melt viscosity.

Joncryl® ADR 4468 can be used during processing to increase the melt strength of polycondensates to improve the processability during extrusion of films, sheets, foams, paper coatings, and blow-molded objects.
For food contact notification, see BASF Regulatory Information Sheet.

Key Features & Benefits

- Reacts and modifies polycondensation polymers
- Increases molecular weight and melt strength
- Improves hydrolytic stability
- Improved processability and accelerated polycondensation reaction

Appearance	Solid flakes
Specific gravity, 25° C	1.08
Mw	7250
T_g (°C)	59
Non-volatile by GC (%)	>99
Epoxy equivalent weight (g/mol)	310

These typical values should not be interpreted as specifications

1. Product Form

Form	Particle Size [1]/ Physical Characteristics	Description
ADR 4468 (Flakes)	2.5 – 4.0 mm mean <2% (w/w) smaller than 0.15 mm	Efficient for dry blending with cold plastics pellets of flake, or for separate feeding
Pre-compounded masterbatch (supplied by recommended masterbatcher)	Appearance will depend on pelletization and carrier resin.	Masterbatches are recommended for single screw extrusion or injection molding applications where mixing is limited.

[1] Particle size distribution may shift toward smaller particle sizes with handling due to the brittle nature of this additive.

2. Recommended dosage for Joncryl® ADR 4468

Every chain extension problem is unique and you may consult our technical service team should you need help with determining the right dosage for your specific operation. In general, the recommended initial trial dosage should be 0.2%. You may increase or decrease the dosage after your initial trial depending on the outcome and your target requirements in the following applications for different type of resins:

Resin Types
Polyesters (PET, PETG, PBT, PLA, etc.)
Polycarbonates (PC, PC/ABS)
Others (TPU etc.)

Applications
Injection molding (compound of recycled polycondensates)
Extrusion (film, sheet, tape, strap profile)
Blow molding (extrusion blow molding, ISBM of recycled polyesters)
Hydrolytic stabilization
Foam
Compatibilization (e.g. alloying of PA-PET, etc.)

3. Feeding Method

Dry-Blending

Procedure

a) Flake or masterbatch can be dry-blended with pre-dried and cold (<40ºC) plastic pellets or flakes with the aid of low shear mixer such as tumble mixer or conical mixer.

b) All solid forms of Joncryl® ADR 4468 can be mixed with other materials in a high shear mixer such as a Henschel mixer below

50ºC. Cold mixing may be aided with 0.2% of Joncryl® ADP-1200, acrylic plasticizer.

Feeding of Joncryl® ADR 4468 on a single screw extruder, twin screw extruder or kneader

a) Dry-blends prepared as in (1) can be volumetrically, gravimetrically or flood fed directly into the mixing zone of the extruder (see temperature recommendations in the Processing Conditions in Section 4.)

b) Gravimetric feed metering systems can be used to feed any solid product form in a parallel stream with the plastic directly into the feeding zone of the extruder. Belt and disc feeders are particularly recommended for the flake form.

- Single Screw Feeders – clearance of 3 to 5 mm (0.76 – 1.27 in) between the screw and the tube recommended.

- Twin-Screw Feeders – non-intermeshing spiral screw with 6 mm (1.52 in) clearance between the screw and the tube recommended. Eliminate agglomeration at the throat or feed zone by maintaining tube temperature below 80 °C.

c) Volumetric Feeders: Well calibrated feeders with variation of less than 0.5% are recommended. Clearance of 3 to 5 mm (0.76 – 1.27 in) between the screw and tube is also required to reduce fines.

Eliminate agglomeration at the throat or feed zone by maintaining tube temperature below 80 °C.

d) Side feed systems and other types of forced dosing extruders may be employed with all solid product forms, except for fine powder, to feed the products downstream. Residence time recommendations are given below in reference to downstream feeds.

e) Direct gravimetric/volumetric addition of the chain extender in any form to the plastic melt may be carried out through any suitable downstream venting or degassing port.

4. Processing Method

Pre-drying

Procedure

Pre-dry the base plastic at manufacturer's recommended conditions.
In some instances small amounts of Joncryl® chain extenders can compensate for poor/incomplete drying, thus bringing robustness and savings to your operations. For example in polyesters, degradation brought about by 100 ppm of moisture can be compensated by 0.2 % of Joncryl® ADR 4468.
Hygroscopicity: there is no evidence of bulk absorption of moisture over extended periods of time for Joncryl® ADR 4468.

- At normal conditions of temperature and relative humidity (i.e. 25°C and 50% RH) its surface reaches equilibrium saturation

through adsorption at less than 0.25% moisture.

- At extreme conditions (i.e. fine powder at 35°C and 100 % RH) its surface reaches equilibrium saturation at less than 0.50 % of moisture.

Therefore, Joncryl® ADR 4468 can generally be processed without any drying, even after long exposure to drastic conditions bringing no more than 5 ppm moisture per every 0.1% used.
In systems where moisture sensitivity is extreme, Joncryl® ADR 4468 can be dried in a desiccant dryer at 30°C for 1 hour, prior to use
Masterbatches of Joncryl® ADR 4468 should not be dried above 120°C to prevent pre-reaction within the masterbatch from happening.

Extruder Temperature Profile

When feeding solid Joncryl® ADR 4468 into the 1st zone of the extruder or injection molder, we recommend operating this zone at 20°C to 40°C lower temperature than normal. This will prevent early melting and agglomeration of the additive.

Refer to masterbatch suppliers' directions for additional information and instructions regarding how to use chain extender masterbatches.

All other zones should employ normal processing conditions as recommended by the plastic's manufacturer.

Additive Thermal Stability

Neat Joncryl® ADR 4468 has a better thermally stable than Joncryl® ADR 4368C / 4368CS. Therefore Joncryl® ADR 4468 has better chances for more strict food contact approvals.

Residence Time

Joncryl® ADR 4468 reacts quickly. Its reaction will be over 99% complete if at least 120 sec residence time is provided at 200°C in a well-mixed system. Alternatively, 30 sec residence time at 280°C will provide 99% completion. These limits accommodate most extrusion processes for the recommended thermoplastics and applications.

Maximum Process Temperature

Joncryl® ADR 4468 should not be processed at temperatures higher than 320°C (see Thermal Stability in Section 4)

Extruder pressure effects

The use of Joncryl® ADR 4468 in reactive extrusion operations produces significant increases in molecular weight of the plastic being modified. This increase in molecular weight raises the melt viscosity, which in turn raises the pressure observed in the equipment.

It is important that operators be aware of these expected pressure changes. Alarms, automatic shut-offs, screen purging set-points, and other operation variables should be adjusted to accommodate these normal and expected pressure increases.

Instantaneous pressure variations and spikes are due to large instantaneous changes in melt viscosity. At constant temperature, changes in melt viscosity are often due to variable feed rate and/or poor mixing Fluctuations in the feed rate of Joncryl® ADR 4468 larger than 10% of the target value may cause large instantaneous extruder pressure

EV/BX, Rev. March 2014   Page 5 of 6   Joncryl® ADR 4468

spikes. To attain steady and consistent pressure, homogenous dry blends or robust co-feed systems are essential.

Finer screen mesh will produce even higher pressures during chain extension process.

5. Troubleshooting

In case of unexpectedly high pressure:

1. Decrease the feed rate of Joncryl® ADR 4468

2. Decrease the RPM. This decreases pressure on single screw extruders and flood-fed twin-screw extruders, and will decrease heating on starve-fed twin- screw extruders

3. Slowly increase the temperature, starting from the die and then from the last to the zone.

4. In a typical extruder with an L/D >24 normally most of the extension reaction takes place in the first half of the extruder length. In-creasing the temperature in the zones of the final half of the extruder will generally result in lower viscosity and pressure.

5. With pressure under control, increase the Joncryl® ADR 4468-C/CS feed slowly.

6. For steady operation follow recommendations given in the section 5 above.

7. Keep in mind that chain extension will always result in higher pressure at constant extruder settings.

8. In case extruder stopped on high torque caused by overdosing of Joncryl® ADR 4468, increase barrel temperature up to 320°C and purge the extruder with raw material.

6. Note

The data contained in this publication are based on our current knowledge and experience. In view of the many factors that may affect processing and application of our product, these data do not relieve processors from carrying out their own investigations and tests; neither do these data imply any guarantee of certain properties, nor the suitability of the product for a specific purpose. Any descriptions, drawings, photographs, data, proportions, weights, etc. given herein may change without prior information and do not constitute the agreed contractual quality of the product. It is the responsibility of the recipient of our products to ensure that any proprietary rights and existing laws and legislation are observed.

It is the responsibility of those to whom we supply our products to ensure that any proprietary rights and existing laws and legislation are observed. Some uses of Joncryl® and products obtained by use of Joncryl® are subject of intellectual property rights. Purchase of Joncryl® does not entitle the buyer or any third party to produce, offer or use any blends protected under property rights and all their equivalents as listed here: EP-B 1656423 and EP-B 1838784

EV/BX, Rev. March 2014   Page 6 of 6   Joncryl® ADR 4468

Europe, Africa and Middle East	**US and Canada**	**Latin and South America**	**Asia / Pacific Rim:**
BASF Nederland B.V.	BASF Corporation	BASF Mexicana, S.A. de C.V.	BASF East Asia Regional Headquarters Limited
Innovatielaan 1	100 Campus Dr.	Av. Insurgentes Sur #975	45th Floor, Jardine House
8467 SN Heerenveen	Florham Park,	Col. Ciudad de los Deportes	No. 1 Connaught Place
The Netherlands	NJ 07932	C.P. 03710, Mexico. D.F.	Central, Hong Kong
Tel: 31-513-619619	USA	Tel: (52-55) 5325-2787	Tel: (852) 2731-4316
Fax: 31-513-619600	Tel: (973) 245-7829	(52-55) 5325-2687	Fax: (852) 2731-5633
		Fax: (52-55) 5611-4897	

C ANOVA

For the ANOVA the E2 sample and the samples E2x1x0.2%, E2x1x0.6%, and E2x1x1% for each Joncryl® are considered.

All samples were checked on normality with the *Shapiro-Wilk* test. The samples for the Joncryl® 4400 for the elongation at break at a concentration of 0.6 wt% and the crystallinity of the second heating scan with a weight percentage of 0.2 are not normally distributed.

The null-hypothesis (equal variance) for the *Barlett*-test has to be rejected for the tangent modulus of the Joncrly® 4468 in table 15, this is due to the use of different processing settings for the sample E2 1x0.6% 4468 (see table 3, page 32).

Table 14: *p-values for test on equal variance and ANOVA for the Joncryl® 4400.*

Property	p-value *Bartlett*	p-value ANOVA
Peak crystallization temperature	0.945	0.000
Crystallinity	0.301	0.000
Tangent modulus	0.808	0.000
Ultimate tensile strength	0.531	0.174
Elongation at break	0.719	0.000
Notched charpy impact	0.284	0.000

Table 15: *p-values for test on equal variance and ANOVA for the Joncryl® 4468.*

Property	p-value *Bartlett*	p-value ANOVA
Peak crystallization temperature	0.479	0.000
Crystallinity	0.847	0.000
Tangent modulus	0.001	0.016
Ultimate tensile strength	0.319	0.097
Elongation at break	0.052	0.003
Notched charpy impact	0.050	0.009

D   Amplitude Sweep

Table 16: Relevant testing parameters of the amplitude sweep in dynamic oscillatory rheology measurement.

Parameter	4400	4468, multiple
Preparationg time in min	~10	~10
Plate diameter in mm	25	25
Gap in mm	1	1
Temperature in °C + max. value	190+0.5	190+0.5
Deformation in %	0.1 to 100	0.1 to 100
Measurement time in s	~4.1	~2
Angular freqeucny in %	10	100

Legend:
- G' E2 1x0.2% 4400
- G'' E2 1x0.2% 4400
- G' E2 1x0.6% 4400
- G'' E2 1x0.6% 4400
- G' E2 1x1% 4400
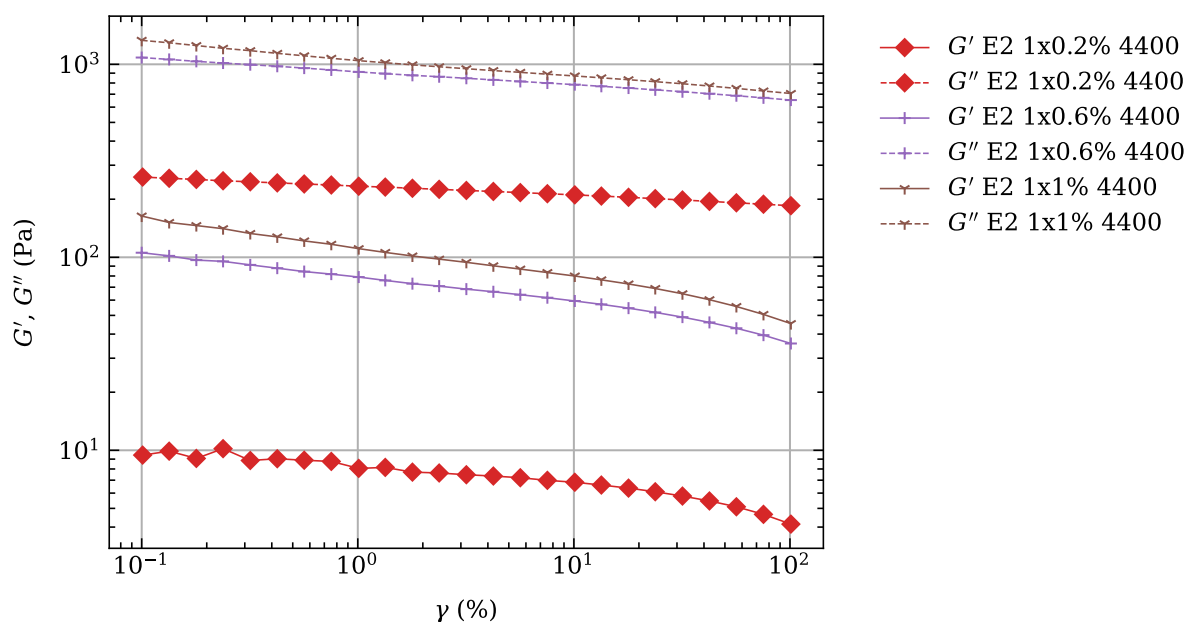- G'' E2 1x1% 4400

Axes: G', G'' (Pa) versus γ (%)

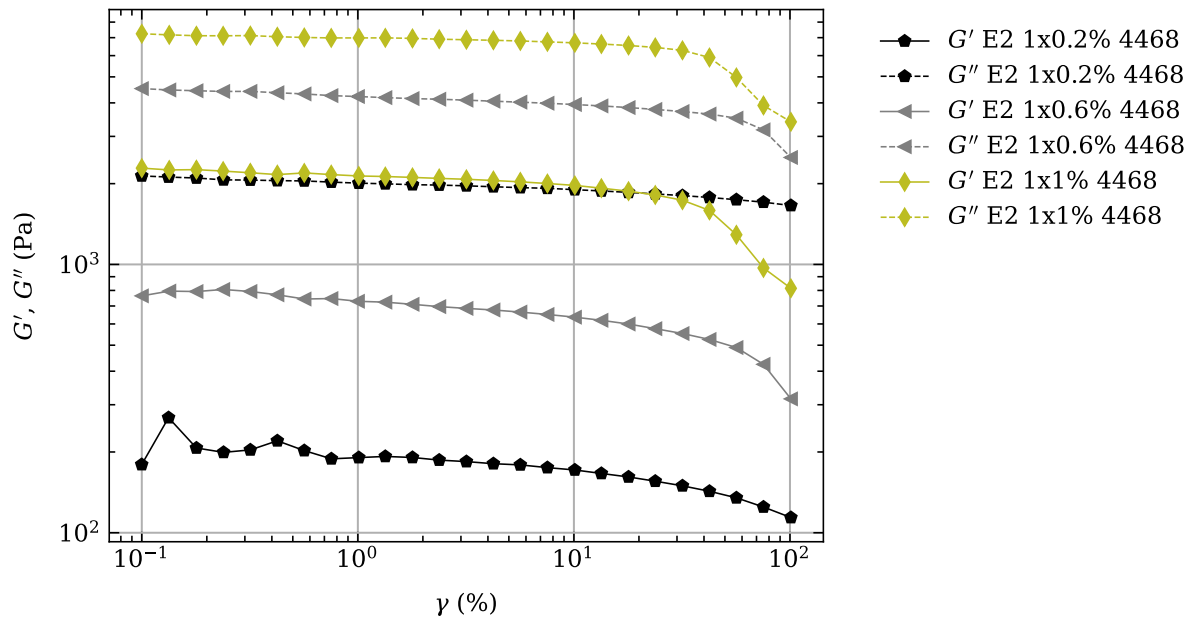*Figure 60: Amplitude sweeep for different concentrations of Joncryl® 4400.*

Figure 61: Amplitude sweeep for different concentrations of Joncryl® 4468.
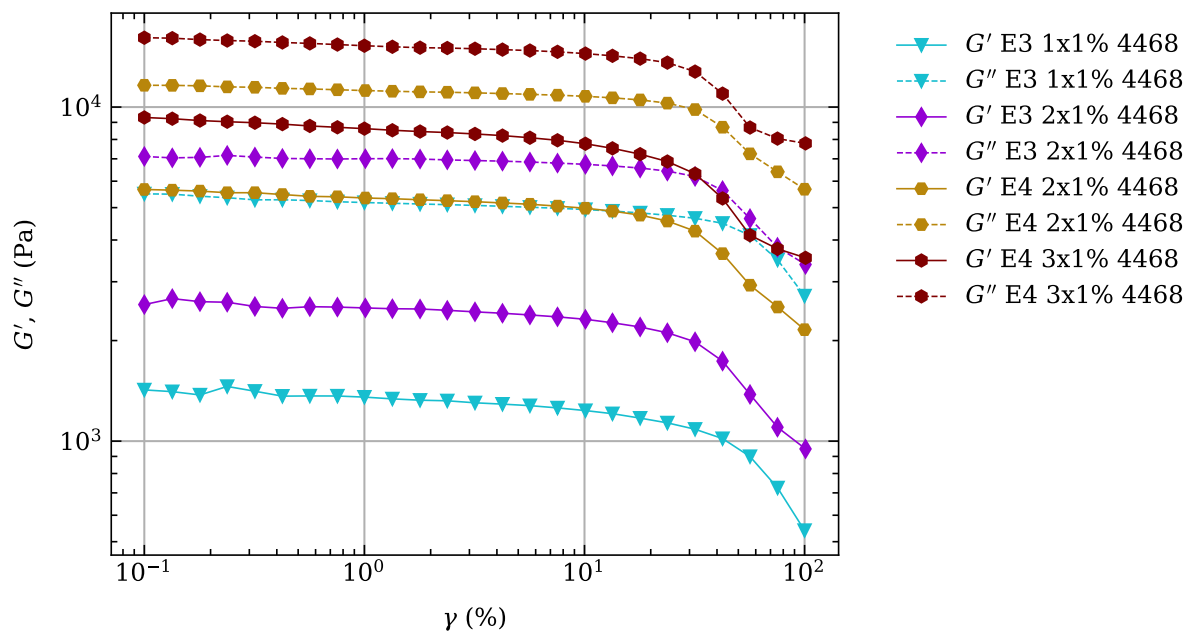

Figure 62: Amplitude sweep for multiple addition of Joncryl® 4468 at different processing steps.